Posted
A&F
OHH

GEORGIA INSTITUTE OF TECHNOLOGY

OFFICE OF RESEARCH ADMINISTRATION

RESEARCH PROJECT INITIATION

Date: January 29, 1975

Project Title: Exploratory Research on Ultrasonic and Audible Acoustic Emissions from Composite Solid Propellants

Project No: E-16-659

Principal Investigator: Dr. W. C. Strahle

Sponsor: Air Force Office of Scientific Research

Agreement Period: From 1/1/75 Until: 6/30/75

Type Agreement: Grant No. AFOSR-75-2805

Amount: $10,000 AFOSR
1,893 GIT (E-16-350)
$11,893 Total

Reports Required:

Final Scientific Report
Interim Scientific Report (if extended beyond 6 months)
Fiscal Report

Sponsor Contact Person (s):

Administrative Matters
thru ORA
Ms. Jean O. Marshall, Buyer
AFOSR
1400 Wilson Boulevard
Arlington, Va. 22209

Technical Matters
Maj. Wilbur C. Simmons
AFOSR
1400 Wilson Boulevard
Arlington, Va. 22209

Assigned to: Aerospace Engineering

COPIES TO:

- Principal Investigator
- School Director
- Dean of the College
- Director, Research Administration
- Director, Financial Affairs (2)
- Security-Reports-Property Office
- Patent Coordinator
- Library
- Rich Electronic Computer Center
- Photographic Laboratory
- Project File
- Other

RA-3 (6-71)

GEORGIA INSTITUTE OF TECHNOLOGY
OFFICE OF CONTRACT ADMINISTRATION

SPONSORED PROJECT TERMINATION

Posted 10 a.m.

Date: 12/20/77

Project Title: Exploratory Research on Ultrasonic and Audible Acoustic Emissions from Composite Solid Propellants.

Project No: E-16-659

Project Director: J. I. Craig

Sponsor: Air Force Office for Scientific Research

Effective Termination Date: 9/30/77

Clearance of Accounting Charges: 9/30/77

Grant/Contract Closeout Actions Remaining:

- _ Final Invoice and Closing Documents
- X Final Fiscal Report
- _ Final Report of Inventions
- _ Govt. Property Inventory & Related Certificate
- _ Classified Material Certificate
- _ Other _____

Assigned to: Aerospace Engineering (School/Laboratory)

COPIES TO:

- Project Director
- Division Chief (EES)
- School/Laboratory Director
- Dean/Director—EES
- Accounting Office
- Procurement Office
- Security Coordinator (OCA)
- Reports Coordinator (OCA)
- Library, Technical Reports Section
- Office of Computing Services
- Director, Physical Plant
- EES Information Office
- Project File (OCA)
- Project Code (GTRI)
- Other _____

CA—4 (3/76)

B 108
BOUND BY THE NATIONAL LIBRARY BINDERY CO. OF GA.
Have you checked, to be sure, volume is complete, with all issues, index and title page? Imperfect volumes delay return of binding. Thanks.

AFOSR Interim Scientific Report

AFOSR-TR-

Audible and Ultrasonic Acoustic Emissions from Composite Solid Propellants

prepared for

Air Force Office of Scientific Research
Aerospace Sciences Directorate

by

James I. Craig
Warren C. Strahle
John Palfery

School of Aerospace Engineering
Georgia Institute of Technology
Atlanta, Georgia 30332

Approved for Public Release; distribution unlimited

Grant No. AFOSR-75-2805 July 1975

Conditions of Reproduction

Reproduction, translation, publication, use and disposal in whole or in part by or for the United States Government is permitted.

UNCLASSIFIED

SECURITY CLASSIFICATION OF THIS PAGE *(When Data Entered)*

REPORT DOCUMENTATION PAGE		READ INSTRUCTIONS BEFORE COMPLETING FORM
1. REPORT NUMBER	2. GOVT ACCESSION NO.	3. RECIPIENT'S CATALOG NUMBER
4. TITLE *(and Subtitle)* AUDIBLE AND ULTRASONIC ACOUSTIC EMISSIONS FROM COMPOSITE SOLID PROPELLANTS		5. TYPE OF REPORT & PERIOD COVERED Feb 1975 - June 1975 INTERIM 6. PERFORMING ORG. REPORT NUMBER
7. AUTHOR(s) JAMES I CRAIG WARREN C STRAHLE JOHN PALFERY		8. CONTRACT OR GRANT NUMBER(s) AFOSR 75-2805
9. PERFORMING ORGANIZATION NAME AND ADDRESS GEORGIA INSTITUTE OF TECHNOLOGY SCHOOL OF AEROSPACE ENGINEERING ATLANTA, GEORGIA 30332		10. PROGRAM ELEMENT, PROJECT, TASK AREA & WORK UNIT NUMBERS 681308 9711-01 61102F
11. CONTROLLING OFFICE NAME AND ADDRESS AIR FORCE OFFICE OF SCIENTIFIC RESEARCH/NA 1400 WILSON BOULVEARD ARLINGTON, VIRGINIA 22209		12. REPORT DATE July 1975 13. NUMBER OF PAGES 51
14. MONITORING AGENCY NAME & ADDRESS*(if different from Controlling Office)*		15. SECURITY CLASS. *(of this report)* UNLCASSIFIED 15a. DECLASSIFICATION/DOWNGRADING SCHEDULE

16. DISTRIBUTION STATEMENT *(of this Report)*

Approved for public release; distribution unlimited.

17. DISTRIBUTION STATEMENT *(of the abstract entered in Block 20, if different from Report)*

18. SUPPLEMENTARY NOTES

19. KEY WORDS *(Continue on reverse side if necessary and identify by block number)*

ULTRASONICS
NOISE
SOLID PROPELLANT COMBUSTION
ACOUSTIC EMISSIONS

20. ABSTRACT *(Continue on reverse side if necessary and identify by block number)*

An apparatus to test the audible and ultrasonic acoustic emissions from composite solid propellants was designed, constructed and checked out. Tests were conducted at 300 psia for eight aluminized HTPB-AP propellants supplied by the Air Force Rocket Propulsion Lab. The tests were conducted under both nitrogen and air pressurization. For the audible emissions in the range 100-2500 Hz there is a marked effect of the pressurization fluid. In air the noise output is 10^4 higher than in nitrogen. There is a definite possibility that the noise output is responsible for observed chamber pressure roughness level. For the ultrasonic

DD FORM 1 JAN 73 1473 EDITION OF 1 NOV 65 IS OBSOLETE

UNCLASSIFIED

SECURITY CLASSIFICATION OF THIS PAGE *(When Data Entered)*

signal in the range 50 to 300 kHz there are strong spectral peaks observed but their origin is not clear and they do not correlate with observed deflagration behavior. For audible signals a striking effect of AFCAM aluminum coating is the reduction of signal strength.

Abstract

An apparatus to test the audible and ultrasonic acoustic emissions from composite solid propellants was designed, constructed and checked out. Tests were conducted at 300 psia for eight aluminized HTPB-AP propellants supplied by the Air Force Rocket Propulsion Lab. The tests were conducted under both nitrogen and air pressurization. For the audible emissions in the range 100 - 2500 Hz there is a marked effect of the pressurization fluid. In air the noise output is 10^4 higher than in nitrogen. There is a definite possibility that the noise output is responsible for observed chamber pressure roughness level. For the ultrasonic signal in the range 50 to 300 kHz there are strong spectral peaks observed but their origin is not clear and they do not correlate with observed deflagration behavior. For audible signals a striking effect of AFCAM aluminum coating is the reduction of signal strength.

Table of Contents

Nomenclature

A_p	propellant surface area
c	speed of sound
f	frequency of maximum radiated sound power
h	combustion noise monopole source strength
k	wavenumber, $\omega/\bar{c}$
ℓ	tube length
ℓ_e	mean granularity distance
$\dot{m}$	mass flow of propellant
p	acoustic pressure
$\bar{p}$	mean chamber pressure
r	distance from source or burn rate
S	tube cross-section area
S_ω	power spectral density (PSD)
t_o	sampling time of Fourier transform
$< >$	time average
α	95% confidence limits for PSD
γ	ratio of specific heats
ζ	specific acoustic impedance
ρ	density
η	mass flow noise efficiency, $P/\dot{m}$

Subscripts

—	steady state value
ℓ	at tube length

ω	Fourier transform
s	solid phase
r	real part
i	imaginary part

Superscripts

*	Complex conjugate

Introduction

There have been three recent studies [1], [2], [3] of the acoustic emission properties of deflagrating composite solid propellants. These studies have been concerned with both the audible and ultrasonic emissions from the propellants. In Ref. (3) it has been suggested that the sound power generation capability of a propellant may be responsible for the normal roughness in chamber pressure level during solid rocket motor burning. Furthermore, it has been suspected that a spectral analysis of this roughness would show that it may be mistaken for an instability in the motor. That is, the chamber pressure fluctuation magnitude in the frequency range about an acoustic mode of the motor cavity may be driven by noise and not be a feedback mechanism with the propellant.

While the origin of the audible signal appears reasonbaly clear, as explained below, the origin of the ultrasonic signal is open to wide interpretation. In Refs. (1) and (2) the ultrasonic signal from burning propellants has been investigated for possible value in deflagration behavior diagnostics. Principal attention in these studies has been directed to the spectral features of what is basically a continuous, random waveform. There has been little success, however, in correlating particular features of the spectra with the combustion process. The issue is further clouded by uncertainties in the frequency response of the piezoelectric transducers employed for detecting the ultrasonic emissions. Not only may the piezoelectric elements themselves be contributing substantial and unknown response peaks to the spectra, but also, it is possible that the emissions may have characteristic frequencies well above the transducer limits. The problem is presently unresolved since neither

a flat response transducer nor a satisfactory calibration procedure has yet been devised.

The objectives of the current program are to a) determine the magnitude and spectra of the audible signal and to b) obtain ultrasonic measurement with a cleaner transmission path than has been used before. The results are still exploratory and further work will eliminate many of the uncertainties which will be shown to exist.

Facilities and Instrumentation

The acoustic tube designed and built for these experiments is shown in Fig. 1. It is a 5 foot long by 5 inch diameter tube capable of a safe working pressure of 1000 psia. Nitrogen or air is used as the pressurization gas and the tube is capable of initial air evacuation. At one end of the tube fiberglass insulation is used to absorb part of the incident acoustic waves. Initial measurements of audible signals were made by a B & K Model 4134, $\frac{1}{2}$ inch condensor microphone, shown in Fig. 1, which is also pressurized. As shown in Fig. 1, the solid propellant sample is epoxyed to an aluminum sample holder which is bolted to the steel endplate. Directly behind this endplate the ultrasonic transducer, a Dunegan-Endevco Model D 9201 flat response transducer, is held in place by an elastic cord and a coupling grease.

Tape recording of the signals is made in the FM mode for the audible signal and in the AM mode for the ultrasonic signal at a recording tape speed of 60 inches per second. The upper limit of response for the tape recorder is 300 kHz. Later signal processing is made by digital Fourier analysis. During a run the cumulative number of excursions of the ultrasonic signal above a preset level is monitored on an X-Y recorder and the overall sound pressure level of the audible signal is monitored on a microphone amplifier. The details of the data acquisition and analysis configurations are shown in Fig. 2.

The tube dimensions are chosen to satisfy three criteria. These are: (a) the volume of the tube should be sufficient that the mean pressure level does not increase by more than 10% during a run for a propellant strand of dimensions 3" x $\frac{1}{4}$", (b) the tube should be long enough that plane wave propa-

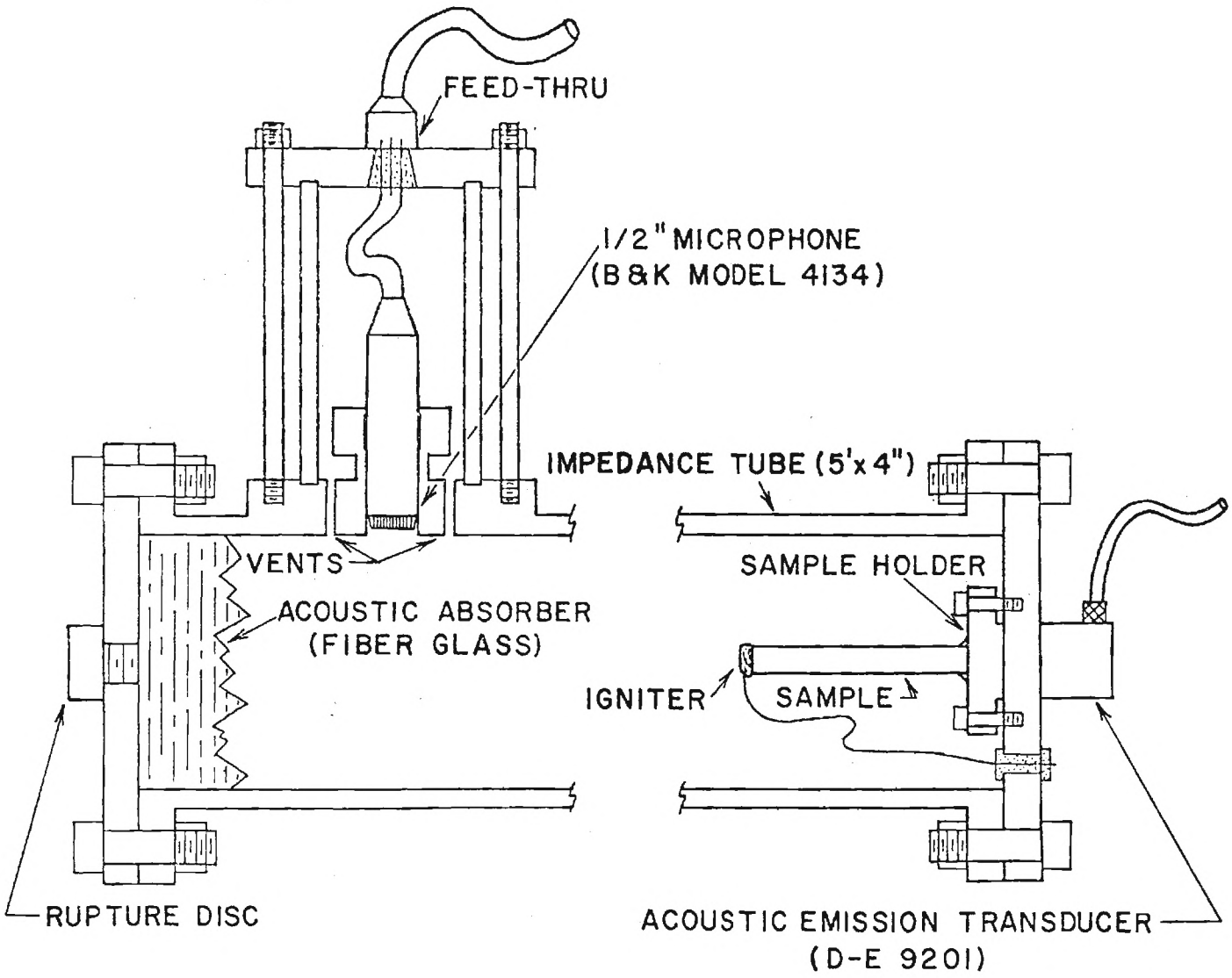

FIGURE 1. SCHEMATIC OF THE SAMPLE HOLDER, AUDIBLE TRANSDUCER AND ULTRASONIC TRANSDUCER INSTALLED IN THE TUBE

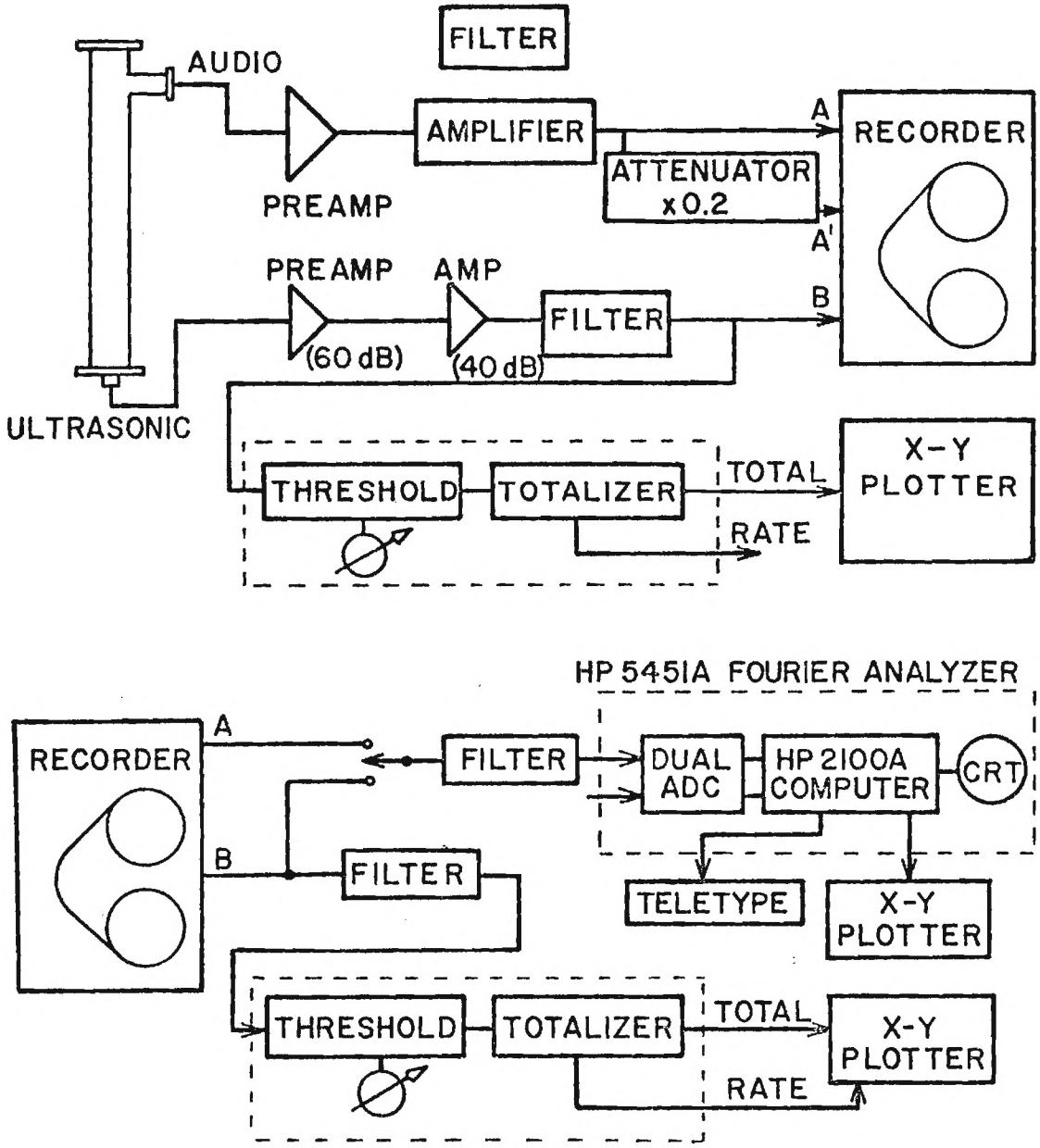

FIGURE 2. DATA ACQUISITION AND ANALYSIS SCHEMATIC

gation is taking place at the microphone end of the tube for frequencies below the first transverse mode of the tube and (c) the first transverse mode should have a frequency higher than that expected for the peak of the sound power spectrum emitted from the propellant. The above criteria are satisfied in the given design with the exception that criterion (a) is only satisfied above 300 psia. A photograph of the facility is shown in Fig. 3.

The design for the ultrasonic emissions is chosen to minimize uncertainties concerning the transmission path of the ultrasonic signal. Here it is directly through the propellant to the bonding plate and through the end plate to the transducer.

Later in the test program it was decided to use air as the pressurization fluid as opposed to nitrogen to obtain afterburning of the aluminum. One B & K transducer was destroyed in the nitrogen tests, and a B & K Type 4149 quartz coated transducer was tried during the afterburning tests. This transducer was also destroyed before a good burn could be obtained. It was decided to use a cheap Quasar $3\frac{1}{2}$ inch speaker as the microphone, placed at the B & K position and with a metal face plate to protect it from the burning aluminum impact. The speaker used as a microphone was calibrated against the B & K under pressurization by recording their respective outputs from a noise generator input from another speaker placed at the propellant end of the tube.

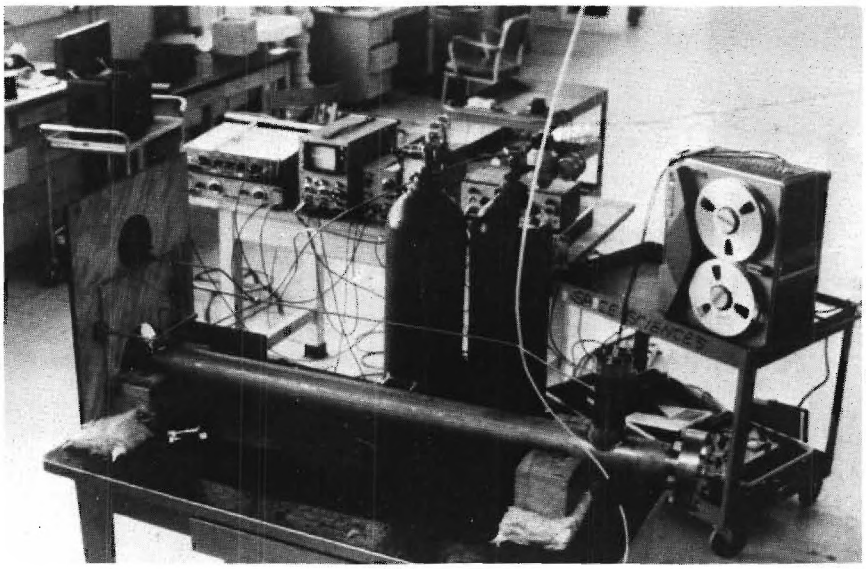

Figure 3. Test Facility Showing Instrumentation and Recording Equipment in Position for a Test

Results

Burn Rate

The propellants were supplied by the Air Force Rocket Propulsion Laboratory and are shown in Table 1. Although no direct observation of burn rate was possible the rate may quite accurately be inferred from the rather precise onset and termination of the audible and ultrasonic signals. These burn rates, for successful tests, are shown in Table 1 at the single pressure of 300 psia. Although all propellants were tested at least once, tests were rejected if the burn rate was not comparable to that measured on the same propellant by the Princeton group.[2]

As may be seen from Table 1, the propellants are basically hydroxyl terminated polybutadiene - ammonium perchlorate (AP) - aluminum (AL) propellants with some additives. Parameter variations are systematically made in AP particulate size, aluminum coating (AFCAM), and catalyst.

In the test sequence reported here one microphone was damaged after obtaining nitrogen pressurized data on four propellant samples including three propellant types. Bad burns were encountered on some of the other tests, and, coupled with a tape recorder malfunction on two other tests, this accounted for the lack of complete ultrasonic data. Severe difficulty was encountered in obtaining a good burn in air; at least seven samples of MC170 and 178 burned to completion in less than a second. Various coatings were tried to protect the propellant from recirculating, burning aluminum. Finally, a thick ($\approx \frac{1}{4}$ in) coat of Dow Corning 140 RTV adhesive was used to protect the propellant and a good burn was obtained. This difficulty, coupled with the microphone problem mentioned above, allowed only one test (MC 179) to be obtained for burning in air at 300 psi. The burn rate obtained was consistent with that obtained in nitrogen.

Table 1. PROPELLANTS FOR ACOUSTIC TESTING, AND BURN RATES AT 300 PSIA

Specimen	R-45M	AP		AL	Dioctyl dipate	Indopol	IPDI	Catalysts	Acoustic data	Burn rate (in/sec)
		Size	%							
MC-170	9.31%	200μ 14μ 6μ	26.8 20.4 20.8	20% 5μ		2.0%	0.69%		Good audible Bad ultra-sonic	0.31 ±0.3
MC-172	9.31%	200μ 14μ 6μ	26.8 20.4 20.8	20% 5μ AFCAM		2.0%	0.69%		Good audible Good ultra-sonic	0.37 ±0.01
MC-173	9.31%	200μ 14μ 6μ	26.8 20.4 18.8	20% 5μ	2%		0.69%	Fe_2O_3 2%	No audible Bad ultra-sonic	0.52
MC-179	9.31%	200μ 14μ 6μ	26.8 20.4 18.8	20% 5μ	2%		0.69%	Copper fluoride 2%	Bad	Bad burn
MC-174	10.24%	6μ 0.5μ	26 40	20% 5μ		3.0%	0.76%		No audible *	0.57
MC-175	10.24%	6μ 0.5μ	26 40	20% 5μ AFCAM		3.0%	0.76%		No audible *	0.81
MC-177	9.31%	400μ 200μ 50μ	44 18 6	20% 5μ		2.0%	0.69%		Good audible Good ultra-sonic	0.21 ±0.02
MC-178	9.31%	400μ 200μ 50μ	44 18 6	20% 5μ AFCAM		2.0%	0.69%		Burned in air Fair audible Good ultra-sonic	0.21 ±0.03

* Ultrasonic data with uncertain level calibration

Audible Acoustic Emissions

Theory

The overall measured sound pressure level and the spectrum, of course, depend upon the acoustic properties of the tube. Resonances will appear at the natural mode frequencies of the tube, and, since the only absorbant material is located at the microphone end of the tube, this is the only acoustic surface which can control the strength of the tube resonant response. The data would be useless in an engineering sense if the data could only be interpreted as unique to this configuration. What are actually desired are the sound power and spectra characteristics of the propellant in the absence of reflecting surfaces, i.e., the characteristics that would be obtained if the propellant were burning in a pressurized anechoic chamber. If this information can be extracted then theoretical acoustics may be employed to determine the acoustical behavior of any rocket chamber the propellant might be placed into. Stated another way, the question is asked, what must the propellant source characteristics be in order to produce the observed sound pressure and spectra in the given apparatus?

If the noise radiator (the propellant) is unaffected by a feedback mechanism through wall-reflected pressure waves, it is sufficient to determine the free field radiation characteristics of the source in order to determine the behavior when enclosed. Solid propellants are known to only exhibit strong feedback effects when the radiating area (propellant surface area) is comparable to the nozzle exhaust area.[4] In the current experiments the propellant area is much smaller than the tube cross-sectional area, which is the same as the fiberglass cross-sectional area. Since it is determined later

that the fiberglass has sound attenuation characteristics at least as good as those of a rocket nozzle, the feedback effect is negligible for these tests.

The theory for this configuration follows closely the theory of Ref. (5). Neglecting flow effects since the Mach number is small, the governing equation for the noise generation and propagation processes may be approximated by an inhomogeneous Helmholtz equation(6)

$$\nabla^2 p_\omega + k^2 p_\omega = h_\omega \tag{1}$$

Averaging Eq. (1) over the chamber cross-section, and assuming the side walls are hard, the equivalent plane wave equation is obtained as

$$\frac{d^2 p_\omega}{dx^2} + k^2 p_\omega = \frac{1}{S}\int_S h_\omega dS \equiv \bar{h}_\omega \tag{2}$$

where p_ω is now a cross-section average of the pressure transform. Assuming the end plane at $x=\ell$ is far enough away from the combustion region that nearly plane waves are impinging on it and that the plane may be characterized by a specific acoustic impedance ζ_ℓ, the solution for $p_\omega(\ell)$ may be written

$$p_\omega(\ell)\ p_\omega^*(\ell) = \frac{\zeta_\ell^2\left[\left(\int_o^\ell \bar{h}_{\omega_r} \cos kx dx\right)^2 + \left(\int_o^\ell \bar{h}_{\omega_i} \cos kx dx\right)^2\right]}{k^2\left[\cos^2 k\ell + \zeta_\ell^2 \sin^2 k\ell + 2\zeta_{\ell_i} \sin k\ell \cos k\ell\right]} \tag{3}$$

where it has been assumed that velocity oscillations at x=0 are zero.

If the combustion zone is short enough that h_ω falls to zero in a fraction of a wavelength, $\cos kx \approx 1$ in the integrands of Eq. (3). Then Eq. (3) becomes

$$p_\omega p_\omega^* = \frac{\zeta_\ell^2}{S^2 k^2} \frac{I I^*}{\left[\cos^2 k\ell + \zeta_\ell^2 \sin^2 k\ell + 2\zeta_{\ell_i} \sin k\ell \cos k\ell\right]} \tag{4}$$

$$I = \int_V h_\omega \, dV$$

and I is the total combustion source strength transform. The assumption of a short combustion zone is probably only true when burning in nitrogen, beacuse of extended aluminum reaction. However, the cosine factors can, at most, alter the results by a factor of two, which is not of concern here. Consequently, Eq. (4) will be used in the following theory.

From Ref. (6) for a flame burning in a free field

$$p_\omega p_\omega^* = \frac{I I^*}{(4\pi r)^2} \tag{5}$$

so that measurement of $I I^*$ by measuring $p_\omega p_\omega^*$ in the tube [Eq. (4)] directly gives information on the free field source behavior through Eq. (5). Measurement of $I I^*$ from the tube data, in which $S_\omega = p_\omega p_\omega^* 2\pi/t_o$ is directly measured, is greatly aided by observation of the large ζ_ℓ limit for Eq. (4). Near a spectral trough ($\sin k\ell = 1$) for $\zeta_\ell \to \infty$,

$$p_\omega\, p_\omega^{*}\ (\min) = \frac{I\, I^{*}}{S^2 k^2} \tag{6}$$

while near a peak ($\sin k\ell = 0$)

$$p_\omega\, p_\omega^{*}\ (\max) = \frac{\zeta_\ell^{\,2}\, I\, I^{*}}{S^2 k^2} \tag{7}$$

Consequently, if the peak to trough height is large, ζ_ℓ is large and may be directly measured by the peak to trough height from Eqs. (6) and (7), if the peaks are narrowly spaced in frequency so that $I\, I^{*}$ and k do not vary appreciably between the peak and the trough. More importantly, if these conditions are satisfied, the measurement of the trough envelope is analytically described by Eq. (6) which is independent of ζ_ℓ. The coefficient of $I\, I^{*}$ in Eq. (4) is plotted as the "not filtered"curve in Fig. 4, which is used for graphical construction of $I\, I^{*}$ later. Also shown is a "filtered" curve which will be described later. The assumption of large ζ_ℓ has been met in the experiments.

There are two items which are sought. There are (a) the shape of the $I\, I^{*}$ curve to give deflagration behavior diagnostic information and (b) the magnitude of $I\, I^{*}$, or, equivalently the acoustic power generation capability of the propellant. As put forth in Ref. (3) there is the possibility that the noise generation capability of the propellant may be strong enough to account for pressure roughness levels commonly seen in rocket motors. Assuming that the rocket nozzle is the only source of damping of acoustic waves and that the rocket nozzle is short compared with a wavelength, the following formula for

the mean square pressure at the nozzle entrance may be readily worked out:

$$\frac{\langle p'^2 \rangle}{\bar{p}^2} = \frac{2\gamma^2}{\gamma-1}\frac{\eta}{\bar{c}^2} \tag{8}$$

For $\langle p'^2 \rangle/\bar{p}^2$ to correspond to 10^{-4} (a 1% chamber pressure roughness level), and $\gamma = 1.2$ and $\bar{c} = 10^5$ cm/sec, $\eta = 7 \times 10^4$ $(\text{cm/sec})^2 = 7$ m^2/sec^2. This is an "installed" number; that is, it is the necessary power generation capability of the propellant when installed in the motor chamber and, consequently, depends upon the acoustic properties of the chamber. As will be seen, since a rocket chamber has resonant modes, the above number is an upper limit on the value of the equivalent free flame η required to be of importance to the roughness problem. Once $I\,I^*$ is deduced from Eq. (4) the equivalent open flame acoustic power may be derived from Eq. (5) and the knowledge that $P = \frac{\langle p'^2 \rangle 4\pi r^2}{\bar{\rho}\bar{c}}$ for a monopole source

$$P = 4\pi r^2 \int_{-\infty}^{\infty} \frac{2\pi\, p_\omega p_\omega^*}{t_o\, \bar{\rho}\bar{c}} = \frac{1}{4\pi} \int_{-\infty}^{\infty} \frac{2\pi}{t_o} I\, I^*\, d\omega \tag{9}$$

Finally, $\dot{m}$ may be completed from the measured burn rate and used to determine η.

Combustion noise is basically produced by a velocity source in other flame types[7] and there is no reason to suspect this is not the case here. Velocity roughness downstream of the flame may easily be caused by the heterogeneous character of the propellant. Following the developments of Ref. (7) the equivalent open flame acoustic power may be expected to scale like

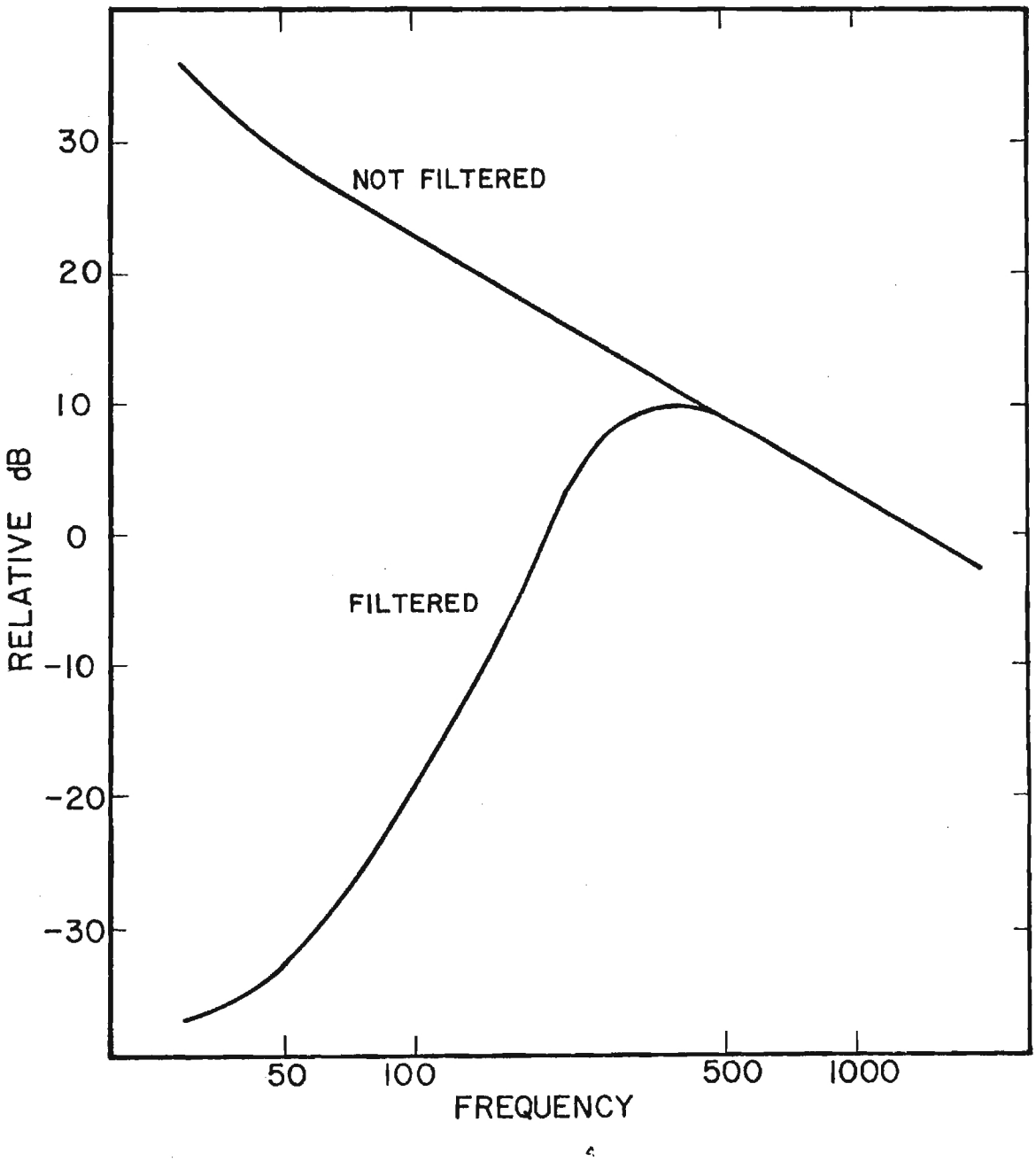

FIGURE 4. ENVELOPE OF TROUGHS IN PSD OF THE SOUND PRESSURE LEVEL TO BE EXPECTED IF THE COMBUSTION NOISE IS WHITE NOISE

$$P \propto \frac{\bar{\rho}}{c} A_p \left(\frac{\rho_s r}{\bar{\rho}} \right)^4 \tag{10}$$

A test of this relation can be made with the current propellants. That is, the power should scale directly with the propellant surface area and, for the same propellant energetics ($\bar{\rho}$), the higher the burn rate the higher should be the acoustic power. Again, following the lead of Ref. (7) the majority of the frequency content of the noise should be located near

$$f \propto (\rho_s r/\bar{\rho})/\ell_e \tag{11}$$

According to Eq. (11) if the mean granularity (particle size) is reduced, the frequency content of the noise should rise and if the burn rate is higher for fixed $\bar{\rho}$ the higher should be the frequency. In the current tests $\bar{\rho}$ has been held constant so the only variables which may be investigated are propellant burn rate, burn area and particle size.

Experiment

The spectra for $\frac{1}{4}$" square and 3/8" square strands of MC177 propellant are shown in Fig. 5 for the case of burning in nitrogen. The result for the $\frac{1}{4}$" strand is an unfiltered spectrum whereas the result for the 3/8" square strand has been obtained with a high pass filter inserted between the microphone and the recording apparatus. The filter, which has known characteristics, was used to improve the signal to noise ratio in the higher frequency portions of the trace. That is, it was used to attempt to make the spectrum more uniform with frequency. In these spectra, which were taken with fixed frequency bandwidth analysis ($\approx$ 8 Hz), a Hanning window has been used to improve the low frequency information. This was necessary because of the high

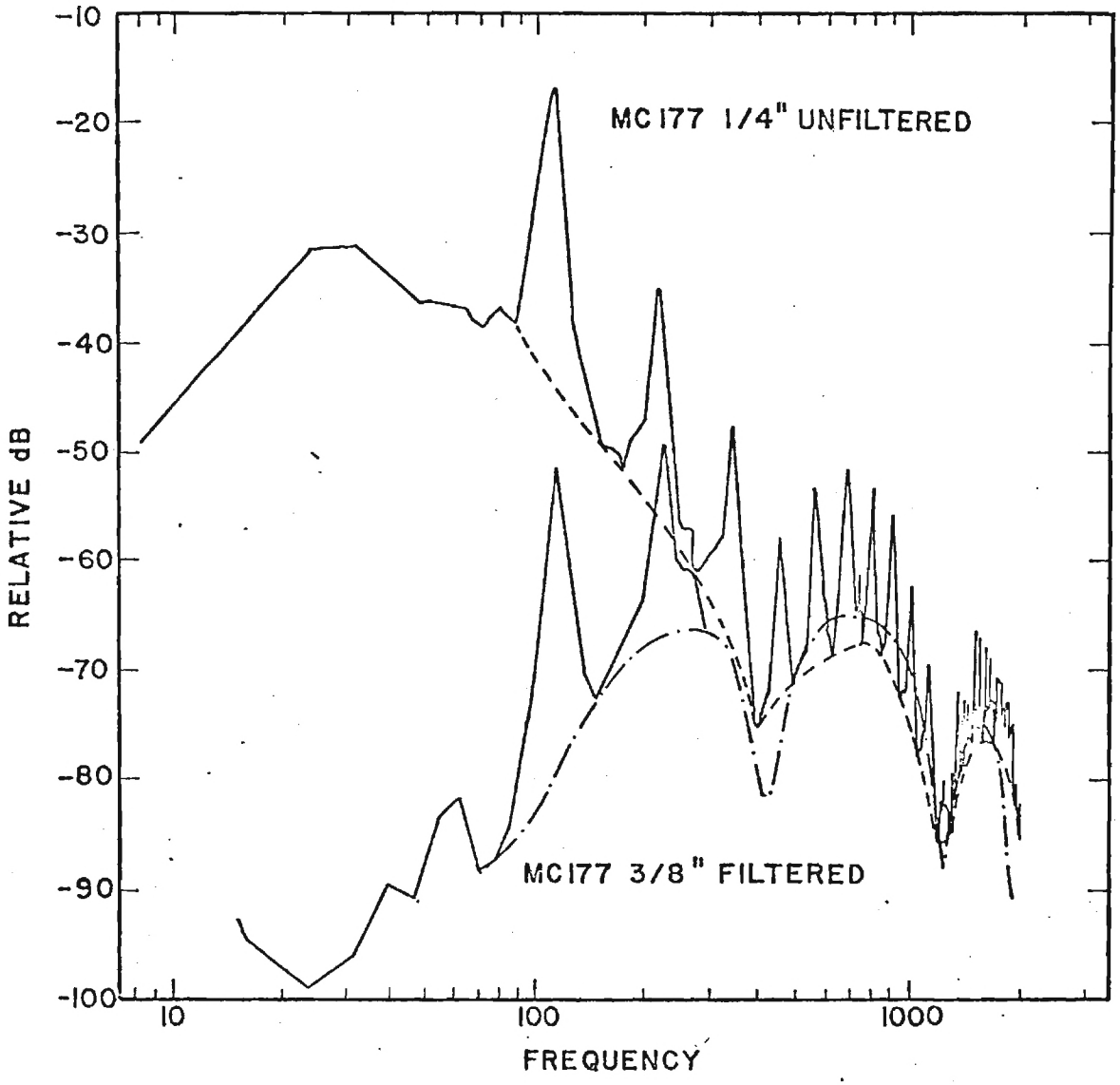

FIGURE 5. EXPERIMENTAL AUDIBLE SPECTRA FOR MC-177 PROPELLANT

peak to trough height ratio of the lower modes which tends to "leak" information into the lower frequency results. The high peaks here are due to rather poor absorbtion of the fiberglass at low frequencies and in future tests a better low frequency absorber should be sought. However, the high peak to trough height confirms the validity of the simplified data reduction procedure based upon a large ζ_ℓ assumption and use of the trough envelope.

Also shown in Fig. 5 is the envelope of the troughs which is used with Fig. 4 to deduce the pure source behavior. In Fig. 4 the "filtered" curve is merely the upper curve as constructed for the experimental filter characteristics. The deduced free field spectra for both the runs of Fig. 5 and for $\frac{1}{4}$" square strands of MC170 and 172 propellant are shown in Fig. 6. Above 80 Hz the similarity in the two MC177 curves is to be expected with the 3/8" square strand on average being above the $\frac{1}{4}$" square strand curve in accordance with Eq. (10). Below about 80 Hz the data are suspect because of the "leakage" problem in the Fourier analysis. Future tests will correct this problem.

Restricting the frequency range to 100-2000 Hz, integration of the two MC177 curves shows that the acoustic power of the 3/8" square strand is 2.2 times the power of the $\frac{1}{4}$" strand. According to Eq. (10) the power ratio should be $\left[(3/8)/(\frac{1}{4})\right]^2 = 2.25$; consequently, the scaling with respect to propellant area is confirmed.

Shown on Fig. 6 are the burn-through frequencies, using the MC170 burn rate for the various particle sizes of AP and Aℓ in these propellants. It is seen that the spectrum is rather densely occupied by available frequencies due to granularity. No apparant correlation of the observed spectra with these frequencies is evident; none was really expected to be clear because of the roughness of the estimate of frequency, the usual spread of particle size

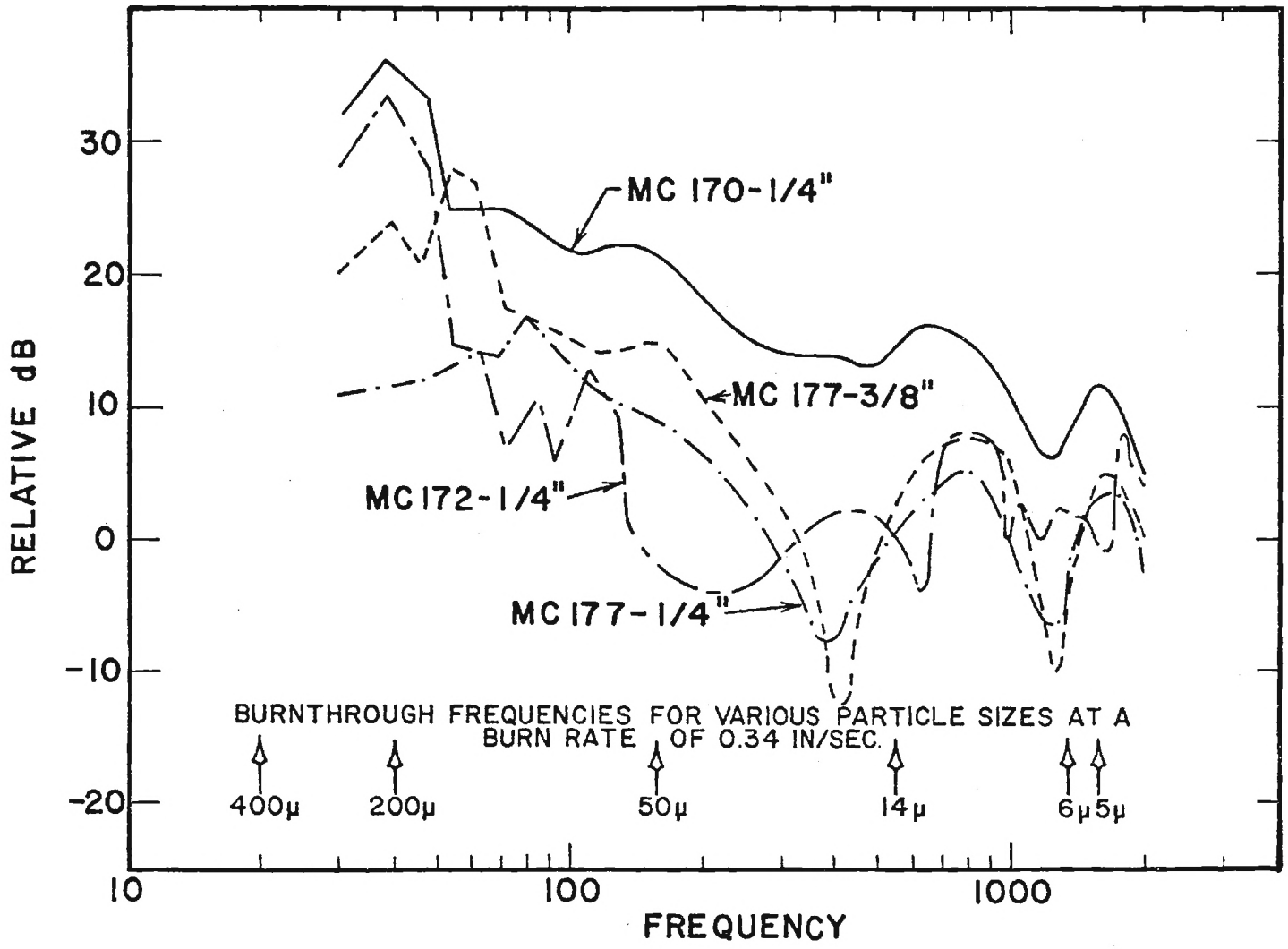

FIGURE 6. DEDUCED FREE - FIELD SPECTRA FOR SEVERAL PROPELLANTS

about the stated value and the dense population of the spectrum with these particle frequencies. Nevertheless, moving from MC177 to MC170 propellant, which decreases the mean particle size and increases the burn rate (see Table 1), there is a general rise in the spectrum and a filling of the spectrum in the mid-frequency range (perhaps due to the 14 μmAP). Integration of the spectrum shows that the acoustic power of the MC170 propellant is roughly 10 times that of the MC177 propellant. Referring to Eq. (10) and the burn rates of Table 1, the power indeed appears to scale as the fourth power of the burn rate, for fixed propellant energetics. It may be concluded that solid propellant noise generation proceeds by the same mechanism as with other flame types because of the confirmation of the A_p and r scaling of Eq. (5).

In moving to the MC172 propellant, however, interesting phenomena occur. The only change from MC170 is a coating on the aluminum and the overall sound level is depressed from the MC172 propellant by 10-20 dB. This strongly suggests that the aluminum behavior is the major determinant of the noise behavior and further tests to document this are necessary.

For the MC177 propellant, integration of the spectrum of Fig. 6 yields $\eta \approx 2$ $(cm/sec)^2$. Calculating ζ_ℓ from the peak heights in the spectra of Fig. 5 shows that in the vicinity of 200 Hz the fiberglass is behaving with a ζ of the same order of magnitude as a rocket nozzle. Consequently, in an installed configuration η could only be raised by a maximum of 20 dB or to a value of about 400 $(cm/sec)^2$. Even assuming the MC170 propellant the installed η could not be above 4000 $(cm/sec)^2$. This is still an order of magnitude too low to be considered significant from a chamber roughness standpoint. Consequently, it was suggested that burning in nitrogen suppresses the noise from aluminum burning and that tests in air should be tried to oxidize the aluminum, as

would occur in a real rocket motor.

Several difficulties appeared with the in-air testing, as has been mentioned before. Consequently only one good test was achieved. The data accuracy is not as good as with the previous tests because of poor speaker (microphone) response at low frequencies. Shown on Fig. 7 is the source spectral behavior. The major difference, as compared with the nitrogen cases, is the majority of the noise comes in the frequency range 150-700 Hz. The tube was quite hot along its length after the test and the pressure rise during a test was substantially greater than that which was obtained with nitrogen used as the pressurization fluid. Consequently, the difference in results is most probably due to aluminum afterburning.

The most important result, however, comes from the integration of Fig. 7 and construction of η. For this case $\eta = 3\ m^2/sec^2$. In fact, the sound pressure level in the tube was 145 dB re $2 \times 10^{-5}\ N/m^2$ as compared with 100 dB typically for the nitrogen-pressurized runs. Although the data accuracy was poor in the air-pressurized run, there is a strong indication that the aluminum burning may be responsible for severe roughness in a real rocket motor chamber pressure history.

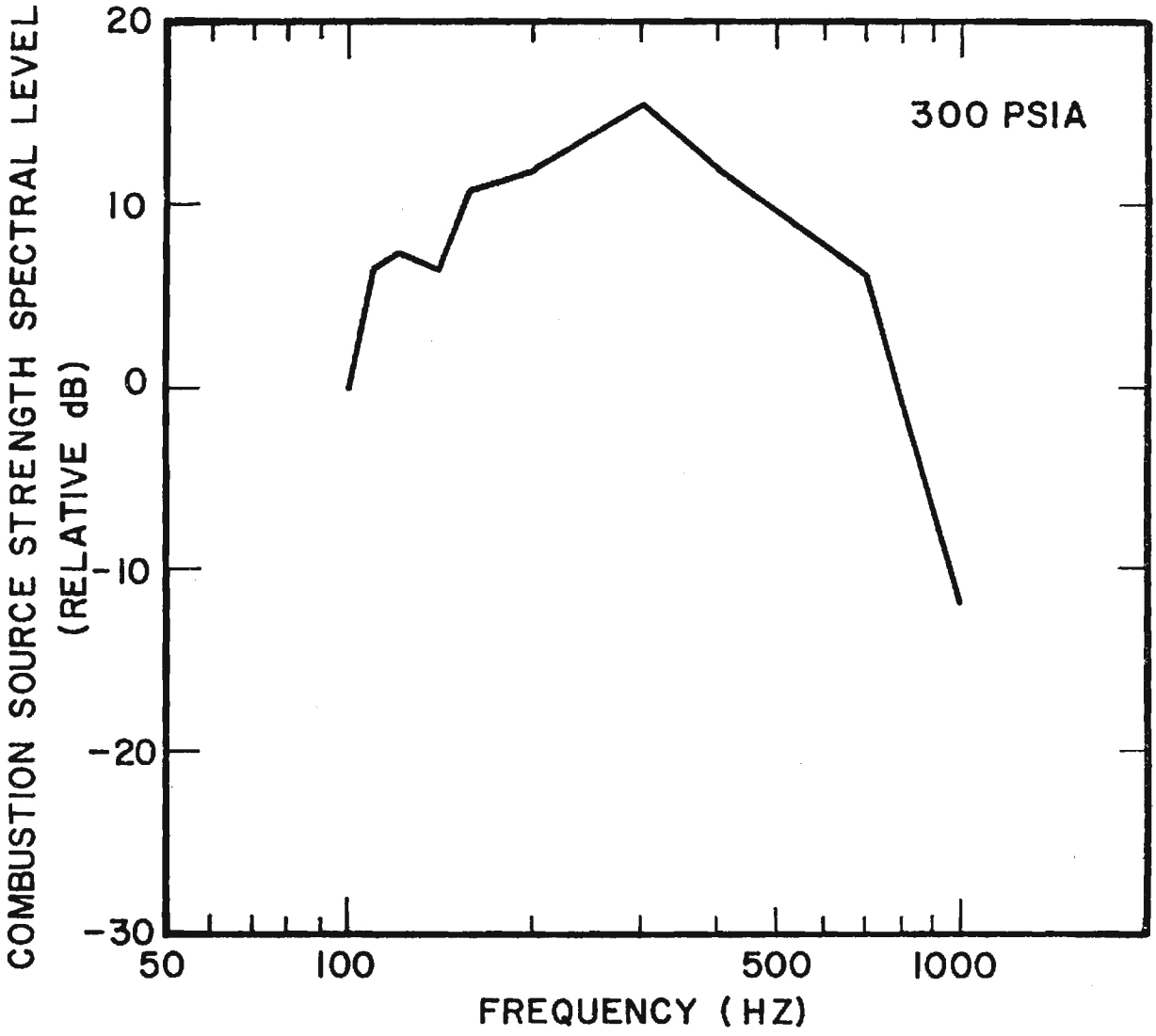

FIGURE 7. DEDUCED FREE FIELD SPECTRUM FOR A 1/4 INCH STRAND OF MC178 PROPELLANT BURNING IN AIR.

Ultrasonic Acoustic Emissions

Theory

Acoustic emissions can be broadly defined as stress wave emissions generated from within a solid material in response to some type of loading. The emission levels are generally well below those associated with audible disturbances and for many materials are on the order of microbars.

The temporal characteristics of the emissions may range from continuous to pulsatile although a burst type activity is commonly observed in materials studies. From the earliest investigations into the acoustic emission phenomenon to the present (for summaries see Refs. 8, 9, 10), attention has been directed primarily to the amplitude characteristics of signals that were basically impulsive in nature. The most popular technique has been to use a piezo electric ceramic disc encapsulated in an epoxy shoe. Each time an emission stress wave is received a proportional electrical charge is produced on faces of the ceramic. Unfortunately, most elements exhibit strong mechanical resonances in the range from 100 kHz to 1 MHz and consequently the electrical output commonly observed is a ringing type response at one of these natural frequencies. This performance is satisfactory for event detection where the frequency of occurence (and the location) of an event are of prime importance. The approach is also useful when an analysis of the emission energy per event is considered. On these grounds, acoustic emission analysis has been successfully employed for flaw location in pressure vessels and other structures, weld inspection, fatigue studies and fracture mechanics in metals and composite fiberous materials.

The spectral features of acoustic emissions are not as well understood and a general meaning of the spectrum has yet to be formulated in any present area of study. The situation is due principally to three reasons. First, the emissions originate in finite, bounded materials so that the features of the emission process are combined with the response characteristics of the medium itself.

The problem is identical to that posed in the audible acoustics portion of this report where the propellant acoustics are combined with the tube response. The solution, which involves accounting for the medium response, is vastly more complex due not only to the inability to precisely define the medium but also to its nonhomogeneity, (e.g., crystal structure) at frequencies of interest.

The second reason is the lack of a suitable acoustic emission transducer with adequate bandwidth and relatively uniform response. Transducers with high fidelity are readily available only for use below about 100 kHz. A number of transducers have been designed for use above this point, but invariably, they are beset with local response peaks of 15dB or more and have poorly defined phase characteristics. The only transducer reported to date with reasonably flat response[11] is useful from 8 MHz but even this range may be insufficient since emission energy has been observed at frequencies above 30 MHz in metals.

Finally, the third reason for concern is the attenuation presented by the medium to stress waves emanating from an emission site. The fact that emission energy has been found over a wide range of frequencies strongly suggests that the mechanisms responsible either are operating at many frequencies or else occur over a very short time interval and are basically impulsive events. A short duration pulse propagating in a solid material will change its shape because of a combination of frequency dependent attenuation and reflection at interfaces where there are changes in material properties.

There are a number of points that can be drawn from these observations which apply to the study at hand. For transient type signals amplitude or energy per emission measurements can be accomplished using simple resonant piezoelectric transducers. So long as the resonant characteristics of the transducer remain unchanged, its total response considered over a reasonably broad band (compared to resonance spacings) can be directly related to emission energy. The application of amplitude analysis to a continuous acoustic emission signal is not so clear. The number of signal excursions above a threshold basically defines one point on the amplitude

"cumulative probability distribution function" curve for the signal.

Spectral analysis of either transient or continuous acoustic emissions is not a straightforward procedure. The immediate problem is in properly accounting for the resonant characteristics of the transducer since flat response designs are not presently available. The correction process itself is a relatively simple task: for example, when the PSD is available in digital form, this can be accomplished by a point-by-point division of the raw spectrum by the transducer calibration spectrum. The major obstacle to this approach is the lack of precision in the transducer calibration. There are essentially 3 techniques that may be used for calibration: (1) direct excitation by a piezoelectric element driven at a known power level, (2) excitation by an impulse of known strength, for example, that due to a spark discharge from a known energy source [12], and (3) broadband excitation by a random noise source such as friction noise[13]. Unfortunately, each method produces a markedly different spectrum for the same transducer. The overall power levels agree reasonably well but there is substantial difference in the "fine" spectral features.

Experiment

Ultrasonic acoustic emissions were recorded from $\frac{1}{4}$ inch square by 3 inch strands of each of the 8 propellant formulations in Table 1 at 300 psi in nitrogen. In addition one sample was burned in air at 300 psi. Single samples of each propellant were tested, and because of a combination of improper burning and signal level saturation in the instrumentation system, useful ultrasonic data was obtained from 6 of the 9. As shown in the "Acoustic Data" column of Table 1; however, these 6 tests cover the range of AP particle sizes from 400 μ to 0.5 μ for both coated and uncoated aluminum and with relatively constant proportions of indopol and IPDI. Consequently, while it is not possible at this time to make reproducibility checks, the data does cover the extreme formulations and test conditions expected to have the most pronounced effect on ultrasonic acoustic emissions.

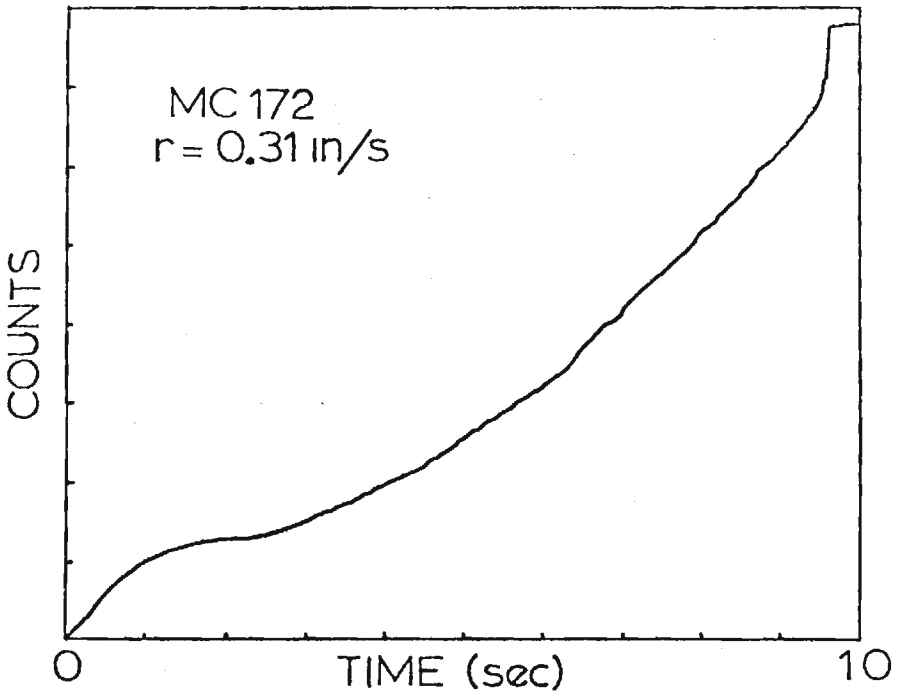

FIGURE 8. NUMBER OF SIGNAL EXCURSIONS ABOVE A PRESET THRESHOLD

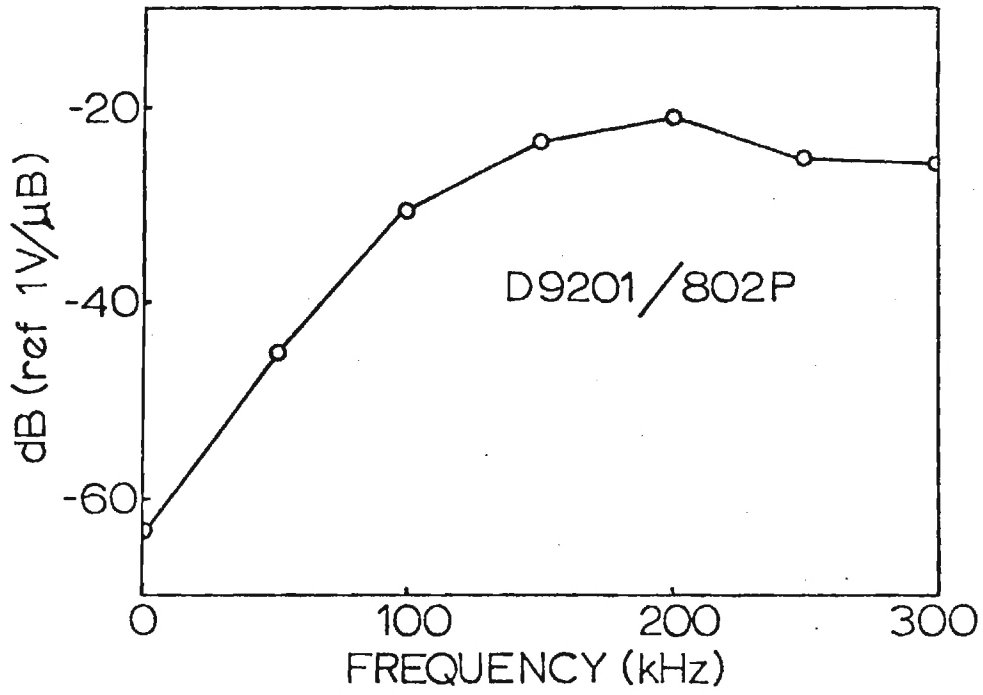

FIGURE 9. CALIBRATION CURVE FOR TRANSDUCER AND PREAMPLIFIER USED IN THE STUDY

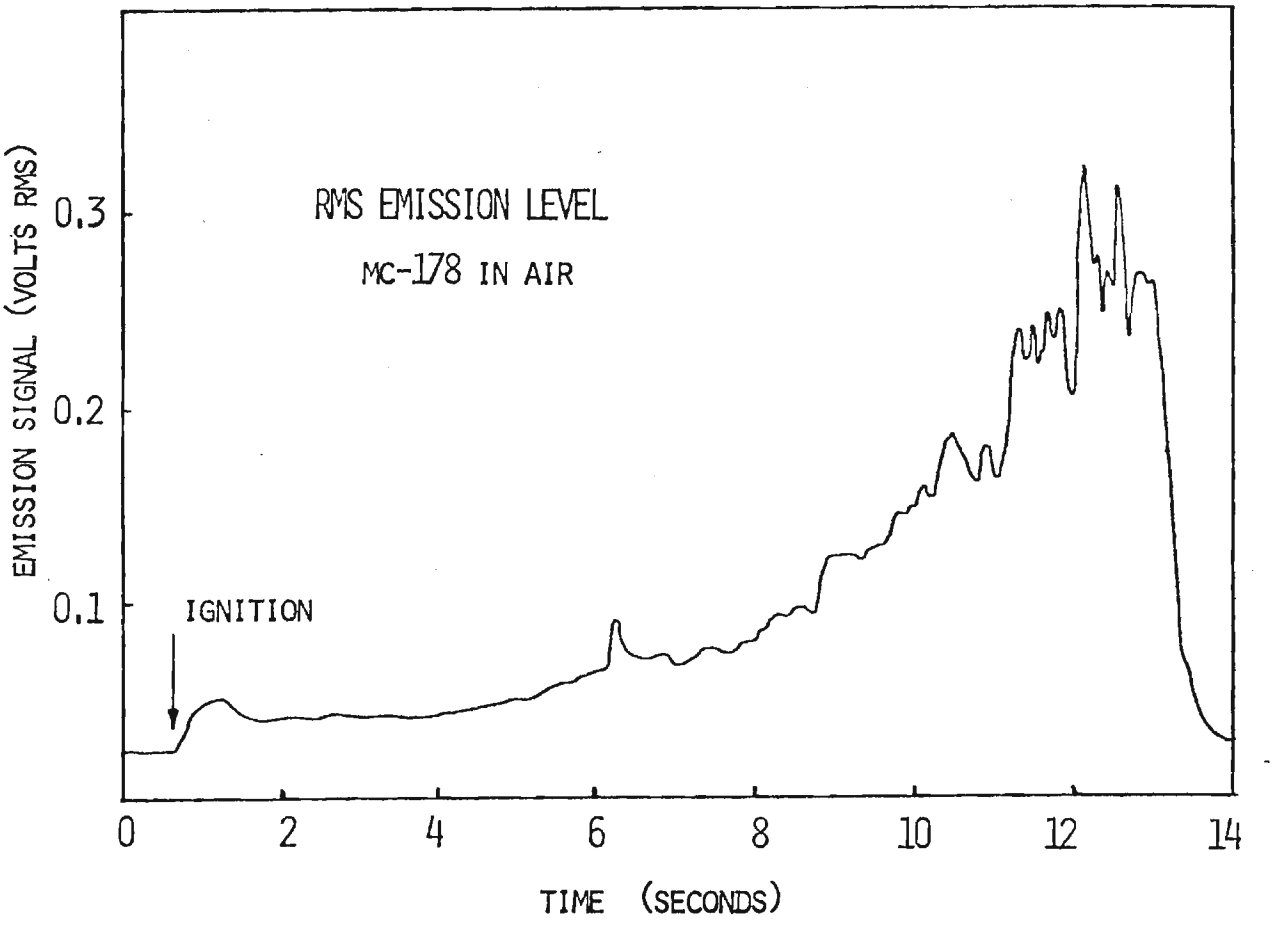

FIGURE 10. RMS SIGNAL LEVEL OVER 300 kHz BANDWIDTH

The instrumentation for these tests is shown in Figure 2. A piezo-electric transducer (Dunegan-Endevco D9201) was used for this work and was selected primarily for its relatively flat response over the 100 - 800 kHz range. The response curve for this particular transducer as obtained from a spark type calibration (done by the manufacturer) is shown in Figure 9. After amplification of 80 - 100 dB and bandpass filtering from 100 kHz to 400 kHz, the signal was recorded on an AM tape recorder at 60 ips. All analysis of the data was done by replaying the tapes at 15 or 1 7/8 ips.

Signal analysis was carried out in both the time and the frequency domain. A threshold crossing scheme was applied in the time domain to determine the number of signal excursions above several preset levels. This approach is similar to the usual acoustic emission analysis in materials testing where burst or transient emissions are encountered. For the present study, however, the technique appears to provide relatively little information because the propellant emissions appear to be basically continuous stress waves with broadband characteristics. Consequently, the cumulative number of excursions above a fixed level is most sensitive to the overall signal level. A typical plot, shown in Figure 8, illustrates the point. The principal features here are the appearance of an ignition transient at the beginning and a burn-out transient at the end of the test. The former is due to the igniter behavior while the latter is produced as the propellant burns through the epoxy mounting. In between, there often appear small changes in slope (rate) and momentary periods of low activity that are at present unexplained.

A typical plot of the (rms) signal level over the 300 kHz instrument bandwidth is shown for comparison in Figure 10. The ignition and burnout transients are clearly present along with several other perturbations during the burn. The most notable feature, however, is the generally monotonic increase in the level during the burn. At present several one dimensional wave propogation models are being examined in an attempt to adequately explain the behavior.

The presentation of the spectral data from these exploratory tests is arranged in four groupings:

(1) PSD computed over progressive time intervals during the deflagration of a single strand.

(2) Comparison of PSD from propellants with different sized particles of AP, other factors being held fixed (burned in nitrogen).

(3) PSD from a propellant burned in air.

(4) Comparison of PSD from a propellant with and without the AFCAM aluminum coating, burned in nitrogen.

The data is presented for several cases in both linear and log form to better accentuate the characteristics of the emission spectra.

PSD During Burn: From 200 to 900 sample records of 256 points each were taken in successive order from the tape recording of each burn. Figure 11A shows a sequence of raw PSD plots constructed from ensemble averages of successive subsets of these records; it shows, in effect, the PSD averaged over equi-spaced time intervals during the deflagration. The same data corrected as outlined previously is shown in Figure 11B where the vertical scale is in (dB) referenced to $(1\ \mu B)^2/Hz$. Note that no data is shown below about 100 kHz in these latter plots. This is a consequence of the high pass cut-off filter in the 802P preamplifier. The small peak near 90 kHz in the raw spectra is due to tape recorder FM interference and does not appear in the corrected plots.

The plots in Figure 11 have several other interesting features. First, it is apparent that the ignition and burn-out transients noted in the amplitude analysis have their counterpart in the frequency domain. Not only is the PSD of considerably lower level during ignition, but also it has a significantly different shape, tending more to lower frequencies. The PSD during burn-out, on the other hand, is much higher level (because at that point the transducer is closer to the emission source) and has a more uniform distribution. This is

Spectral analysis of the recorded emission signals was done using a minicomputer-based Fourier Analyzer that digitized the waveform and performed a direct FFT operation on successive sample records. The emission PSD was computed by self-complex conjugate multiplication of the linear spectrum and ensemble averaging over from 50 to 900 sample records. A double-Hanning window was used to minimize spectral leakage and enhance peaks in the PSD.

Ensemble averaging of random signal power spectra yields an estimate of the true PSD that, according to the Central Limit Theorem, follows the normal distribution for many ($\sim$ 100) averages. It can be shown that:

$$\frac{\sigma_{PSD}}{\mu_{PSD}} = \frac{1}{N}$$

where σ and μ refer to the standard deviation and mean for the PSD and N is the number of averages. With 95% confidence, the true mean will fall within $\pm$ 1.96 σ of the estimated mean for a Normal Distribution. Therefore, the 95% confidence limits for the PSD are given by

$$\alpha = \pm \frac{1.96}{\sqrt{N}}$$

That is, there is a 95% probability that the true PSD lies within these limits.

Two significant corrections were made to the raw PSD in an attempt to define as accurately as possible the true PSD. The first correction consisted of subtracting an ensemble-averaged PSD of the instrumentation background noise as recorded immediately before and after each test. The second correction consisted of using the D9201/802P transducer-preamplifier calibration curve to account for their frequency response effects on the PSD. The calibration curve of Figure 8 was digitized and the correction performed directly in the digital analyzer. The final result was a corrected, ensemble averaged, acoustic emission stress wave PSD in units of $(\text{microbar})^2/\text{Hz}$ as received at the D9201 transducer.

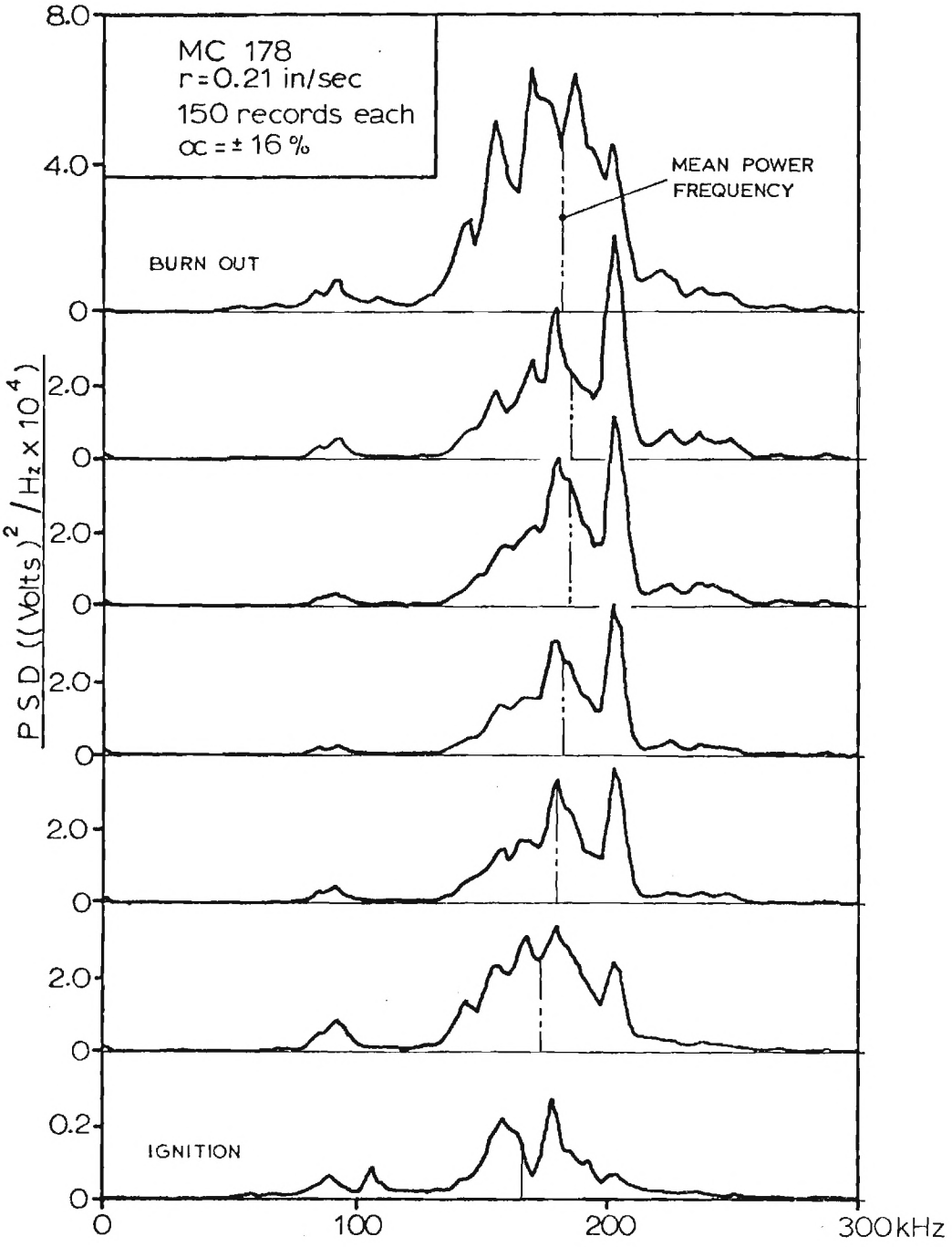

(11A LINEAR PLOTS)

FIGURE 11. EMISSION PSD AVERAGED OVER EQUALLY SPACED TIME INTERVALS FROM IGNITION TO BURN - OUT

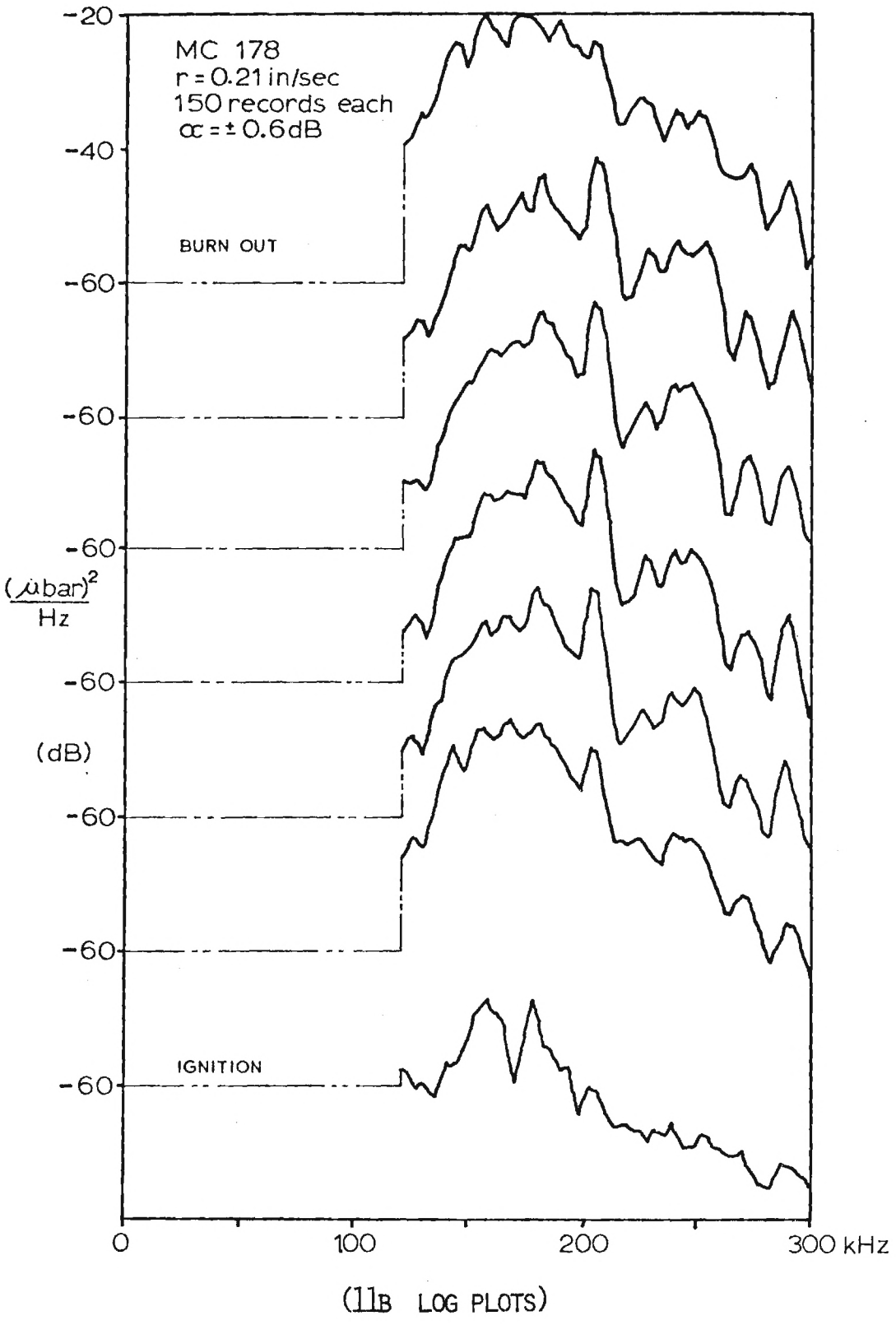

(11B LOG PLOTS)

FIGURE 11. (CONTINUED)

most likely due to some interaction of the epoxy mounting with the combustion process. In between, the PSD plots reflect a basically stationary process but do show the development of several strong spectral peaks, especially ones at 181 and 204 kHz. The interpretation of these peaks will be discussed in the next section. While it is not readily apparent from Figure 11, there is a consistent tendancy in the spectra to higher frequencies as the burn progresses. The vertical dashed line in each spectra locate the "mean power frequency" above (and below) which half the signal power occurs. This point was computed by inte - grating the linear raw spectra from 110 - 300 kHz and normalizing to yield a cumulative power distribution function whose 50% point defines the mean power frequency. The meaning of this shift is not clear at present, but a possible explanation may be that it reflects frequency dependent attenuation of the propellant at these frequencies. One would then expect the emission spectra to show a reduction in higher frequency content as the distance between the source and transducer increase. This behavior has been observed in most but not all of the tests to date. Further exploratory tests are required in this area.

Comparison of Propellants with Different AP Sizes: Useable emission recordings were obtained from 3 propellant samples, MC-178,-172, and -175, which differ only in the distribution and size of AP particles (except for MC-175 which has slightly larger quantities of binder). The predominant features in a comparison of PSD for these samples should be directly related to AP proportions and particle sizes. The plots in Figures 12A and 12B are, respectively, linear and log PSD curves that have been corrected for tape noise and transducer response. The 95% confidence limits are narrower (uncertainty is lower) for the coarser grained samples because their lower burn rates allowed more sample records to be analyzed. Again, as before, the PSD below about 110 kHz is not available because of heavy filtering in the instrumentation below 100 kHz. The plot for MC-178 does include, however, an estimate of the PSD below 110 kHz that is based on the stated roll-off of the

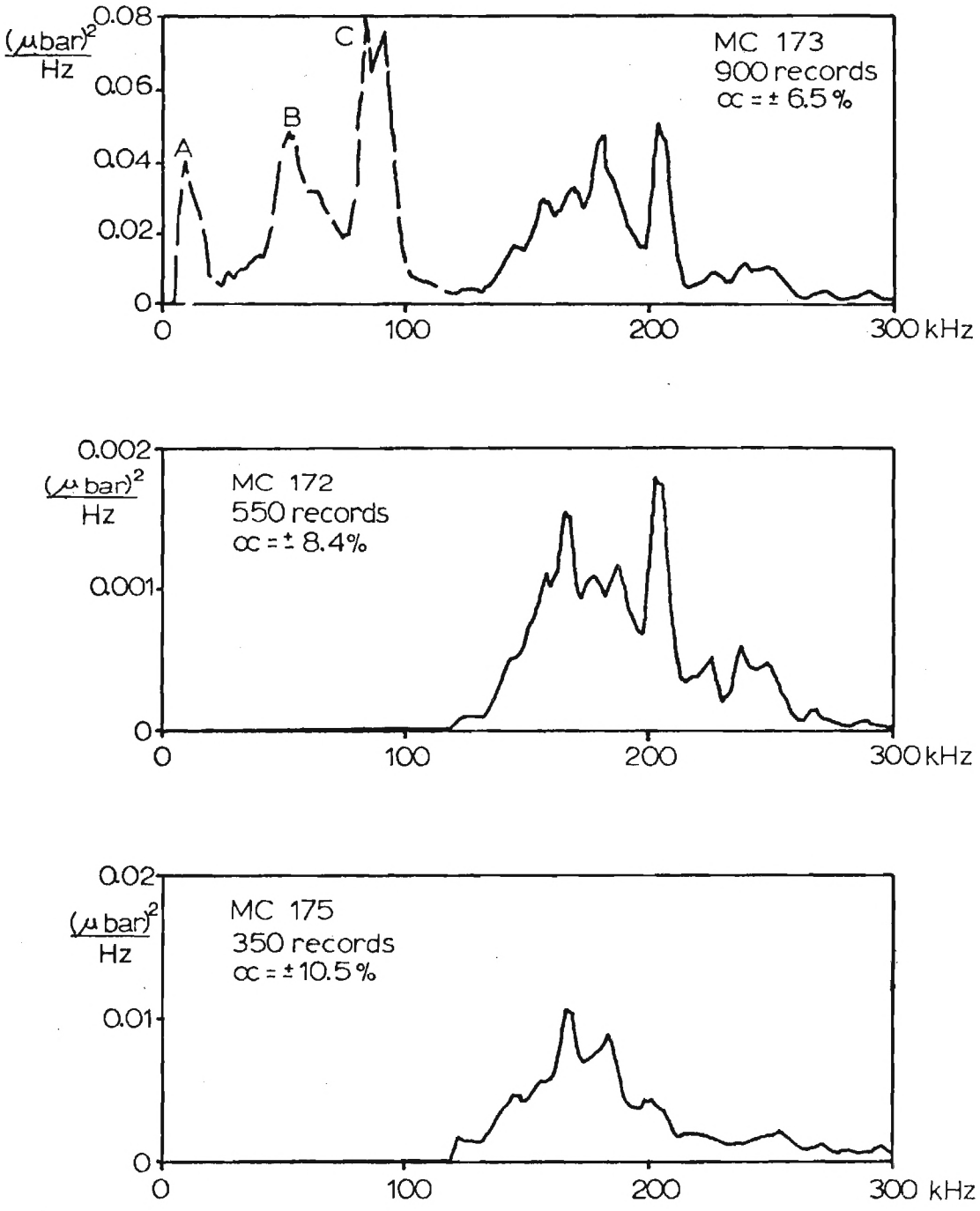

(12A LINEAR PLOTS)

FIGURE 12. COMPARISON OF PSD WITH DECREASING AP PARTICLE SIZE FROM TOP TO BOTTOM OF FIGURE

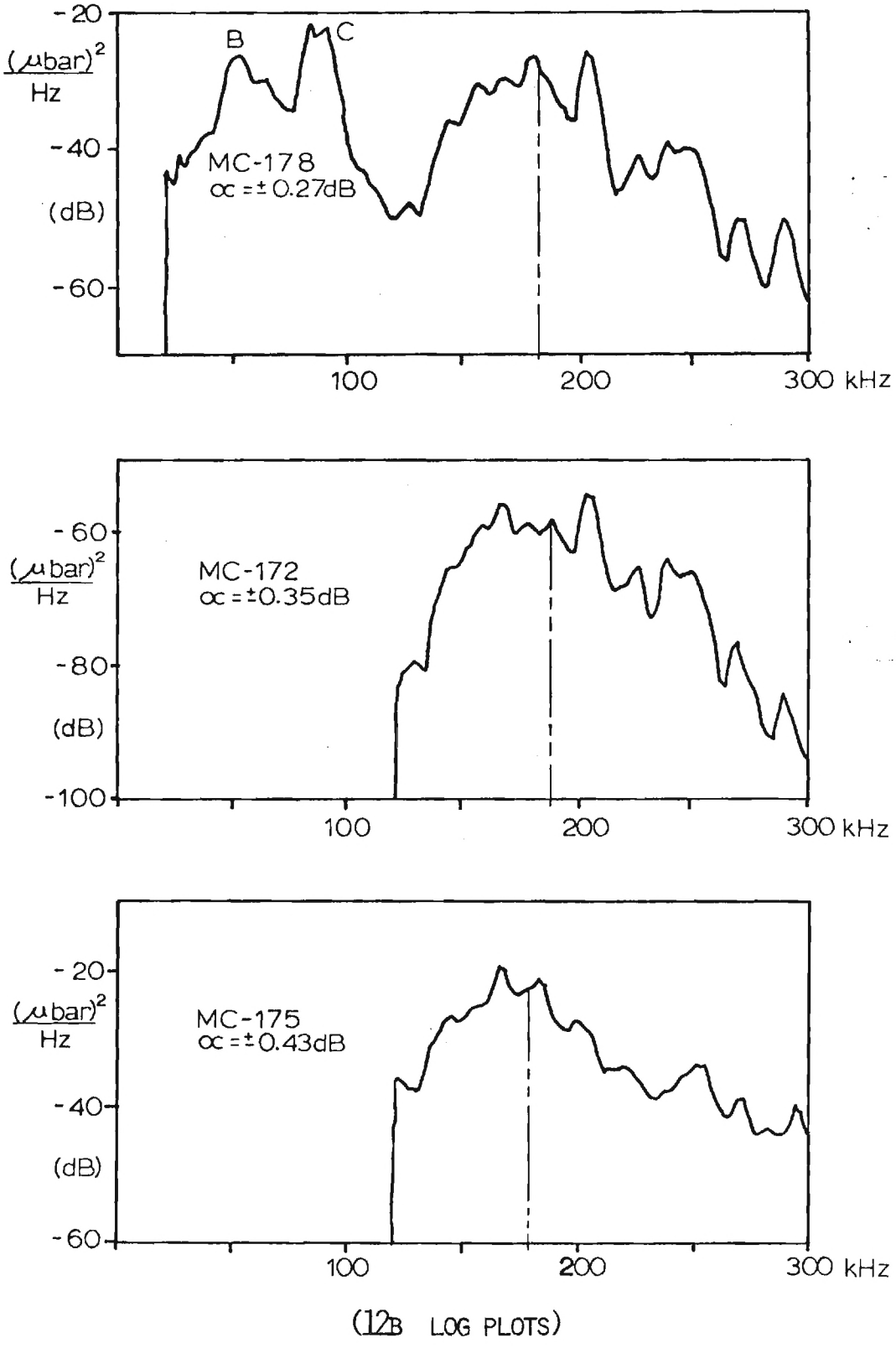

(12B LOG PLOTS)

FIGURE 12. (CONTINUED)

preamplifier filter and an assumed flat response of the D9201 transducer. Of the three peaks, A and C are due to interchannel crosstalk from FM electronics in the tape recorder, while the origin and meaning of B is unclear and may be due to propellant emissions. It should be noted, however, that the uncertainty in the PSD below 110 kHz is at least 10 - 20 dB greater because of the large response correction factor that has been applied.

A comparison of the PSD shapes indicates that those for the coarse and medium sized propellants (MC-178,172) are very similar and differ only in the relative location of several peaks. This is clearest in the log plots where it is also apparent that both log PSD's also decrease in a roughly linear fashion with frequency. A notable feature of these two PSD's is the presence of many peaks at common frequencies with the only difference being the relative strengths of each. Moving to the finer sized MC-175 propellant, it is apparent that a definite change occurs in the PSD with a marked tendancy to a more uniform distribution of power and a more gradual decrease in this power with increasing frequency. Again, there appear several peaks, most notably at 168 and 252 kHz, that are also present in the coarser propellants, but in contrast, the previously strong peak at 204 kHz is barely noticeable. A meaningful quantitative comparison of the spectra is not possible because of a malfunction in the tape recorder for the MC-175 test which resulted in an unknown attenuation of the signal. Data from all other tests was unaffected.

There does not at this time appear to be any simple correlation between the spectrum peaks and the AP composition. The issue requires further study, especially tests with samples having different areas. For example, if the peaks are caused by the rate at which individual particles in the propellant are consumed, then their frequencies should depend on the propellant area, burn rate, and the particle volumetric density.

Propellant Burning in Air: Considerable difficulty was encountered in performing a test in air and it was only possible to obtain data from a single MC-178 sample. The PSD computed over the entire record from ignition to burnout is shown in Figure 13 and the PSD for a similar specimen with nitrogen as the pressurization fluid is shown for comparison.

The most striking difference appears to be the stronger low frequency components in the PSD in air. In nitrogen the peak power occurs slightly below 200 kHz while in air it occurs at around 100 kHz. There is, however, some degree of similarity in the fine structure with both PSD exhibiting a local peak near 200 kHz. In fact the broad peak between 160 and 200 kHz in nitrogen may be present as a flattened region at similar frequencies for air. In both cases the power density seems to fall off uniformly with frequency.

Finally, there appears to be a significant difference in the spectral levels above about 130 kHz with the PSD in air being approximately 10dB lower than in nitrogen. The total power is, however, higher in air because of the strong contribution at around 100kHz. The PSD computed progressively over equispaced intervals is shown in Figure 14. Here it is apparent that while the general shape of the spectrum remains the same the overall level increases by roughly 25dB during the burn.

Comparison With and Without AFCAM: PSD plots for the coarse sized propellant with and without AFCAM coating on the aluminum are shown in Figure 15. There is a strong similarity in the shape of the spectra, and in fact, some of the smaller scale differences are due to the fact that the MC-177 recording was analyzed without the double-Hanning window. The major difference is the approximately 7 dB increase in the PSD for the AFCAM sample.

To conclude the presentation, several general observations can be made. First, it is not at all clear that the spectral response curve used for the D9201 transducer represents its actual as-mounted performance for these types of tests. Certain of the features observed in the PSD plots may actually be characteristic of

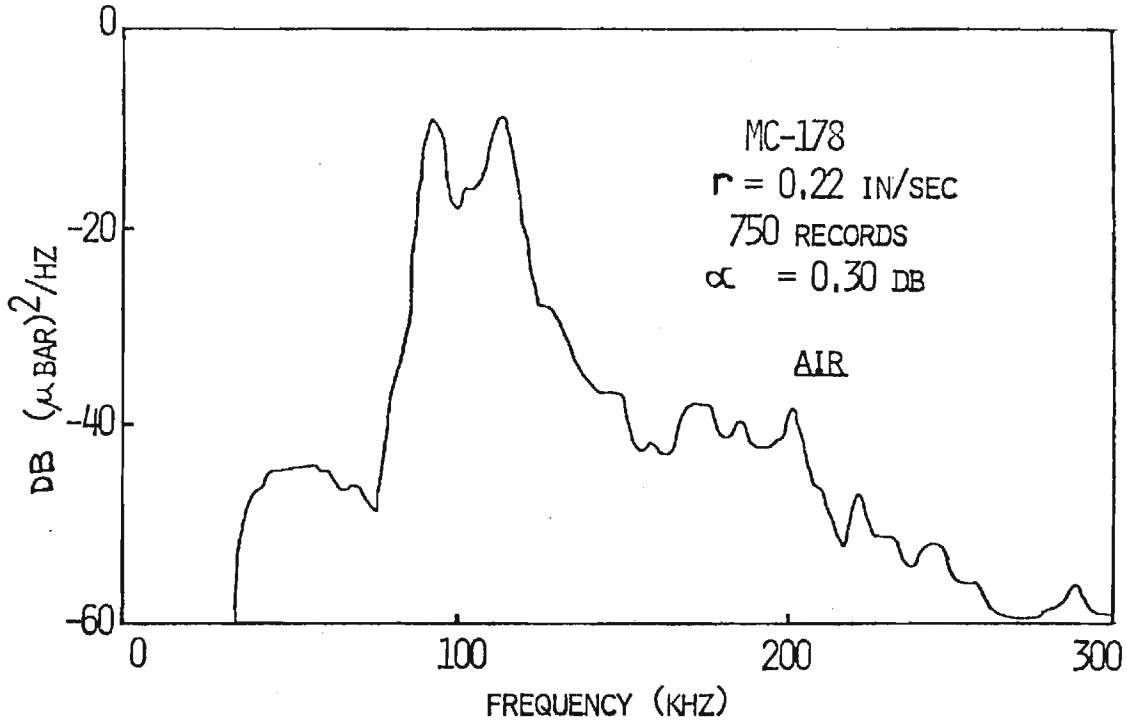

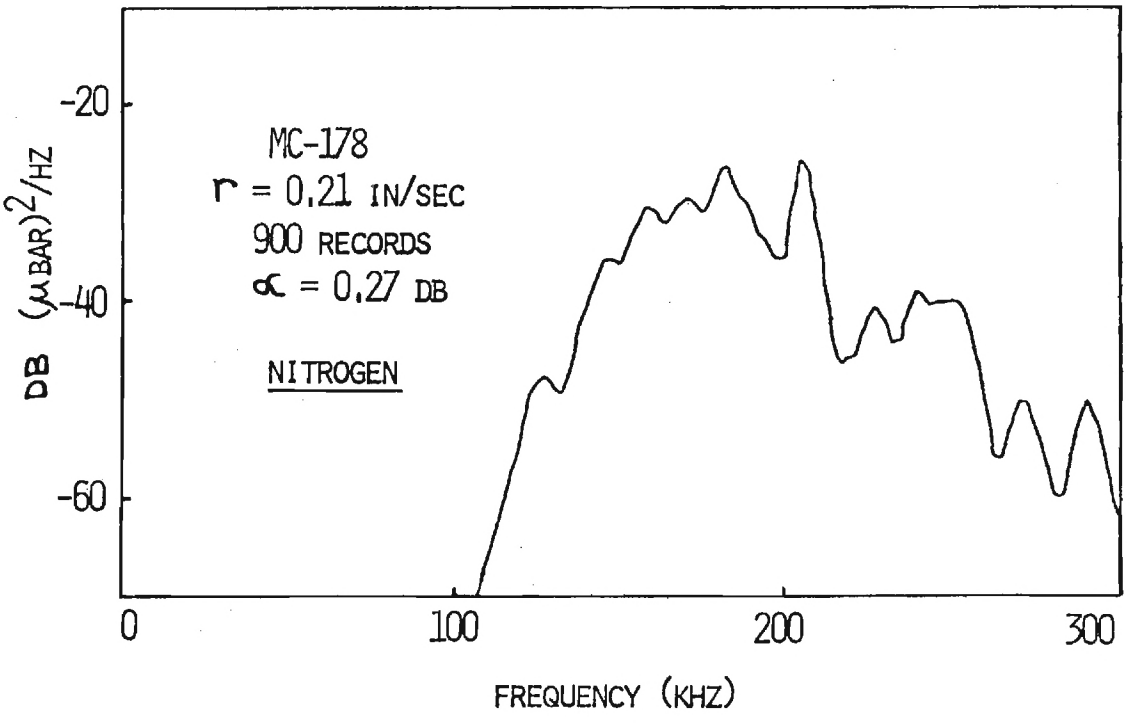

FIGURE 13. COMPARISON OF PSD IN AIR AND NITROGEN AT 300 PSIA

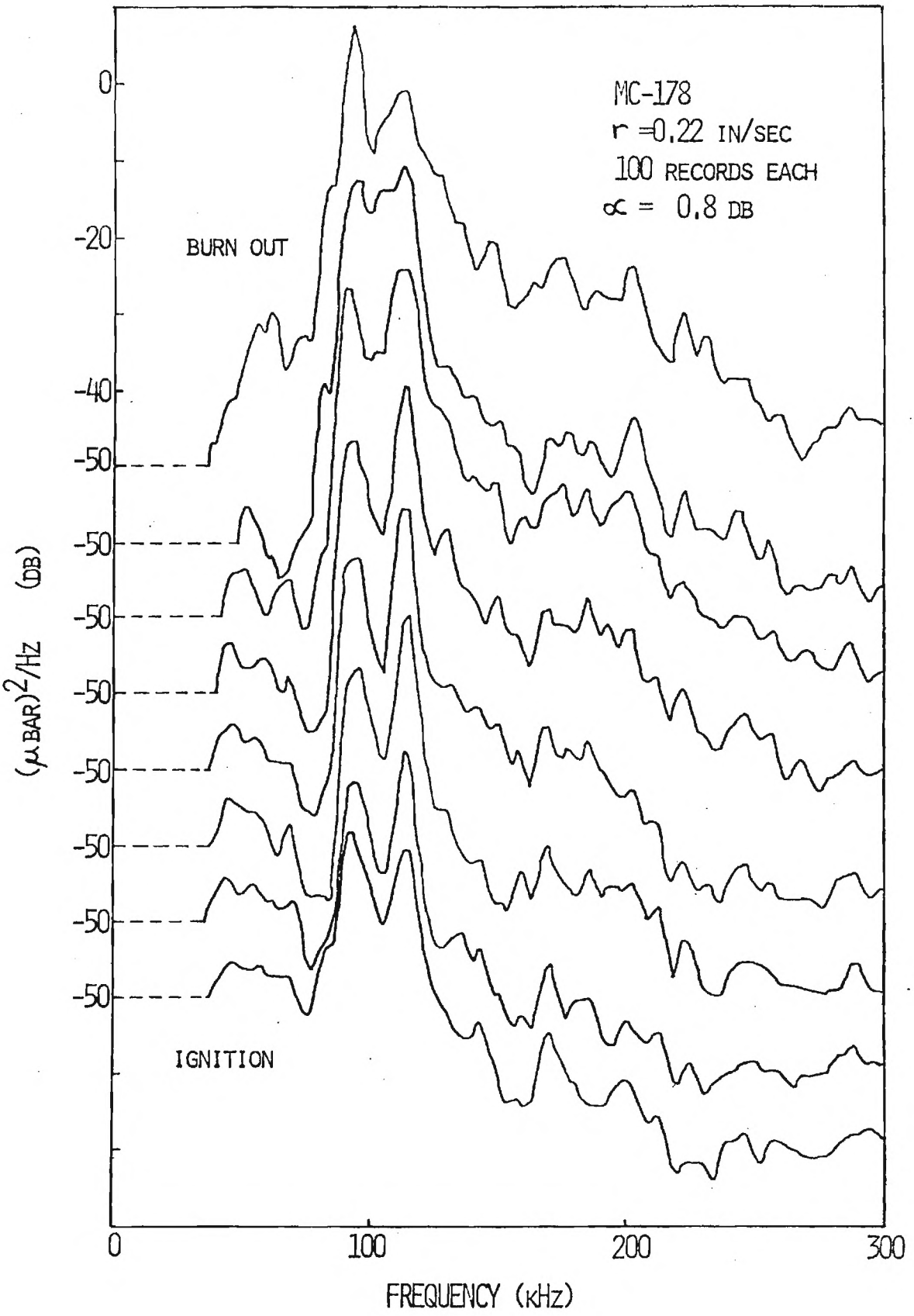

FIGURE 14. EMISSION PSD AVERAGED OVER EQUALLY SPACED TIME INTERVALS FROM IGNITION TO BURN-OUT FOR A SAMPLE BURNED IN AIR AT 300 PSIA

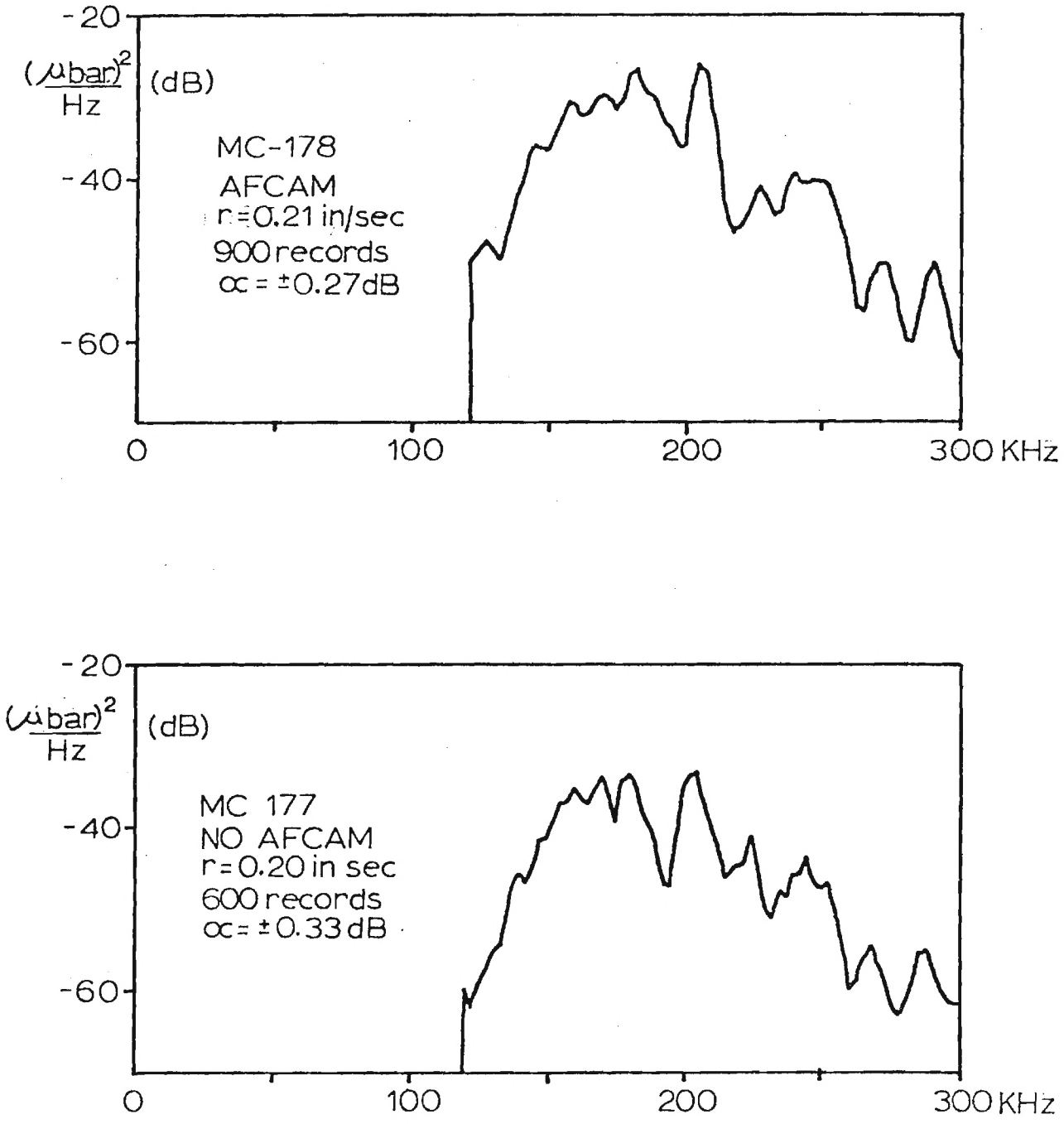

FIGURE 15. COMPARISON OF PSD FOR THE SAME PROPELLANT FORMULATION BOTH WITH AND WITHOUT AFCAM COATING

the transducer and its mounting details rather than the propellant deflagration. As noted previously there is no straightforward means for quantitatively determining the transducer response; however, the possibility of developing qualitative calibration techniques must be explored. A promising approach under development at the present time is a technique for electrically driving the piezoelectric transducer with a very low level signal and measuring its electrical impedance. Since the impedance is a function of both the electrical and mechanical loading it should be possible to indirectly estimate the mechanical (stress wave) response. In this approach, the mounted transducer would be calibrated before each series of tests and the impedance versus frequency data recorded on tape for later conversion to an as-mounted calibration.

In addition, the measurement bandwidth must be expanded beyond the original 100-300 kHz. In the most recent air pressurization tests, an improved tape recorder was used along with instrumentation modified to handle signals in the 40-100 kHz range as well. Extension of the bandwidth upwards to 1MHz will be explored in the continuing work.

Conclusions

1. There is a marked effect on audible emissions due to the pressurization fluid. For the propellants tested at 300 psia in nitrogen the pure combustion noise is insufficient to account for observed chamber pressure fluctuations. In air the noise output is 10^4 times higher with the definite possibility that this behavior is responsible for observed chamber pressure roughness levels.
2. There is a preliminary confirmation of theory and experiment in the audible noise output from solid propellants indicating that the mechanism of the noise is a velocity source caused by the heterogeniety of the propellant.

3. A striking effect of aluminum coating (AFCAM) is the general reduction in audible noise output in nitrogen. An opposite similar behavior was observed for the ultrasonic emissions.
4. Preliminary data appears to indicate, in contrast to the audible results, that use of air as a pressurization fluid does not substantially affect the overall level of ultrasonic emissions but does increase the lower frequency components. Aluminum afterburning in air does not affect ultrasonic emissions as strongly as it does the audible.
5. No correlation is possible at present between the ultrasonic emission PSD and deflagration behavior. Strong peaks are observed in the spectrum but their origin is not clear.

References

1. Koury, J., "Solid Strand Burn Rate Technique for Predicting Full Scale Motor Performance," AFRPL TR 73-49, October, 1973.
2. Saber, A.J., Johnston, M.D., Caveny, L.H., Summerfield, M., and Koury, J., "Acoustic Emissions from Burning Propellant Strands," 11th JANNAF Combustion Meeting, CPIA Publications 261, December, 1974 1 pp 409-428.
3. Strahle, W.C., "The Role of Combustion Noise in Solid Propellant Combustion Instability," 11th JANNAF Combustion Meeting, CPIA Publication 261, December, 1974, pp. 399-408.
4. Culick, F.E.C. (ed.), "T-Burner Testing of Metalized Solid Propellants," AFRPL TR 74-28, October, 1974.
5. Strahle, W.C. and Shivashankara, B.N., "Wall Reflection Effects in Combustion Generated Noise," AIAA Paoer No. 75-127, 1975.
6. Strahle, W.C., "Some Results in Combustion Generated Noise," Journal of Sound and Vibration, 23, 113-125, 1972.
7. Strahle, W.C. and Shivashankara, B.N., "A Rational Correlation of Combustion Noise Results from Open Turbulent Premixed Flames," Fifteenth Symposium (International) on Combustion, The Combustion Institute, Pittsburgh (to be published in 1975).
8. Liptai, R.G., Harris, D.O., Engle, R.B. and Tatro, C.A., "Acoustic Emission Techniques in Materials Research," International Journal of Nondestructive Testing, Vol. 3, pp. 215-275. 1971.
9. Dunnegan, H.L. and Harris, D. O., "Acoustic Emission Techniques," Experimental Techniques in Fracture Mechanics, ed. A.S. Kobayashi, SESA Monograph No. 1, Iowa State University Press, p. 38, 1973.
10. Acoustic Emission, American Society of Testing and Materials, Special Technical Publication. STP-505, Philadelphia, 1972.
11. Curtis, Graham,"Spectral Analysis of Acoustic Emission - Acoustic Emission

4, " Non-Destructive Testing, 7, April, 1974, p. 82-91.

12. Bell, R.L., "Acoustic Emission Transducer Calibration - Transient Pulse Method," Tech. Rept. DE-73-3, Dunegan - Endevco, San Juan Capistrano, California.

13. Chambers, R.H., ARPA Semi-Annual Report, March, 1968 - August, 1969, University of Arizona, Tucson, Arizona, 1969.

AFOSR INTERIM SCIENTIFIC REPORT

AFOSR-TR-76-1193

AUDIBLE AND ULTRASONIC ACOUSTIC EMISSIONS FROM COMPOSITE SOLID PROPELLANTS

Prepared for

Air Force Office of Scientific Research/NA
Bolling Air Force Base, D. C. 20332

by

William A. Bell
James I. Craig
Warren C. Strahle

School of Aerospace Engineering
Georgia Institute of Technology
Atlanta, Georgia 30332

Approved for public release; distribution unlimited

Grant No. AFOSR-76-1193 September 1976

Conditions of Reproduction

Reproduction, translation, publication, use and disposal in whole or in part by or for the United States Government is permitted.

UNCLASSIFIED

SECURITY CLASSIFICATION OF THIS PAGE *(When Data Entered)*

REPORT DOCUMENTATION PAGE		READ INSTRUCTIONS BEFORE COMPLETING FORM
1. REPORT NUMBER AFOSR-TR-76-1193	2. GOVT ACCESSION NO. ADA032875	3. RECIPIENT'S CATALOG NUMBER
4. TITLE *(and Subtitle)* AUDIBLE AND ULTRASONIC ACOUSTIC EMISSIONS FROM COMPOSITE SOLID PROPELLANTS		5. TYPE OF REPORT & PERIOD COVERED July 1975-September 1976 INTERIM
		6. PERFORMING ORG. REPORT NUMBER
7. AUTHOR(s) WILLIAM A. BELL JAMES I. CRAIG WARREN C. STRAHLE		8. CONTRACT OR GRANT NUMBER(s) AFOSR 75-2805
9. PERFORMING ORGANIZATION NAME AND ADDRESS GEORGIA INSTITUTE OF TECHNOLOGY SCHOOL OF AEROSPACE ENGINEERING ATLANTA, GEORGIA 30332		10. PROGRAM ELEMENT, PROJECT, TASK AREA & WORK UNIT NUMBERS 681308 9711-01 61102F
11. CONTROLLING OFFICE NAME AND ADDRESS AIR FORCE OFFICE OF SCIENTIFIC RESEARCH/NA 1400 WILSON BOULEVARD ARLINGTON, VIRGINIA 22209		12. REPORT DATE July 1976 13. NUMBER OF PAGES 35
14. MONITORING AGENCY NAME & ADDRESS*(if different from Controlling Office)*		15. SECURITY CLASS. *(of this report)* UNCLASSIFIED 15a. DECLASSIFICATION/DOWNGRADING SCHEDULE

16. DISTRIBUTION STATEMENT *(of this Report)*

Approved for public release; distribution unlimited.

17. DISTRIBUTION STATEMENT *(of the abstract entered in Block 20, if different from Report)*

18. SUPPLEMENTARY NOTES

19. KEY WORDS *(Continue on reverse side if necessary and identify by block number)*

ULTRASONICS
NOISE
SOLID PROPELLANT COMBUSTION
ACOUSTIC EMISSIONS

20. ABSTRACT *(Continue on reverse side if necessary and identify by block number)*

Audible and ultrasonic acoustic waves are generated during deflagration of composite solid propellants. The audible waves can be sensed by microphones while special high frequency pressure transducers are required to measure the ultrasonic signals. These acoustic emissions have a potential use both as diagnostics of the combustion and as a means for the study of fundamental burning processes. To date a family of composite HTPB-AP propellants have been tested. Results which show the effects of pressure level, atmosphere in which burned, AP particle size, aluminum addition, and aluminum coating are presented and discussed.

DD FORM 1 JAN 73 1473 EDITION OF 1 NOV 65 IS OBSOLETE

SECURITY CLASSIFICATION OF THIS PAGE *(When Data Entered)*

AFOSR INTERIM SCIENTIFIC REPORT

AFOSR-TR-76-1193

AUDIBLE AND ULTRASONIC ACOUSTIC EMISSIONS FROM COMPOSITE SOLID PROPELLANTS

Prepared for

Air Force Office of Scientific Research/NA
Bolling Air Force Base, D. C. 20332

by

William A. Bell
James I. Craig
Warren C. Strahle

School of Aerospace Engineering
Georgia Institute of Technology
Atlanta, Georgia 30332

Approved for public release; distribution unlimited

Grant No. AFOSR-76-1193 September 1976

Conditions of Reproduction

Reproduction, translation, publication, use and disposal in whole or in part by or for the United States Government is permitted.

Abstract

Audible and ultrasonic acoustic waves are generated during deflagration of composite solid propellants. The audible waves can be sensed by microphones while special high frequency pressure transducers are required to measure the ultrasonic signals. These acoustic emissions have a potential use both as diagnostics of the combustion and as a means for the study of fundamental burning processes. To date a family of composite HTPB-AP propellants have been tested. Results which show the effects of pressure level, atmosphere in which burned, AP particle size, aluminum addition, and aluminum coating are presented and discussed.

Table of Contents

I. Introduction

Deflagration of composite solid propellants is a complex, unsteady process involving a heterogeneous material. Consequently, experimental studies of the combustion dynamics are difficult to perform because of both the inaccessability of the process and the relatively small scale of heterogeneities. Average or integrated properties, such as the burn rate or the characteristic acoustic impedances of the propellant surface, have been measured during deflagration; but the details of the combustion processes must generally be studied by microscopic examination of the quenched propellant surface. Recent studies have been made[1,2] which relate ultrasonic acoustic emissions to the details of the combustion process.

This investigation is concerned with the use of audible and ultrasonic acoustic waves generated during deflagration to assist in the study of the combustion dynamics. These emissions are a direct result of unsteadiness caused by the heterogeneity of the propellant, and their measurement exemplifies the use of acoustic analysis in "turbulence" diagnostics. This technique consists of analyzing the frequency spectra of the noise produced by the deflagrating solid propellant and relating spectral characteristics to specific combustion processes. Deduced free-field audible emission measurements were taken and cover a range of frequencies from 40 Hz to 10 kHz. Ultrasonic emissions were also measured and reliable data were obtained from 50 kHz to 300 kHz. The acoustic fields for a family of AP-HPTB composite propellants, including coated and uncoated aluminized as well as nonaluminized formulations, were analyzed. The AP particle sizes range from 0.5 to 400 microns, and the propellants were burned in air, CO_2, and N_2 at pressures from 10 to 30 Atm.

The effects of mean pressure, pressurization gas, AP particle size, aluminum addition, and aluminum coating are discussed. Theories are presented which explain low frequency behavior (0-300Hz) although the high frequency behavior, which accounts for most of the noise, is open to interpretation.

II. Experiment

The deflagration tube shown in Fig. 1 is used in this study and can operate at pressures up to 70 Atm. The tube consists of a stainless steel pipe 162.5 cm in length with a nominal ID of 10.16 cm and an O.D. of 15.25 cm. The tube dimensions were originally chosen to satisfy the following criteria: (1) the volume of the tube should be sufficient so that the mean pressure level does not increase more than 10% during a run for the propellant strands used in this study; (2) the tube should be long enough to ensure fully developed wave propagation at some axial distance sufficiently far from the propellant; and (3) the first transverse mode should have a frequency higher than that expected for the peak of the sound power spectrum emitted from the propellants. Recent developments in accounting for three-dimensional waves in the tube have made it possible to relax this last assumption. Provisions are made along the tube for pressurization and evacuation. The gases used in this study were N_2, air and CO_2.

At one end of the tube, the solid propellant sample is held with epoxy to an aluminum sample holder which is bolted to a steel endplate 2.5 cm thick. Behind this endplate directly opposite the sample, a Dunegan-Endevco Model D 9201 flat response transducer is mounted to measure the ultrasonic acoustic emissions. To ensure a clean transmission path for the signal, high-vacuum grease is used between the

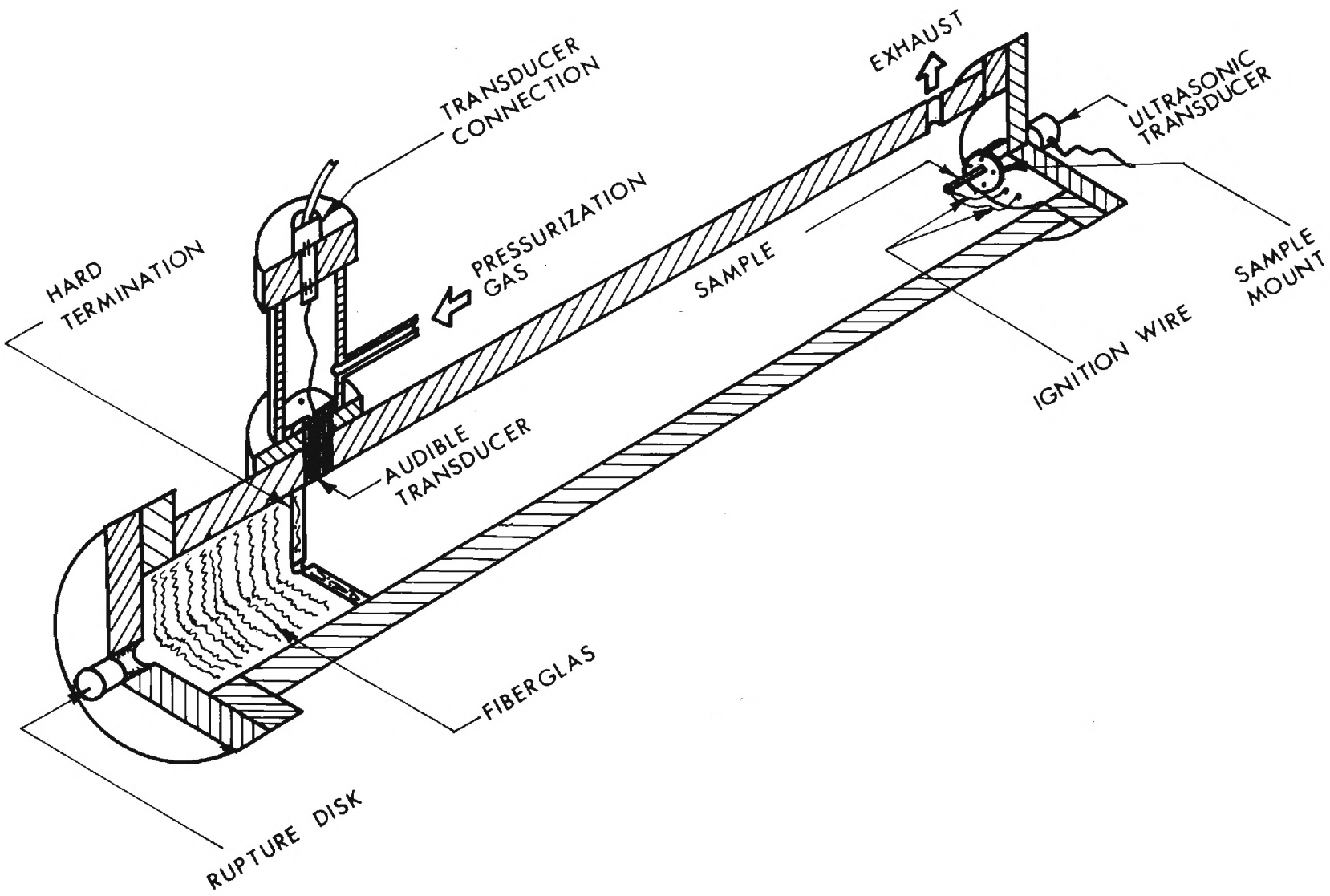

FIGURE 1. SCHEMATIC OF DEFIAGRATION TUBE.

sample holder and the endplate and a coupling grease is employed at the transducer-endplate interface. Electrical connections on the endplate allow the ignition wire to be joined to the igniter.

At the other end of the tube is another endplate to which a rupture disc is attached, as shown in Fig. 1. Twenty cm away along the axis of the tube a termination disc is located with a vent hole in the center. Fiberglass is placed between the disc and endplate to prevent acoustic feedback. The cavity between the disc and the endplate acts as a Helmholtz resonator and reduces the high amplitudes which occur at the lower resonant frequencies of the tube so that better signal resolution can be achieved at the higher frequencies. Directly in front of the termination disc, the audible transducer - a BBN Model 376A piezoelectric sensor - is located. To minimize pressure differentials across the transducer, it is surrounded by a cylindrical cavity which is coupled to the deflagration tube.

As shown in Fig. 2, the signals from both the audible and ultrasonic transducers are amplified, filtered, and then recorded on an Ampex 14-channel tape recorder at a speed of 60 inches per second. The FM mode is used for the audible signals and the AM mode is selected for the ultrasonic signals. The upper limit of response for the tape recorder is 300 kHz. The signals are then played back at a reduced rate for digital Fourier analysis using an HP5451A Fourier Analyzer. Typical results are presented in Fig. 3 for the audible signal and consist of the power spectrum over a specified frequency range. The narrow peaks occur at the resonant frequencies of the tube. A theory has been developed to deduce the equivalent free field spectra from the tube spectra and is presented in the next section.

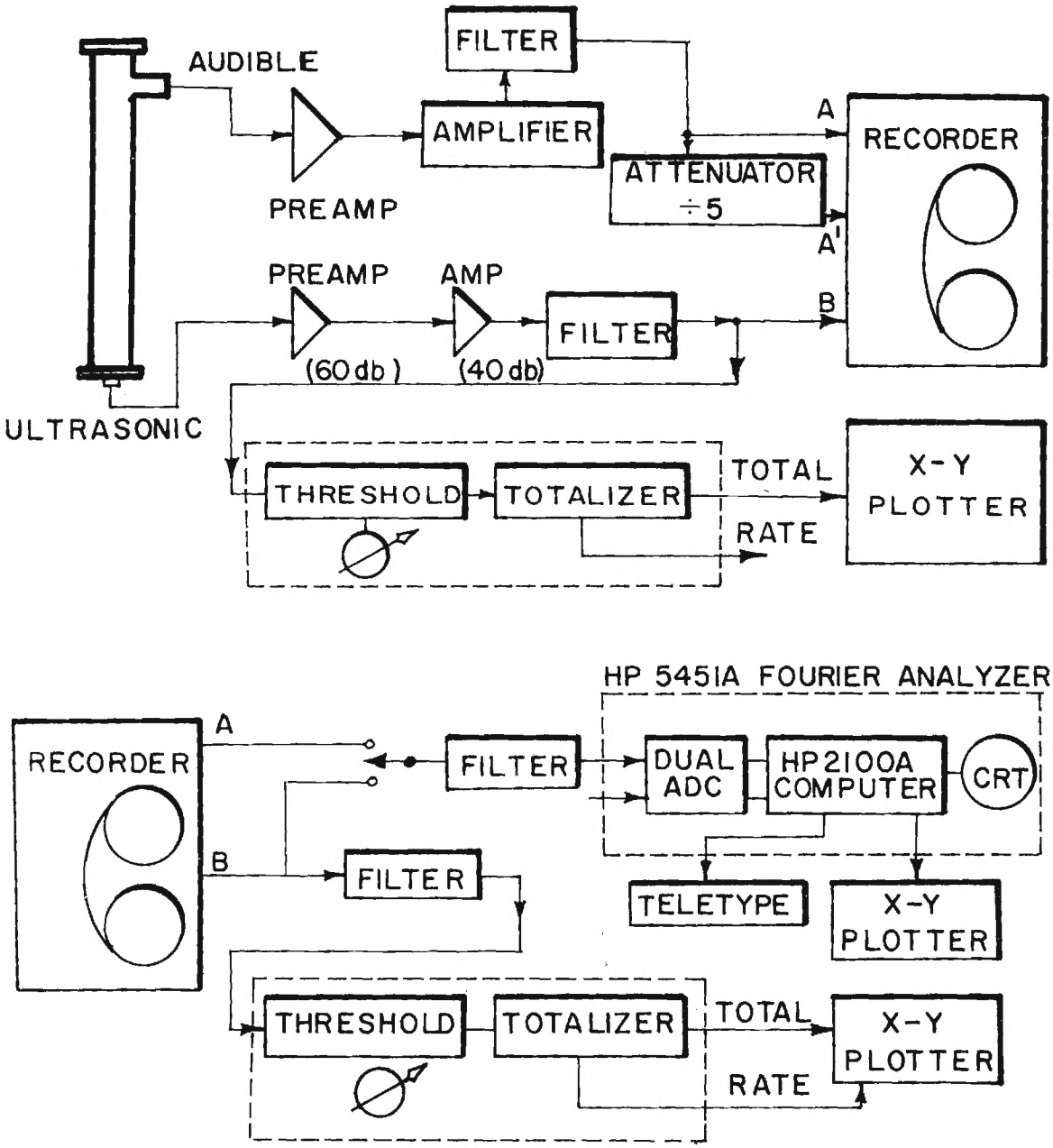

FIGURE 2. DATA ACQUISITION AND ANALYSIS SCHEMATIC

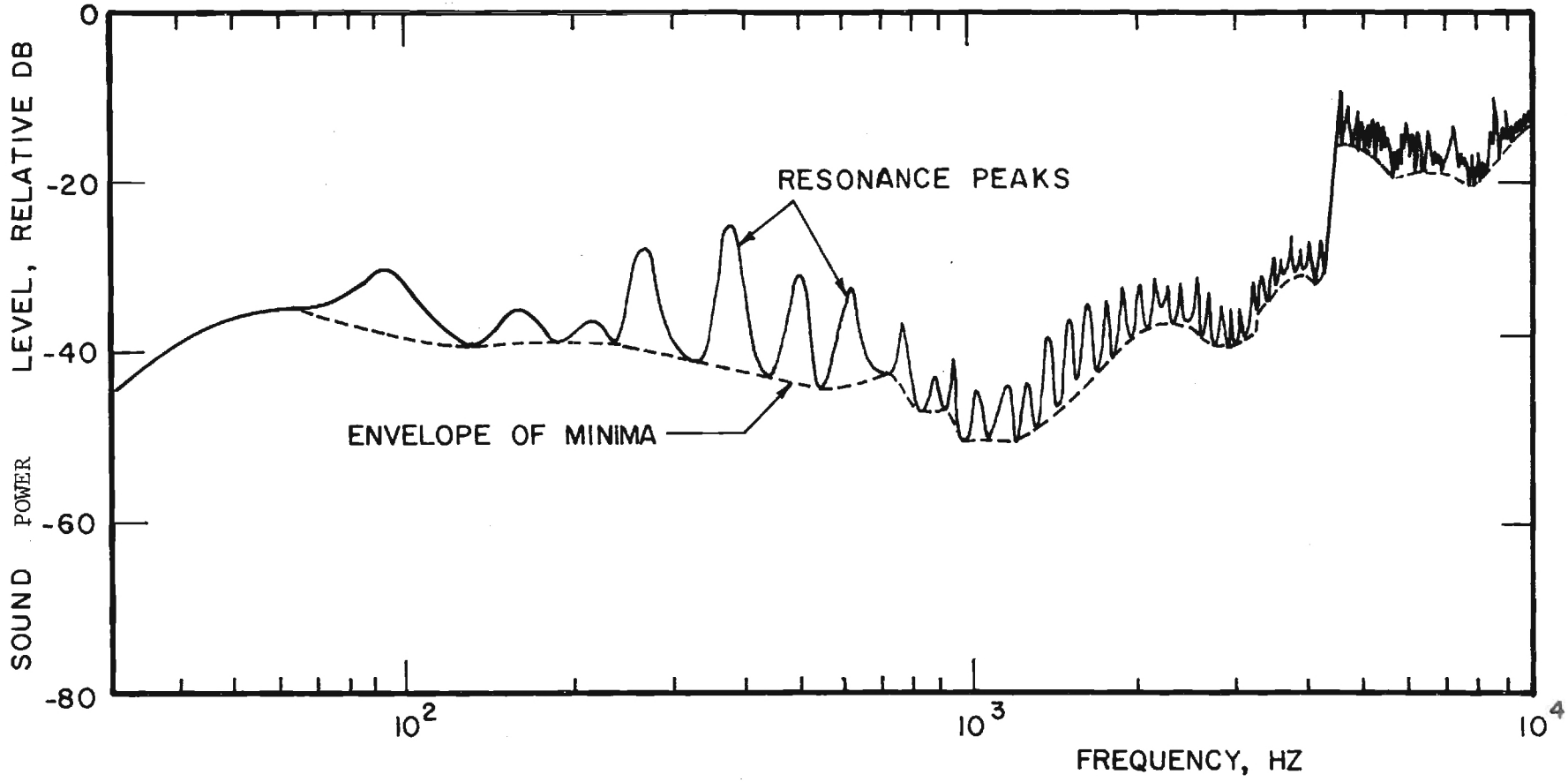

FIGURE 3. RAW SPECTRUM FOR NT-2 BURNING IN NITROGEN AT 300 PSIA.

III. Theory

Audible

The theoretical investigation for the audible emissions include (1) calculation of the equivalent free field sound power level and spectrum from the deflagration tube measurements, (2) determination of the mass flow noise efficiency $P/\dot{m}$, and (3) formulation of scaling laws to assist in combustion analysis.

The overall measured sound pressure level and the spectrum, of course, depend upon the acoustic properties of the tube. As shown in Fig. 3, resonances will appear at the natural mode frequencies of the tube. The data would be useless in an engineering sense if they could only be interpreted as unique to this configuration. What are actually desired are the sound power and spectral characteristics of the propellant in the absence of reflecting surfaces, i.e., the characteristics that would be obtained if the propellant were burning in a pressurized anechoic chamber. If this information can be extracted then theoretical acoustics may be employed to determine the acoustical behavior of any rocket chamber in which the propellant might be placed.

Over the frequency range from 0 to 2000 Hz, plane waves exist in the tube and the theory developed in Ref. 3 can be used to obtain the equivalent free field spectrum and sound power. Above 2000 Hz, however, three-dimensional modes are present, so the one-dimensional theory must be extended.

Since the Mach number is small, flow effects can be neglected. Also, any feedback of the reflected wave from the disc termination can be neglected.[3] The governing equation for acoustics of the tube are given by

the Helmholtz equation[4]

$$\nabla^2 p_\omega + k^2 p_\omega = 0 \qquad (1)$$

In the present experiment, cylindrical coordinates are applicable and the tube walls are assumed rigid ($\frac{\partial p_\omega}{\partial r} = 0$). The boundary conditions at the ends of the tube are

$$\frac{\partial p_\omega}{\partial x} = A_\omega \, \delta(r) \qquad (2)$$

at the propellant's end where the sample is assumed to be a point source of axial velocity fluctuations located at r = 0, and

$$\frac{\partial p_\omega}{\partial x} - i k y_\ell p_\omega = 0 \qquad (3)$$

at the other end of the tube. At frequencies greater that about 100 Hz, the admittance y_ℓ is about the same as a short nozzle.[3] A solution of the form

$$p_\omega = \sum_{m,n=0}^{\infty} (A_+ e^{-ik_{mn}x} + A_- e^{ik_{mn}x}) J_m \left(\frac{S_{mn} r}{a} \right) \cos m\theta \qquad (4)$$

is assumed. Applying Eq. (2) gives

$$(-A_+ + A_-) \sum_{m,n=0}^{\infty} \left[ik_{mn} J_m \left(S_{mn} \frac{r}{a} \right) \cos m\theta \right] = A_\omega \, \delta(r)$$

Multiplying both sides of this expression by $J_\mu (S_{\mu\eta} r)$ and integrating over the endplate area gives

$$- A_+ + A_- = \frac{A_\omega}{i \sum_{\substack{n=0 \\ k_{on} < k}} \pi a^2 k_{on} J_o{}^2 \left(\frac{S_{on}}{a} \right)}$$

With the propellant located at r=0, only radial modes exist in the tube.[4] For tangential modes (m > 0) a pressure node is located at the

tube's center. But since the propellant is placed at r=0, a pressure antinode exists at the center which means that the conditions for the formation of tangential modes cannot be maintained.

In the last expression the series in the denominator is restricted to values of k greater than the cutoff frequency k_{on}. At frequencies below the cutoff values the radial modes decay rapidly with axial distance.

Applying Eq. (3), solving for A_+ and A_-, and substituting the expressions into Eq. (4) gives, for the transducer located at x=ℓ, r=a:

$$p\, p_\omega^* = \frac{A_\omega A_\omega^*}{\sum_{n=0}^{k_{on}<k} \left[\pi a^2 J_o\left(\frac{S_{on}}{a}\right)\right]^2 (k^2 |y_\ell|^2 \cos^2 k_{on}\ell + k_{on}^2 \sin^2 k_{on}\ell - 2 k y_i k_{on} \sin k_{on}\ell \cos k_{on}\ell)} \tag{5}$$

For a flame burning in the free field,[5]

$$p_\omega\, p_\omega^* = \frac{A_\omega A_\omega^*}{(\pi R)^2} \tag{6}$$

so that measurement of $A_\omega A_\omega^*$ from $p_\omega\, p_\omega^*$ in the tube directly using Eq. (5) gives information about the free field source behavior through Eq. (6). In addition, once $A_\omega\, A_\omega^*$ is determined it can be used as a boundary condition similar to Eq. (2) in any generally shaped combustion chamber.

To facilitate the computation of $A_\omega\, A_\omega^*$ from typical spectral data shown in Fig. 3, the following observations are noted in Eq. (5). If $y_i = 0$, then at the minimum points of the spectrum where $\sin k_{on}\ell = 1$,

$$\left(p_\omega p_\omega^*\right)_{min} = \frac{A_\omega A_\omega^*}{\sum_{n=0}^{k_{on}<k} \left[\pi a^2 k_{on} J_o\left(\frac{S_{on}}{a}\right)\right]^2} \tag{7}$$

Preliminary tests of the tube using a known sound source indicate that $y_i = 0$ for the termination disc at frequencies above 100 Hz. Below this frequency, the peak-to-trough height in Fig. 3 is about 10 db which indicates that $|y_\ell|$ is small. Thus, Eq. (5) is apparently a good approximation below 100 Hz as long as $\sin k_{on} \ell$ does not approach zero. Equation (7) implies that $A_\omega A_\omega^*$ can be measured directly from the minima of the tube spectra if $A_\omega A_\omega^*$ does not vary appreciably with frequency.

Once $A_\omega A_\omega^*$ is determined, two important propellant combustion characteristics can be obtained. The first is the shape of the free field spectrum from which deflagration behavior diagnostics can be deduced. Secondly, the acoustic power generation capability can be obtained from the relation

$$P = \frac{1}{4\pi} \int_{-\infty}^{\infty} \frac{2\pi}{t_o} A_\omega A_\omega^* \, d\omega \tag{8}$$

By dividing the power P by the mass flow rate $\dot{m}$ computed from the measured burn rates, the mass flow noise efficiency can be obtained.

Combustion noise is basically produced by a velocity source, as assumed in Eq. (2), in other flame types[6] and there is no reason to suspect this is not the case here. Velocity roughness downstream of the flame may easily be caused by the heterogeneous character of the propellant. Following the development of Ref. 6 the equivalent open flame acoustic power may be expected to scale like

$$P \propto \frac{\bar{\rho}}{\bar{c}} A_p \left(\frac{\rho_s r}{\bar{\rho}}\right)^4 \tag{9}$$

A test of this relation was made with the current propellants. That is, the power should scale directly with the propellant surface area A_p and, for the same propellant energetics ($\bar{\rho}$), the acoustic power should increase as the burn rate r to the fourth power. Again, following the lead of Ref. 6 the majority of the frequency content of the noise should be located near

$$f \propto (\rho_s r/\bar{\rho})/\ell_e \tag{10}$$

According to Eq. (10) if the mean granularity (particle size) ℓ_e is reduced, the frequency content of the noise should rise, and an increase in the burn rate for a fixed $\bar{\rho}$ should increase the frequency. In the current tests $\bar{\rho}$ and ρ_s have been held constant so the only variables investigated were propellant burn rate, burn area and particle size.

Ultrasonic Acoustic Emissions

Acoustic emissions can be broadly defined as stress wave emissions propagating within a solid material in response to some type of loading. The emission levels are generally well below those associated with audible disturbances and for many materials are on the order of microbars.

The investigation of deflagrating solid propellants by study of the ultrasonic emission spectrum must, at present, be general in nature for basically three reasons. First, the general meaning of the spectrum has yet to be formulated in any area of study. For solid propellants the inability to precisely define the propellant acoustical properties and its inhomogeneity greatly complicate data interpretation. Secondly, a suitable acoustic emission transducer with adequate bandwidth and relatively uniform response above 100 kHz is unavailable. Finally, frequency dependent attenuation of the waves caused by their dispersive propagation

through the propellant and signal distortion produced by reflection at interfaces complicates data interpretation.

In the present investigation, studies of propellants with greatly different properties were tested to determine if any general trends can be noticed. To account for the lack of flat transducer response at the frequencies tested, a transducer calibration spectrum was used to correct the measured spectra. At the outset, a calibration curve determined by the manufacturer using an impulsive acoustic emission technique (Ref. 7) was used for this purpose. This curve shows a smooth behavior from about 50 kHz to the 300 kHz limit of the tape recorder; however, closer examination and discussion with the manufacturer revealed that the "points" at 50 kHz spacing are simply rms level measurements using a tuned voltmeter and therefore represent overaged output over a band centered every 50 kHz.

In order to provide finer spectrum detail, an alternate qualitative calibration technique was used. Instead of measuring the transducer output for a known input stress wave (pressure), the electrical impedance of the transducer was measured over the frequency range of interest. Piezoelectric material such as that used for the present transducer generally exhibits a reversible behavior, that is, a charge is produced on certain crystal faces in response to an applied stress while a strain state can be produced in the crystal in response to an applied electric field (Ref.8). The relationship is linear, but due to anisotropy may involve extensive cross-coupling (e.g., uniaxial stress may produce charge on several crystal faces). In acoustic emission transducers, the output is measured as a charge on two parallel

element faces produced in response to an applied stress field. Smaller charges are produced on other faces at the same time, but are not detected. Consequently, when electrically driven in order to measure the impedance, the transducer element will vibrate in a manner that is similar to that when subjected to an incident stress wave. Since voltages (fields) are applied to only one pair of faces, a unique inverse to the input condition is not achieved. Ceramic elements, such as are used for most transducers exhibit a strong piezoelectric effect in the poled direction with much smaller cross-coupling effects so that the transducer's driven electrical impedance will generally show a strong qualitative similarity to an actual stress wave calibration. This has been born out in tests to determine the effect of transducer coupling mechanisms on the calibration (9).

In the present work, this electrical technique was used to obtain finer qualitative calibration data than available from the transducer maker. The electrical impedance was measured for the as-mounted configuration and quantitatively matched at the peak response (near 100 kHz) to the absolute calibration wave furnished. The most notable difference was the presence of several small (1-3 dB) peaks near 180 kHz and above 300 kHz. Rolloff at 100 kHz for the "impulse" calibration reflects the rolloff of the preamp used by the manufacturer in this test.

Not only is the transducer spectral calibration subject to question, but as noted earlier, due to essentially intractable nonhomogeneities and geometric irregularities in the transmission media, the received signal may bear little resemblence to the pressure wave produced at the

emission source. Three mechanisms can be immediately noted:

(a) material dispersion in the viscoelastic, heterogeneous propellant

(b) geometric dispersion for a stress wave propagating in a prismatic bar

(c) attenuation due to acoustic impedance mismatch at material interfaces in the transmission path.

The first two are difficult to define quantitatively; however, qualitatively, it is well known (10) that geometric dispersion is most pronounced at wavelengths about equal to the cross-section dimensions of the propagation medium. The table below compares the wavelengths at 100 kHz for longitudinal waves in the three materials making up the path. Geometric dispersion in the propellant should be small, although dispersion due to propagation through the heterogeneous material containing AP particles comparable in size to emission wavelengths will be larger.

Material	$E(MN/m^2)$	c_o(m/s)	c_s(m/s)	λ_s(cm)
MC-XXX	2.75	38.4	22.3	.022
Alum.	68.7×10^3	5120	2970	2.97
Steel	206.2×10^3	5151	2987	2.99

$c_o \doteq \sqrt{E/\rho}$, c_s = Rayleigh speed $\approx 0.58\ c_o$

Attenuation due to acoustic impedance mismatch will occur at the propellant-holder, the holder-endplate, and the endplate-transducer interfaces (Figure 3). To a first approximation the overall attenuation

for complex waves may be represented as:

$$\text{Attenuation} = \frac{2}{1 + \frac{\rho_2 c_2}{\rho_1 c_1}}$$

where ρ = density, c = wavespeed, and propagation is from 1 to 2. For the present configuration, the net attenuation is approximately 0.0026 so that less than 1% of the energy at the source will arrive at the transducer element.

Several mechanisms have been considered as potential sources for the measured emissions. They can be broadly grouped as:

(a) solid phase effects such as dislocation kinetics or crystal fracture,

(b) gas phase phenomena such as ignition transients or combustion kinetics.

Since for these tests, energy has been increased over a 50 kHz to 300 kHz band, the sources can be further grouped according to characteristic frequencies. Solid phase effects are commonly observed as sources for acoustic emissions in materials tests, and it is generally agreed that a combination of dislocation movement and micro-fracture are prime amongst these. However, the characteristic times are in the sub-micro-second range so that the major energy release would occur well above the present band (and outside the range of all but the most exotic equipment). Furthermore, should this energy excite individual particles to vibrate, the characteristic frequencies (AP particles, for example) would again fall above 1MHz. Since definite peaks have been observed in the sub-300 kHz range, it must be concluded that other factors are

responsible.

Chemical kinetics times on the other hand are typically on the order of 10^{-5} seconds so that energy in the 100 kHz area can be anticipated. Three potential mechanisms were quantitatively explored and the conclusions summarized below:

(i) Laminar flame moving through a volume of fuel immediately above an AP particle: In this case, the acoustic pressure of interest is that across the flame as it propagates through the fuel. Using the momentum equation on this scale for a flame speed of roughly 1 cm/s yields an expected pressure fluctuation of about 2×10^4 μ Bar. Considering only path attenuation this would produce a 50 μ Bar signal at the transducer.

(ii) AP ignition transient as the gas above a particle ignites. Here again the momentum equation can be crudely applied across the flame but now using the regression velocity rather than the laminar flame velocity above. For typical burn rates (1cm/s), the gas velocity normal to the surface can be estimated by mass conservation as about 100 cm/s. From the momentum equation, the pressure change will be roughly 100 times that above, or about $2 \times 10^6 \mu$ Bar. This would produce a 5000 μ Bar signal at the transducer.

(iii) Explosive ignition of a fuel-oxidizer mixture near the surface. Considering typical specific heats for the fuel, a rough estimation yields gas velocities over 300 times the previous case. Accordingly, pressures in excess of 1 Bar would be seen at the transducer.

IV. Results

Burn Rate

The propellants were supplied by the Air Force Rocket Propulsion Laboratory and are shown in Table 1. Although no direct observation of burn rate was possible, the rate was determined from the onset and termination of the audible and ultrasonic signals. These burn rates for combustion in nitrogen are shown in Table 1 at the single pressure of 300 psia.

As may be seen from Table 1, the propellants are basically hydroxyl terminated polybutadiene - ammonium perchlorate (AP) - aluminum (Al) propellants with some additives. Parameter variations are systematically made in AP particulate size, aluminum coating (AFCAM), and catalyst.

In the test sequence, no reliable audible data were obtained for MC-174 and MC-175 because of the high burn rates. For these two propellants, steady state conditions were not achieved between the ignition and burnout transients. Data for MC-173 and MC-179 will be run in future tests to determine the effects of catalysts on the acoustic properties of the propellant. With the seven remaining propellants the effect of AP particulate size, aluminum coating, and aluminum addition can be studied. Also, the data are used to investigate the scaling laws presented in Section III. The combustion efficiency is presented along with the burn rates for those propellants for which reliable emission data were obtained. This efficiency is computed by integrating the audible spectrum over the range from 40 to 2000 Hz. Preliminary results for the spectrum from 2000 to 20 kHz indicate that most of the noise is produced at frequencies above 2000 Hz where

Table 1. PROPELLANTS FOR ACOUSTIC TESTING, AND BURN RATES AT 300 PSIA IN NITROGEN

Specimen	R-45M	AP		AL	Dioctyl dipate	Indopol	IPDI	Catalysts	Burn rate (in/sec)	$P/\dot{m}$ $(cm/sec)^2$
		Size	%							
MC-170	9.31%	200μ 14μ 6μ	26.8 20.4 20.8	20% 5μ		2.0%	0.69%		0.31 ±0.3	.65
MC-172	9.31%	200μ 14μ 6μ	26.8 20.4 20.8	20% 5μ AFCAM		2.0%	0.69%		0.37 ±0.01	.55
MC-173	9.31%	200μ 14μ 6μ	26.8 20.4 18.8	20% 5μ	2%		0.69%	Fe_2O_3 2%	0.52	-
MC-179	9.31%	200μ 14μ 6μ	26.8 20.4 18.8	20% 5μ	2%		0.69%	Copper fluoride 2%	Bad burn	-
MC-174	10.24%	6μ 0.5μ	26 40	20% 5μ		3.0%	0.76%		0.57	-
MC-175	10.24%	6μ 0.5μ	26 40	20% 5μ AFCAM		3.0%	0.76%		0.81	-
MC-177	9.31%	400μ 200μ 50μ	44 18 6	20% 5μ		2.0%	0.69%		0.21 ±0.02	.08
MC-178	9.31%	400μ 200μ 50μ	44 18 6	20% 5μ AFCAM		2.0%	0.69%		0.21 +0.03	Transducer Calibration Uncertain
NT-2	?	200μ	100%	NONE					.20±.01	1.2
NT-3	?	90μ	100%	NONE					.22±.02	1.3
NT-4	?	50μ	100%	NONE					.33±.03	2.5

transverse modes can exist in the tube. However, the tube characteristics above 2000 Hz will be thoroughly investigated before data at these higher audible frequencies are presented. The data from 40 to 2000 Hz is sufficient to show the effect propellant properties and to investigate scaling laws.

All tests were run with the propellants coated with about 1/4-inch of Dow Corning 140 RTV adhesive to prevent recirculating burning aluminum from igniting the sides of the propellant. Unless otherwise noted tests were run at 20 atm in nitrogen with 1/2 x 1/2 cm samples approximately eight cm in length.

Audible

According to Eq. (9), the total power of an equivalent open flame can be expected to increase directly with an increase in propellant area and to increase as the burn rate to the fourth power. From Eq. (9) the acoustic efficiency should scale like

$$\frac{P}{\dot{m}} \propto \frac{1}{\bar{c}} \left(\frac{\rho_s \, r}{\bar{\rho}} \right)^3 \tag{11}$$

From Table 1, assuming $\bar{\rho}$, $\bar{c}$, and ρ_s are the same, the combustion noise efficiency for MC-170 and MC-177 should differ as $\left(\frac{r_{MC-170}}{r_{MC-177}} \right)^3$ or by a factor of from 2 to 6 for the burn rates measured. The measured difference of about a factor of 8 is not unreasonable. Similarly the difference in $P/\dot{m}$ for NT-2 and NT-4 bears out Eq. (11) to within experimental error. From the data obtained thus far, Eq. (11) is in qualitative agreement with experimental data.

The scaling of Eq. (9) with respect to area has been investigated in this study and in Ref. 3. The results indicate that, to within 20%, the measured power is linearly proportional to the propellant area.

For the aluminized propellants, the effects of propellant properties and pressurization gas on the measured spectra are presented in Fig. 4. Comparison of the curves for MC-177 burned in air and nitrogen indicates a 10 to 15 db rise in sound power level for the run with air. The difference in the results appears to be caused by aluminum afterburning. The effect of an AFCAM coating can be observed from comparison of the spectra for MC-170 and 172. The propellant without AFCAM appears to have a slightly higher noise output over the frequency range from 200 to 2000 Hz.

Shown on Fig. 4 are the burn-through frequencies computed from Eq. (10) using the MC-170 burn rate for various AP and Al particle sizes. Because of variations in granularity, it is seen that the spectrum is rather densely occupied by available frequencies. No apparent correlation of the observed spectra with these frequencies is evident; none was really expected to be clear because of the roughness of the estimate of frequency, the usual spread of particle size about the stated value and the dense population of the spectrum with these particle frequencies. Nevertheless, moving from MC177 to MC170 propellant, which decreases the mean particle size and increases the burn rate (see Table 1), there is a general rise in the spectrum and a filling of the spectrum in the frequency range from 350 to 1000 Hz (perhaps due to the 14 μ AP). In the 5 μ range between 1000 and 2000 Hz the spectra for the aluminumized propellants are consistently flat and the sound power level is the lowest.

In contrast to the aluminized propellants, the spectra for the non-aluminized propellants, shown in Fig. 5, indicate a general increase in noise with decreasing particle size over the 1000-2000 Hz range. Comparison of the curves show a general increase in the sound levels from 300 to

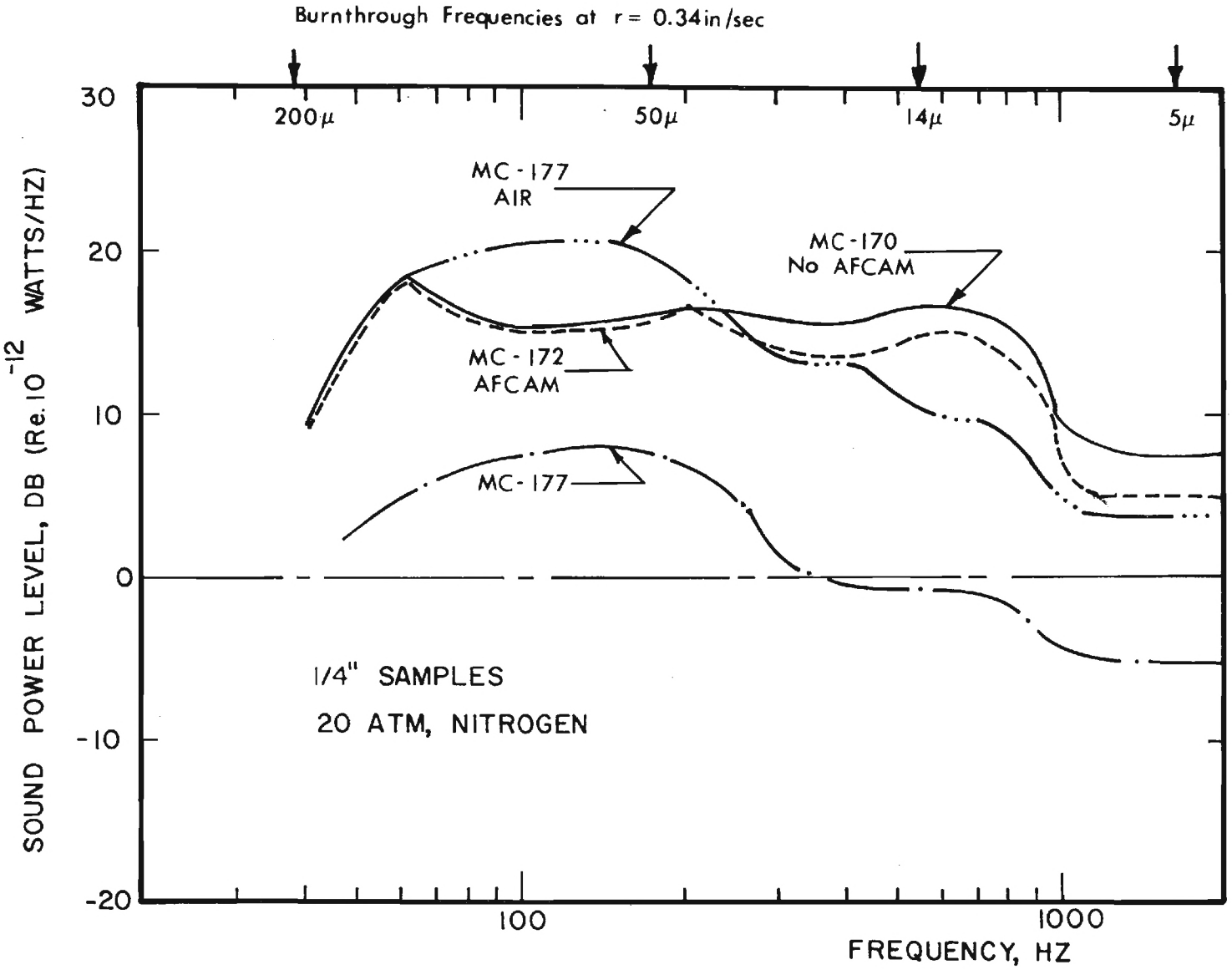

FIGURE 4. EFFECT OF AP PARTICLE SIZE, AFCAM TREATMENT, AND GAS MEDIUM ON DEDUCED FREE FIELD SPECTRA.

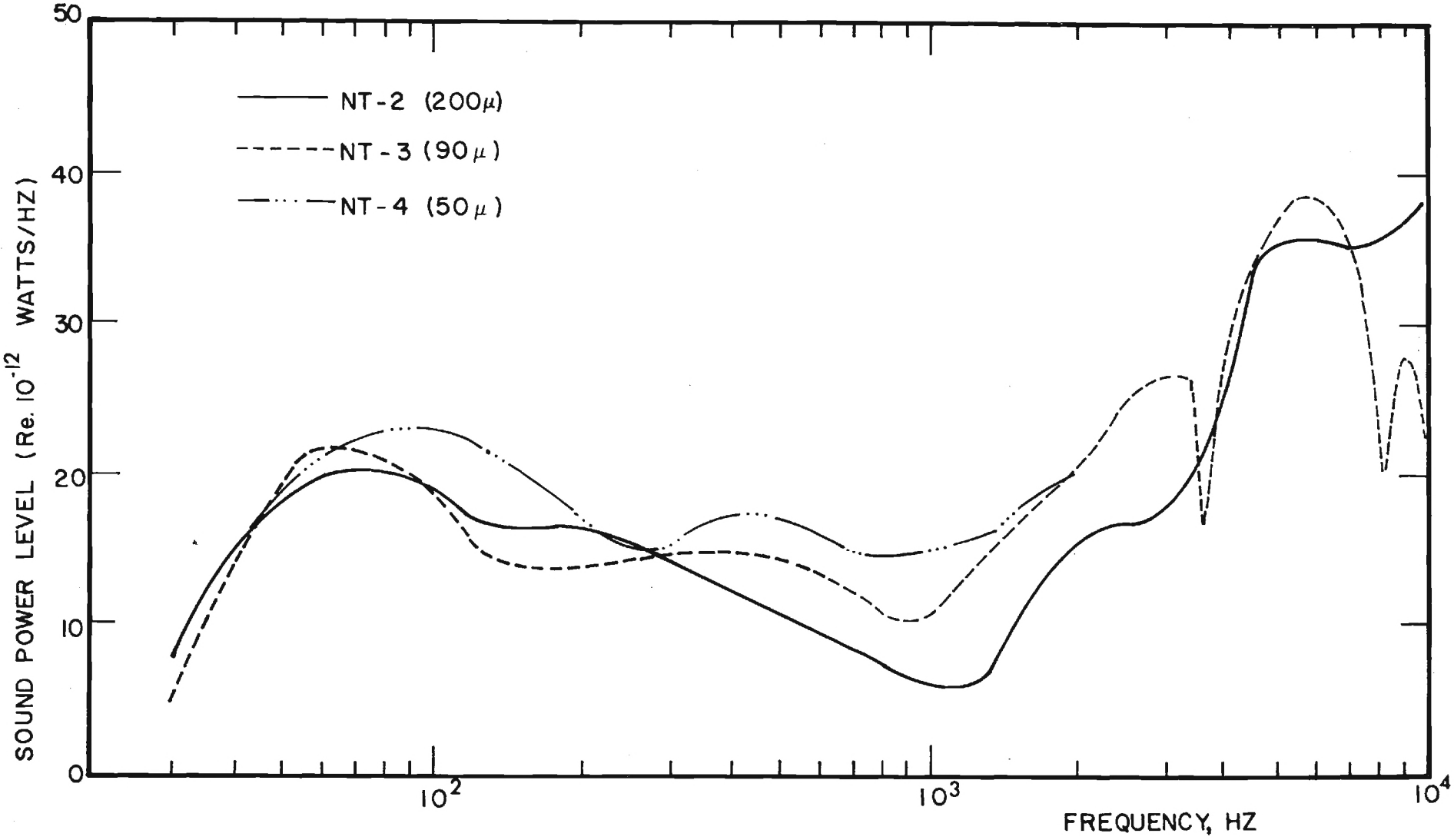

FIGURE 5. COMPARISON OF DEDUCED FREE FIELD SPECTRA FOR NONALUMINIZED PROPELLANTS BURNED AT 300 PSIA IN NITROGEN.

2000 Hz probably caused by the higher burn rate of NT-4 as mentioned previously. Below 300 Hz no general trend can be ascertained. From 2 to 10 kHz there is a 10 to 20 db rise in sound power level over the noise measured below 2000 Hz. Using Eq. (10) this noise is produced by sources on the order of one micron which is of the same order as the reacting surface layer. Including the noise over this frequency range increases the values of $P/\dot{m}$ computed from 0 to 2000 Hz by three orders of magnitude and may explain the observed roughness levels in rocket motors. An investigation is currently underway to check the accuracy of the assumption that the propellant noise output can be approximated by a point source given in Eq. (2). If these preliminary data are valid, the majority of the audible combustion noise falls within the 2000 to 10,000 Hz range.

Ultrasonic

Ultrasonic acoustic emission data were obtained for all propellants in Table 1 except MC-173 and MC-179. The effect of the following variables on the spectral data are presented. (1) AP particle size, (2) pressurization gas, (3) aluminum particles, and (4) AFCAM coating. Details of the data reduction methods are given in Ref. 3 .

AP Particle Size: For the nonaluminized propellants-NT-2, NT-3, and NT-4-AP particle size has little effect on either the overall sound power level or the location of the peaks in the spectrum. Based on these data no correlation appears to exist between the spectral peaks and the particle size as shown in Fig. 6.

Effect of Pressurization Gas: The burning of MC-177 in air as opposed to nitrogen produces a definite shift in both spectral peaks and peak

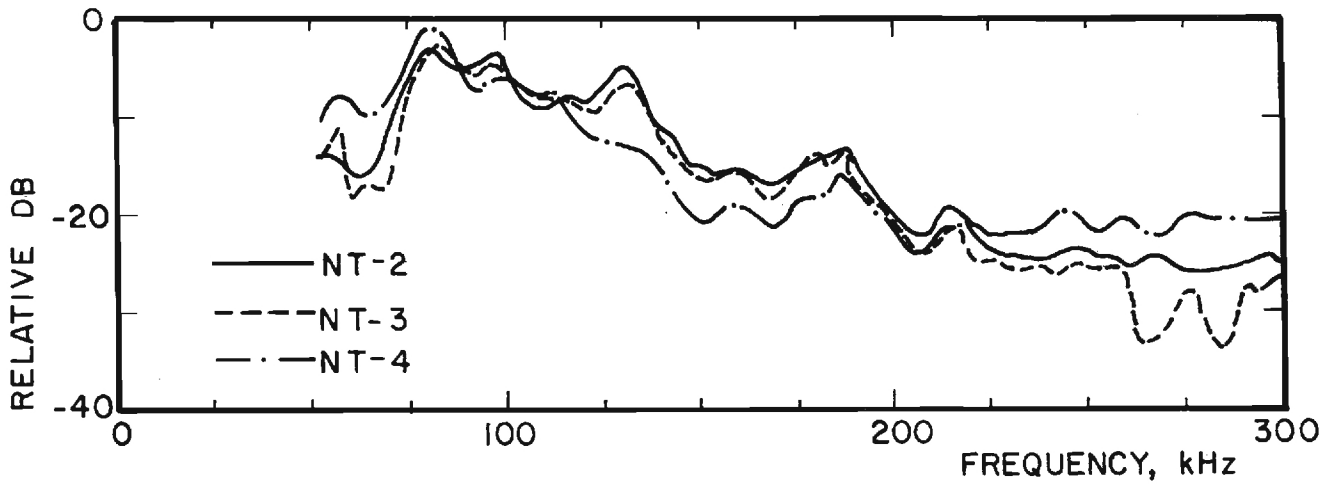

FIGURE 6. EFFECT OF AP PARTICLE SIZE ON THE ACOUSTIC EMISSION SPECTRA FOR NONALUMINIZED PROPELLANTS BURNED IN NITROGEN AT 300 PSIA.

power as shown in Fig. 7. In air there is a stronger high frequency content than in nitrogen. There is also a general smoothing of the spectra for air at the frequencies below 125 kHz. These effects are most probably caused by aluminum afterburning although correlation between the spectral peaks and the combustion process is presently not clear.

Aluminum Particle Addition: As shown in Fig. 6, AP particle size does not have a pronounced effect on the spectra of the acoustic emissions. However, the addition of aluminum does. Comparison of the spectra for aluminized (MC-177) and nonaluminized (NT-2) propellants indicate markedly different spectral features. The spectrum of the aluminumized propellant has a large noise content at the low frequency range below 125 kHz. Also, the peaks in the aluminized propellant spectrum are more distinct in the 125 to 225 kHz range. Above 225 kHz, however, relatively little difference is apparent in the two spectra in Fig. 8. Whether the cause of the differences is the emission source or propagation of the ultrasonic waves through the propellant cannot be ascertained.

Effect of AFCAM Coating: As reported in Ref. 3 there was a general increase in overall sound power when the aluminum is coated with AFCAM for MC-177 and MC-178. This trend also holds for MC-170 and MC-172 as shown in Fig. 9.

Source Characteristics: Based on the earlier observations reported in Ref. 3, it was strongly suspected that the AP deflagration mechanism was primarily responsible for the observed emission spectra. The considerations summarized in Section III of the present report provide a crude

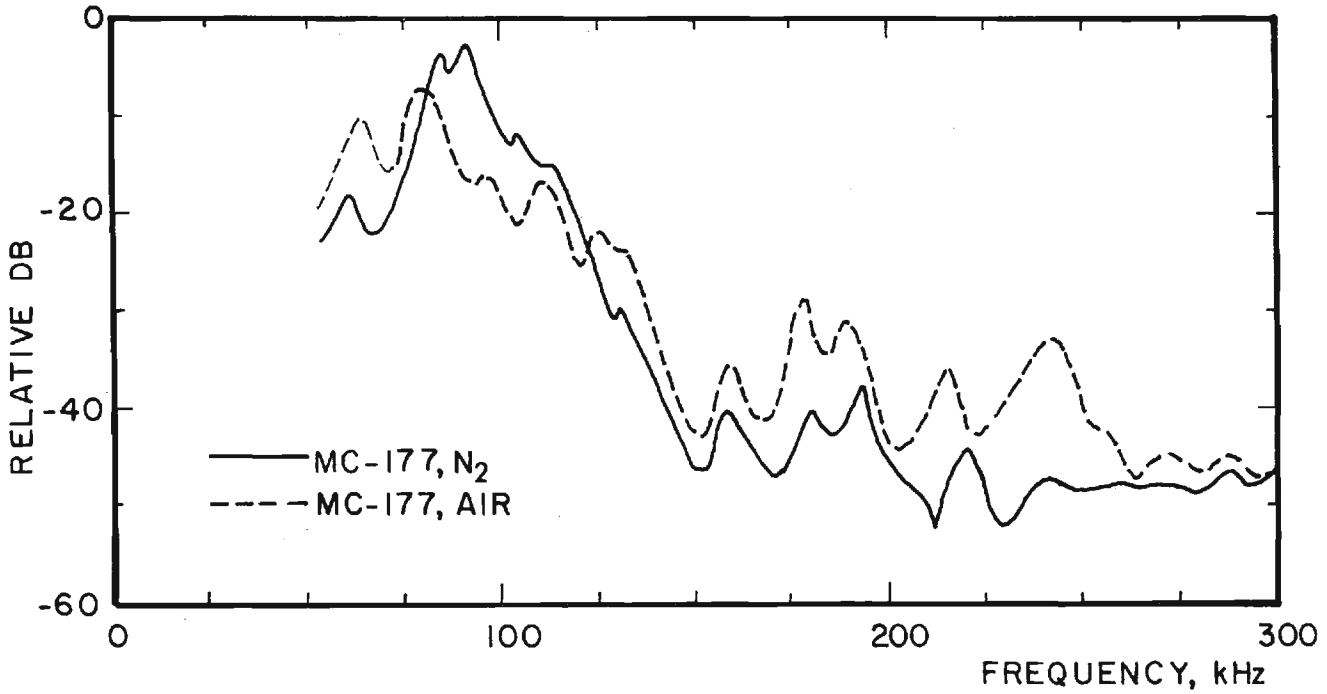

FIGURE 7. EFFECT OF PRESSURIZATION GAS ON THE ULTRASONIC SPECTRA OF MC-177 AT 300 PSIA

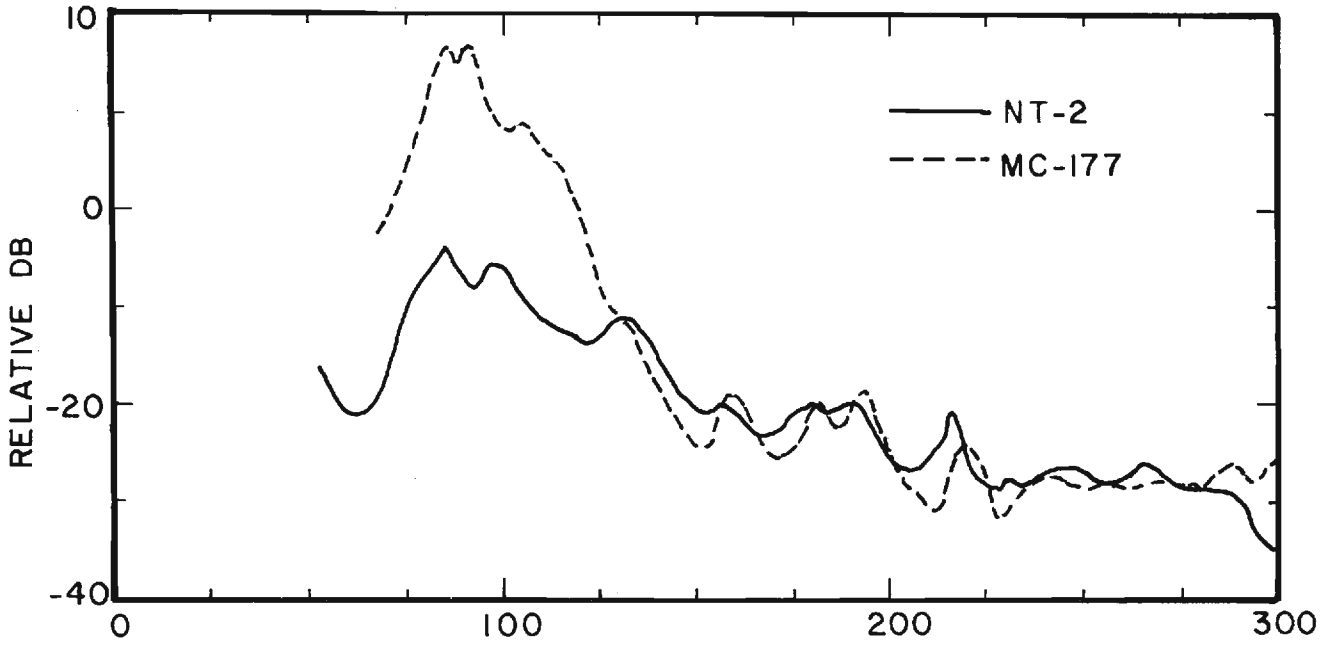

FIGURE 8. EFFECT OF ALUMINUM ADDITION ON THE ULTRASONIC SPECTRA AT 300 PSIA BURNED IN NITROGEN.

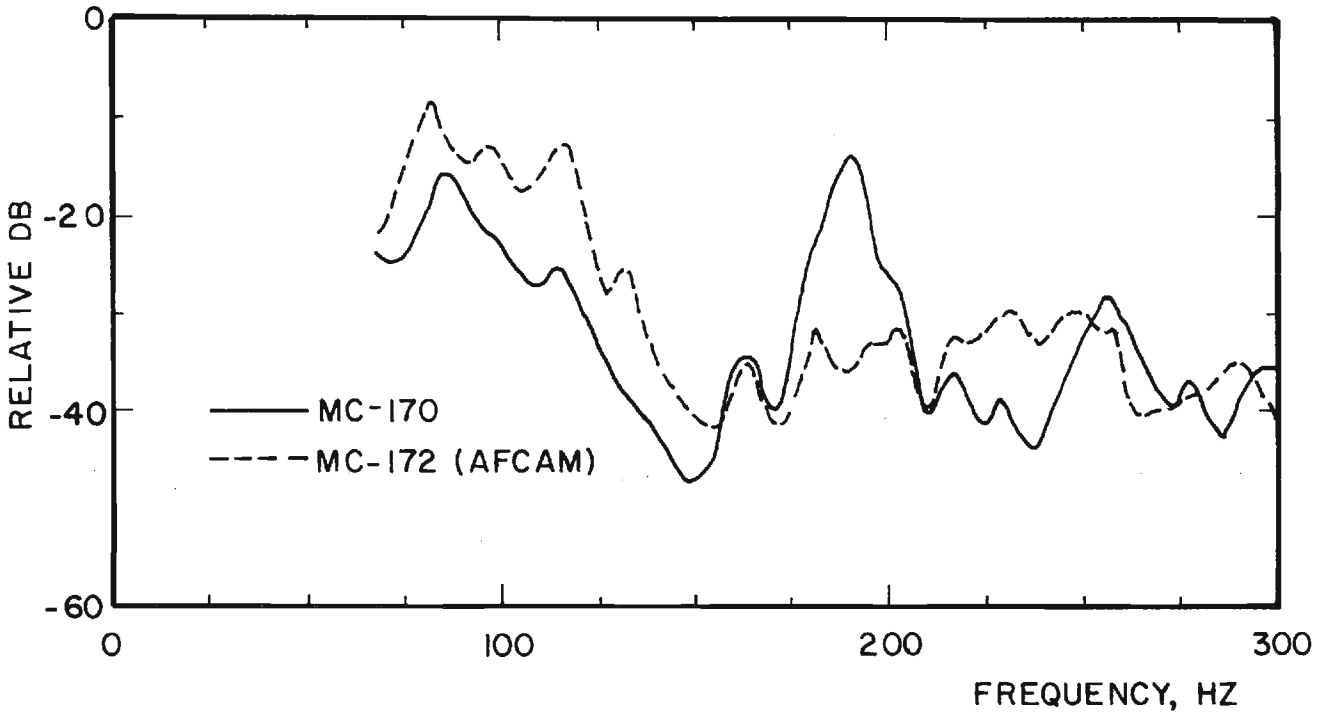

FIGURE 9. EFFECT OF AFCAM COATING OF THE ALUMINUM PARTICLES AT 300 PSIA IN NITROGEN.

theoretical basis for this hypothesis as well. The rms acoustic emission levels at the transducer consistently range between about 800 to 3500 Bar. These levels are somewhat above the range for the laminar flame model, (i), but are generally consistent with the AP ignition transient model, (ii). The chemical kinetics times associated with both of these processes are on the order of 10^{-5} sec so that the accompanying unsteady pressures would be expected to show relatively larger spectral energy content near 100 kHz. Again, this is consistent with the earlier observations of a large, 15 - 25 dB, peak in the emission power spectra around 100 kHz. Furthermore, since these characteristic times should be only weakly affected by pressure and unaffected by AP size, the principal alteration in the emission spectra should be a change in the relative height of the 100 kHz peak as AP sizes and burn rates are varied. In this case, the change in level is associated with the changing source areas.

Unfortunately, as shown in Figure 6, there is no clear difference in the shape or level of the emission spectra as the AP size is varied from 50 m to 200 m (NT series). The spectra show some fine structure but are basically flat within the tolerances of the calibration curve used. On the other hand, as shown in Figure 8, it is much more likely that the observed peak at 100 kHz can be attributed to the Al present in the more complex MC propellants. This possibility has not yet been fully explored in tests to date, although several comments might be made. From the levels involved, the signals would likely be produced before the Al agglomerates have left the burning surface (there is some indication, however, that the peak may be due to Al particle impact on the inner

tube walls). Emissions from the solid phase Al due to dislocation activity or micro-fracture are well above the 100 kHz range. Propellants with a range of Al sizes and quantities will have to be tested in order to further clarify these observations. For example, insensitivity to Al size could indicate a source mechanism associated with the agglomerate phase.

V. Conclusions

There is a marked effect of pressurization gas on the audible and ultrasonic emission. The audible spectra shows a 10 db increase in sound power level. No distinct differences in spectral shape are apparent between two propellants of different AP particle size. However, the audible spectra do indicate an increase in overall power output with a decrease in AP particle size probably caused by the increasing burn rate with decreasing particle size.

The theory presented in Ref. 3 adequately describes the behavior of the audible noise output in the range of frequency from 0 to 2000 Hz. This theory assumes that the mechanism of the noise is a velocity source caused by the heterogeneity of the propellant. Above 2000 Hz the wave characteristics of the tube must be better understood before comparison between the theory and experiment is made.

In contrast to Ref. 3, the effect of aluminum coating (AFCAM) on the audible noise is not significant when burning in nitrogen. However, there is a general increase in the ultrasonic emissions when AFCAM is used.

VI. Nomenclature

A	combustion noise source strength
A_p	propellant surface area
c	speed of sound
f	frequency of maximum radiated sound power
h	combustion noise monopole source strength
k	wavenumber, $\omega/\bar{c}$
ℓ	tube length
ℓ_e	mean granularity distance
$\dot{m}$	mass flow of propellant
p	acoustic pressure
$\bar{p}$	mean chamber pressure
r	radical distance or burn rate
R	distance from the source
S	tube cross-section area
S_ω	power spectral density (PSD)
t_o	sampling time of Fourier transform
X	axial distance
$<>$	time average
α	95% confidence limits for PSD
γ	ratio of specific heats
δ	Dirac delta function
ζ	specific acoustic impedance
ρ	density
η	mass flow noise efficiency, $P/\dot{m}$
θ	tangential coordinate

Subscripts

ℓ at tube length

ω Fourier transform

s solid phase

r real part

i imaginary part

Superscripts

* Complex conjugate

- Steady State Values

VII. References

1. Saber, A. J., Johnston, M. D., Caveny, L. H., Summerfield, M., and Koury, J., "Acoustic Emissions from Burning Solid Propellant Strands," 11th JANNAF Combustion Meeting, CPIA Publication No. 261, December 1974, pp. 409-428.

2. Caveny, L. H., Saber, A. J., and Summerfield, M., "Propellant Combustion and Burning Rate Uniformity Identified by Ultrasonic Acoustic Emissions," AIAA Paper No. 76-696, Presented at the AIAA/SAE 12th Propulsion Conference, Palo Alto, Calif., July 1976.

3. Craig, J. I., Strahle, W. C., and Palfrey, J., "Audible and Ultrasonic Acoustic Emissions from Composite Solid Propellants," AFOSR Interim Scientific Report for Grant No. AFOSR-75-2805, July 1975.

4. Morse, P. M. and Ingard, K. U., Theoretical Acoustics, Mc-Graw Hill, New York, 1964, Chapter 9.

5. Strahle, W. C., "Some Results in Combustion Generated Noise," Journal of Sound and Vibration, 23, 113-125, 1972.

6. Strahle, W. C. and Shivashankara, B. N., "A Rational Correlation of Combustion Noise Results from Open Turbulent Premixed Flames," Fifteenth Symposium (International) on Combustion, The Combustion Institute, Pittsburgh, 1974, pp. 1379-1385.

7. Bell, R. L., "Acoustic Emission Transducer Calibration-Transient Pulse Method," Tech Report DE-73-3, Dunegan-Endevco, San Juan Capistrano, California, 1973.

8. Cady, W. G., Piezoelectricity, McGraw-Hill, New York, 1946.

9. Hill, R. and Stephens, R. W. B., "Acoustic Emission-Evaluation of Transducers and Measuring Systems", Proceedings of the Ultrasonics International 1973 Conference, 5.5, pp. 177-182.

10. Kolsky, H., Stress Waves in Solids, Oxford: University Press, 1953.

AFOSR FINAL SCIENTIFIC REPORT

AFOSR-TR

AUDIBLE AND ULTRASONIC ACOUSTIC EMISSIONS FROM COMPOSITE SOLID PROPELLANTS

Prepared for

Air Force Office of Scientific Research/NA
Bolling Air Force Base, D. C. 20332

by

William A. Bell
James I. Craig
Warren C. Strahle

School of Aerospace Engineering
Georgia Institute of Technology
Atlanta, Georgia 30332

Approved for public release; distribution unlimited

Grant No. AFOSR 75-2805 September 1977

Conditions of Reproduction

Reproduction, translation, publication, use and disposal in whole or in part by or for the United States Government is permitted.

UNCLASSIFIED

SECURITY CLASSIFICATION OF THIS PAGE *(When Data Entered)*

REPORT DOCUMENTATION PAGE		READ INSTRUCTIONS BEFORE COMPLETING FORM
1. REPORT NUMBER AFOSR-TR-	2. GOVT ACCESSION NO. ADA032875	3. RECIPIENT'S CATALOG NUMBER
4. TITLE *(and Subtitle)* AUDIBLE AND ULTRASONIC ACOUSTIC EMISSIONS FROM COMPOSITE SOLID PROPELLANTS		5. TYPE OF REPORT & PERIOD COVERED October 1976 - September 1977 FINAL 6. PERFORMING ORG. REPORT NUMBER
7. AUTHOR(s) WILLIAM A. BELL JAMES I. CRAIG WARREN C. STRAHLE		8. CONTRACT OR GRANT NUMBER(s) AFOSR 75-2805
9. PERFORMING ORGANIZATION NAME AND ADDRESS GEORGIA INSTITUTE OF TECHNOLOGY SCHOOL OF AEROSPACE ENGINEERING ATLANTA, GEORGIA 30332		10. PROGRAM ELEMENT, PROJECT, TASK AREA & WORK UNIT NUMBERS 681308 9711-01 61102F
11. CONTROLLING OFFICE NAME AND ADDRESS AIR FORCE OFFICE OF SCIENTIFIC RESEARCH/NA 1400 WILSON BOULEVARD ARLINGTON, VIRGINIA 22209		12. REPORT DATE September 1977 13. NUMBER OF PAGES 65
14. MONITORING AGENCY NAME & ADDRESS*(if different from Controlling Office)*		15. SECURITY CLASS. *(of this report)* UNCLASSIFIED 15a. DECLASSIFICATION/DOWNGRADING SCHEDULE

16. DISTRIBUTION STATEMENT *(of this Report)*

Approved for public release; distribution unlimited.

17. DISTRIBUTION STATEMENT *(of the abstract entered in Block 20, if different from Report)*

18. SUPPLEMENTARY NOTES

19. KEY WORDS *(Continue on reverse side if necessary and identify by block number)*

ULTRASONICS
NOISE
SOLID PROPELLANT COMBUSTION
ACOUSTIC EMISSIONS

20. ABSTRACT *(Continue on reverse side if necessary and identify by block number)*

The audible and ultrasonic acoustic emissions from deflagrating composite solid propellants were monitored and analyzed to evaluate their potential use as diagnostics of the combustion and as a means for the study of fundamental burning processes. A family of composite HTPB-AP propellants were tested which include a range of AP particle sizes, aluminized and nonaluminized formulations, the effect of the addition of a catalyst, and the presence of an AFCAM aluminum coating.

DD FORM 1 JAN 73 1473 EDITION OF 1 NOV 65 IS OBSOLETE

SECURITY CLASSIFICATION OF THIS PAGE *(When Data Entered)*

For the audible emissions, the frequency behavior in the 0-10 kHz range can be explained by assuming the gas phase reaction time primarily controls the oscillating frequency. The combustion noise efficiency, η, cannot be explained by the theories put forth, so the physical makeup of the noise source is presently unknown.

Analysis of the ultrasonic emission spectra indicates that there are no distinct spectral features which can be used to identify a particular propellant by its acoustic signature. The rms emission levels, however, can be used as a reliable, non-intrusive means for detecting flaws in the propellant, identifying bad burns, and measuring burn rates. The overall level increases with increasing burn rate and chamber pressure and decreasing particle size.

Abstract

The audible and ultrasonic acoustic emissions from deflagrating composite solid propellants were monitored and analyzed to evaluate their potential use as diagnostics of the combustion and as a means for the study of fundamental burning processes. A family of composite HTPB-AP propellants were tested which include a range of AP particle sizes, aluminized and nonaluminized formulations, the effect of the additon of a catalyst, and the presence of an AFCAM aluminum coating.

For the audible emissions, the frequency behavior in the 0-10 kHz range can be explained by assuming the gas phase reaction time primarily controls the oscillating frequency. The combustion noise efficiency, η, cannot be explained by the theories put forth, so the physical makeup of the noise source is presently unknown.

Analysis of the ultrasonic emission spectra indicates that there are no distinct spectral features which can be used to identify a particular propellant by its acoustic signature. The rms emission levels, however, can be used as a reliable, non-intrusive means for detecting flaws in the propellant, identifying bad burns, and measuring burn rates. The overall level increases with increasing burn rate and chamber pressure and decreasing particle size.

Table of Contents

I. Introduction

Deflagration of composite solid propellants is a complex, unsteady process involving a heterogeneous material. Consequently, experimental studies of the combustion dynamics are difficult to perform because of both the inaccessability of the process and the relatively small scale of heterogeneities. Average or integrated properties, such as the burn rate or the characteristic acoustic impedances of the propellant surface, have been measured during deflagration; but the details of the combustion processes must generally be studied by microscopic examination of the quenched propellant surface.

To study the dynamics of localized combustion phenomena, motion pictures using high speed cameras and photographs of the burning propellant surface are often used. With these visual aids phenomena such as binder melts and, with metallized propellants, the formation and burning of the metal particles have been studied. However, the microscopic surface details tend to be obscured by the flame front, smoke, and metal particles.

To augment the visual studies the investigation reported here is concerned with the use of audible and ultrasonic acoustic waves generated during deflagration to assist in the analysis of the combustion dynamics. These emissions are a direct result of unsteadiness caused by the heterogeneity of the propellant, and their measurement exemplifies the use of acoustic analysis in "turbulence" diagnostics. This technique consists of analyzing the frequency spectra of the noise produced by the deflagrating solid propellant and relating the spectral characteristics to specific combustion processes. Deduced free field audible emission measurements were taken and cover a range of frequencies from 40 Hz to 10 kHz. Using combustion noise scaling laws[1-3], the objectives of the audible emission studies are to (1) relate the frequency spectra of the emissions to known propellant properties and (2) determine from overall sound power level the mass flow noise efficiency (acoustic power output per unit mass flow rate). The ultrasonic emissions

(sometimes referred to as acoustic emissions) were also measured and reliable data obtained from 50 kHz to 300 kHz. Recent studies of deflagrating solid propellants[4,5] have attempted to relate variations in acoustic emission levels to instantaneous variations in burn rate. The objectives of the ultrasonic emissions studies reported here are to (1) relate the spectral features to the combustion dynamics and (2) determine the feasibility of using the overall ultrasonic sound power level in both steady and unsteady deflagration diagnostics.

The acoustic fields for a family of AP-HPTB composite propellants, including coated and uncoated aluminized as well as nonaluminized formulations, were analyzed. The AP particle sizes range from 0.5 to 400 microns, and the propellants were burned in helium, air, and N_2 at pressures of from 5 to 30 ATM.

Acoustic data showing the effects of presurization gas, AP particle size, aluminum addition, aluminium coating, and pressure are presented and discussed. The empirical mass flow noise efficiencies and half-power frequencies for the audible emissions are correlated with physical properties of the propellant to obtain scaling laws which are then compared with theory. In the ultrasonic emission studies, both power spectral and rms amplitude data are used to deduce information concerning the combustion dynamics.

II. Experiment

The deflagration tube shown in Fig. 1 is used in this study and can operate at pressures up to 70 Atm. The tube consists of a stainless steel pipe 162.5 cm in length with a nominal ID of 10.16 cm and an O.D. of 15.25 cm. The tube dimensions were originally chosen to satisfy the following criteria: (1) the volume of the tube should be sufficient so that the mean pressure level does not increase more than 10% during a run for the propellant strands used in this study; (2) the tube should be long enough to ensure fully developed wave propagation at some axial distance sufficiently far from the propellant; and (3) the first transverse mode should have a frequency higher than that expected for the peak of the sound power spectrum emitted from the propellants. Recent developments in accounting for three-dimensional waves in the tube have made it possible to relax this last assumption. Provisions are made along the tube for pressurization and evacuation. The gases used in this study were nitrogen, air, and helium.

At one end of the tube, the solid propellant sample is held with epoxy to an aluminum sample holder which is bolted to a steel endplate 2.5 cm thick. Behind this endplate, directly opposite the sample, a Dunegan-Endevco Model D 9201 flat response transducer is mounted to measure the ultrasonic acoustic emissions. To ensure a clean transmission path for the signal, high-vacuum grease is used between the sample holder and the endplate and a coupling grease is employed at the transducer-endplate interface. Electrical connections on the endplate allow the ignition wire to be joined to the igniter.

At the other end of the tube is another endplate to which a rupture disc is attached, as shown in Fig. 1. Twenty centimeters away along the axis of the tube a termination disc is located with a vent hole in the center. Fiberglass is placed between the disc and the endplate acts as a Helmholtz resonator and reduces the high amplitudes which occur at the lower resonant frequencies of the

tube so that better signal resolution can be achieved at the higher frequencies. Directly in front of the termination disc, the audible transducer - a BBN Model 376A piezoelectric sensor-- is located. To minimize pressure differentials across the transducer, it is surrounded by a cylindrical cavity which is coupled to the deflagration tube.

As shown in Fig. 2, the signals from both the audible and ultrasonic transducers are amplified, filtered, and then recorded on an Ampex 14-channel tape recorder at a speed of 60 inches per second. The FM mode is used for the audible signals and the AM mode is selected for the ultrasonic signals. The upper limit of response for the tape recorder is 300 kHz. The signals are then played back at a reduced rate for digital Fourier analysis using an HP5451A Fourier Analyzer. Typical results are presented in Fig. 3 for the audible signal and consist of the power spectrum over a specified frequency range. The narrow peaks occur at the resonant frequencies of the tube. A theory has been developed to deduce the equivalent free field spectra from the tube spectra and is presented in the next section.

III. Theory

Audible Theory - Propellant in Tube

Consider Fig. 4 where a heterogeneous solid propellant is located in the acoustic tube with the propellant surface at the end plate position, x = 0. Because of the propellant heterogeneity, the axial velocity profile will be spatially nonuniform. Moreover, at a fixed space location the velocity will be nonuniform in time due to alternate burnthrough of particles. The "frequency" of the fluctuating velocity is expected to be $\theta(\dot{r}/l_p)$. Typically, for $\dot{r}$ = 0.5 in/sec and l_p = 100μm $\nu \approx$ 130 Hz. The fuel and oxidizer gases mix and react as they travel downstream and the initial velocity profile becomes smoothed as shown in Fig. 4. A typical dimension for this is of the order of hundreds of μm. However, after smoothing, there is still a temporal fluctuation in the axial velocity because the spacewise average mass flow is nonuniform, due to the heterogeneity of the propellant. This fluctuation in the space averaged axial velocity is the source of the acoustic signal.

Consider a sample with $d_p \gg d_R$ so that the mixing layer has penetrated the propellant gas stream a negligible amount by the time the smoothed velocity profile is achieved. Furthermore, for $d_R \ll \lambda$, as is the case under consideration, the smoothed profile may be considered at x = 0 for purposes of acoustic calculations. At $x = d_R$ there will also be spacewise and timewise fluctuations in density because of the space and timewise local mixture ratio fluctuations. The significance of $x = d_R$ is that fluctuations have become small compared with mean values so that small disturbance theory may be used.

It will now be assumed that the propellant properties and solid temperature are such that the mean speed of sound is the gases at $x = d_R$ is equal to that of the tube pressurization gas. This is generally not the case but simplifies the analysis, and a correction will be applied to the results after the analysis

is complete.

Assuming the gas velocity to be primarily axial, the region between x = 0 and d_R may be treated in a quasi-steady manner (mass flow in = mass flow out) if $\omega\, d_R/\bar{u} \ll 1$. For $d_R = 500\,\mu m$ and $\bar{u} = 50$ ft/sec, $\omega\, d_R/\bar{u} \approx 0.02$ for the frequency cited above. Consequently, applying small perturbations to the mass flow per unit area

$$\frac{m'}{\bar{m}} = \frac{\rho'}{\bar{\rho}} + \frac{u'}{\bar{u}} \quad \text{or} \quad \frac{m_\omega}{\bar{m}} = \frac{\rho_\omega}{\bar{\rho}} + \frac{u_\omega}{\bar{u}} \tag{1}$$

This quantity may be locally calculated at $x = d_R$, and the average over the gas flow area must equal the total mass flux fluctuation at the propellant surface.

Assuming perfect gases, the density fluctuation may be written as an isentropic part plus an entropy fluctuation. In transform space this is

$$\frac{\rho_\omega}{\bar{\rho}} = \frac{1}{\gamma}\,\frac{p_\omega}{\bar{p}} + \sigma_\omega \tag{2}$$

Combination of Eqs. (1) and (2) yields

$$\frac{u_\omega}{\bar{u}} = \frac{m_\omega}{\bar{m}} - \frac{1}{\gamma}\,\frac{p_\omega}{\bar{p}} - \sigma_\omega \tag{3}$$

It is well known that $\bar{p}$ is constant to terms of the order of the square of a typical Mach number compared to unity. Moreover, in acoustics, flow effects only enter to terms of the order of the Mach number compared with unity. Since typical Mach numbers for solid propellant gases are approximately 0.01, small Mach number approximations will be valid. Care must be taken here, however, because flow effects are the cause of the emitted sound.

The tube acoustics will obey the Helmholtz equation for the transform of

pressure

$$\nabla^2 p_\omega + k^2 p_\omega = 0 \tag{4}$$

The boundary conditions will assume that the tube side wall is hard and the end plate at x = 1 is characterized by a specific acoustic admittance. These boundary conditions are therefore

$$\left.\frac{\partial p_\omega}{\partial r}\right)_{x,a,\theta} = 0$$

$$\left.\frac{\partial p_\omega}{\partial x}\right)_{1,r,\theta} + i\, k\, \beta\, p_\omega(1,r,\theta) = 0 \tag{5}$$

Eqs. (4) and (5) are homogeneous; the forced oscillation will arise from an inhomogeneous boundary condition at x = 0.

The boundary condition at x = 0 consists of $\partial p_\omega/\partial x = 0$ over all of the tube wall excluding linearized, transformed continuity and axial momentum equations near $x = d_R \approx 0$.

$$i\,\omega\,\rho_\omega + \bar{\rho}\,\nabla\cdot\underset{\rightarrow}{v}_\omega + \bar{u}\,\frac{\partial p_\omega}{\partial x} = 0 \tag{6}$$

$$i\,\omega\,\bar{\rho}\,u_\omega + \bar{\rho}\,\bar{u}\,\frac{\partial}{\partial x}\,u_\omega = -\frac{\partial p_\omega}{\partial x} \tag{7}$$

Combining Eqs. (2), (3), (6) and (7), there results

$$-\frac{1}{\bar{p}}\,\frac{\partial p_\omega}{\partial x} = \gamma\,\bar{M}\left[-\frac{2ik}{\gamma}\left(\frac{p_\omega}{\gamma\bar{p}} + \sigma_\omega\right) + ik\,\frac{m_\omega}{\bar{m}} - \frac{1}{\bar{c}}\,\nabla_{r,\theta}\cdot\underset{\rightarrow}{V}_{\omega_a}\right] \tag{8}$$

where terms of $\theta(\bar{M}^2)$ compared with unity have been neglected. Moreover, the first and last terms on the right hand side of Eq.(8) may be neglected as being of $\theta(\bar{M})$ compared with unity. There results as the boundary condition

at $x = 0$,

$$\left.\frac{\partial P_\omega}{\partial x}\right)_{0,r,\theta} = 0 \quad \text{off of } S_p$$

$$\left.\frac{\partial P_\omega}{\partial x}\right)_{0,r,\theta} = -\, ik\bar{p}\,\gamma M\left[\frac{m}{\bar{m}}\frac{\omega}{} - 2\sigma_\omega\right]$$

$$\equiv -\, D_\omega\, ik\bar{p} \tag{9}$$

where D_ω is the transform of the complicated acoustic source. It is D_ω that is to be measured in the experiments. On the right hand side of Eq. (9) an $\bar{M}$ multiplies the source terms. This cannot be neglected precisely because it is the acoustic source. Previous neglect of terms of the order of $\bar{M}$ compared to unity only was made when derived quantities were being compared, not source quantities.

The solution to Eq. (4) subject to Eqs. (5) and (9) follows by standard acoustics methods.[6,7,8] It is, when evaluated at $x = \ell$, $r = a$ and $\theta = \tilde{\theta}$,

$$p_\omega(\ell, a, \tilde{\theta}) = \sum_{\substack{m,n=0 \\ \sigma = \pm 1}}^{\infty} \frac{\Psi_{mn}^{\sigma}(a,\tilde{\theta})}{i\, k_{mn}\, \Lambda_{mn}} \frac{F_{mn}(\ell)}{S}$$

$$\Psi_{mn}^{\sigma} = J_m(\varkappa_{mn} a) \begin{cases} \cos m\tilde{\theta} & \sigma = +1 \\ \sin m\tilde{\theta} & \sigma = -1 \end{cases}$$

$$k_{mn}^2 = k^2 - \varkappa_{mn}^2 \qquad \varkappa_{mn} J_m'(\varkappa_{mn} a) = 0$$

$$\Lambda_{mn} = \frac{1}{\epsilon_m}\left[1 - \frac{m^2}{(\varkappa_{mn} a)^2}\right] J_m^2(\varkappa_{mn} a) \qquad \begin{aligned} \epsilon_0 &= 1 \\ \epsilon_m &= 2 \quad m > 0 \end{aligned}$$

$$F_{mn} = + \frac{ik\bar{p}}{\dfrac{k}{\bar{k}_{mn}}} \frac{\delta_\omega \; S_p}{\beta_{mn} \cos k_{mn}\ell + i \sin k_{mn}\ell}$$

$$\delta_\omega = \frac{1}{S_p} \int_{S_p} D_\omega\, \Psi_{mn}^{\sigma}(r,\theta)\, dS \tag{10}$$

Equations (10) show the familiar phenomenon of cut-off whereby at sufficiently low frequency the transverse modes are not propagational. In such a case the plane wave mode is dominant and the solution simplifies to

$$k = k_{oo} \qquad \varkappa_{oo} = 0$$

$$p_\omega(\ell) = \frac{\bar{p}}{S} \frac{S_p \int D_\omega \, dS}{\beta_{oo} \cos k\ell + i \sin k\ell} \tag{11}$$

It is also to be noted that in the experiment $S_p << S$ and the propellant is on the axis. Since $\Psi_{mn}^{\sigma}(0,\theta) = 0$ for $m \neq 0$, only the symmetric transverse modes will be substantially excited. This will justify a later experimental procedure of only accounting for the plane and purely radial modes of the tube. Since $\Psi_{o,n}(0,\theta) = 1$, $\delta_\omega \approx S_p \int D_\omega \, dS$ for all modes.

In Eq. (11) resonances can clearly be identified near $\sin k\ell = 0$ as shown in Fig. 3. Note, however, that near minima $\cos k\ell \approx 0$, and the result is independent of β_{oo}. This is used to advantage in the data reduction procedure. From Fig. 3 if a line is drawn connecting the minima in the power spectrum, then the amplitude of the source term at a given frequency is

$$\delta_\omega \approx \int_{S_p} D_\omega \, dS = \frac{S \, p_\omega(\ell)_{min}}{\bar{p}}$$

Thus, the envelope formed by the line drawn through the minima represents the deduced power spectrum of the propellant in the absence of tube effects.

To correct for the speed of sound effect, for propellants which have their gas phase speed of sound different from the tube pressurization gas speed of sound, note that Eq. (9) is valid with k based upon the propellant gas speed of sound. In the limit that the propellant shrinks to a point source, Eq. (4) subject to Eqs. (5) and (9) is still the appropriate acoustics problem

but with k in Eq. (4) based upon the pressurization gas speed of sound. Tracing through the solution the net effect is to place a factor of $\bar{c}/\bar{c}_p$ in the right hand side of Eq. (11). Then constructing the one sided spectral density of the pressure,

$$G_p = \frac{S_p^2 \bar{p}^2 \bar{c}^2 G_\delta}{S^2 c_p^2 \left[\sin^2 k\ell + \beta_{oo}^2 \cos^2 k\ell + \beta_{oo} i \sin 2k\ell \right]} \tag{12}$$

is the formula used in the data reduction procedure when only the plane wave mode is present. It will later be seen that a quantity which is a property of the propellant alone is $\hat{G}_\delta = S_p G_\delta$, and this will be used in what follows.

Audible Theory - Propellant in Free Space

Another way to present the data is to present an acoustic efficiency when radiating to free space. This is the method often used for other flame noise radiation studies. If the flame were radiating to free space and the source dimension is small compared with a wavelength, the solution at distances far from the source is

$$p_\omega = \frac{e^{-ikr}}{4\pi r} \; i \frac{\omega}{\bar{c}_p} \bar{p} \int_{S_p} D_\omega \, dS$$

with a one sided spectral density given by

$$G_p = \frac{1}{(4\pi r)^2} \left(\frac{\omega}{\bar{c}_p} \right)^2 \bar{p}^2 S_p \hat{G}_\delta \tag{13}$$

The mean square value of the acoustic pressure is

$$\langle p'^2 \rangle = \int_0^\infty G_p \, d\omega$$

and the acoustic power is

$$P = 4\pi r^2 \frac{\langle p'^2 \rangle}{\bar{\rho} \bar{c}}$$

An acoustic efficiency is defined as

$$\eta = P/\dot{m}\,\dot{r}^2 \tag{14}$$

which is also used in the data reduction. $\hat{G}_\delta$ is determined from experiment and Eq. (11), and Eqs. (12) and (13) are used to construct the free space radiation properties.

Ultrasonic Theory

Acoustic emissions can be broadly defined as stress wave emissions propagating within a solid material in response to some type of loading. The emission levels are generally well below those associated with audible disturbances and for many materials are on the order of microbars.

The temporal characteristics of the emissions may range from continuous to pulsatile although a burst type activity is commonly observed in materials studies. From the earliest investigations into the acoustic emission phenomenon to the present (for summaries see Refs. (9,10)), attention has been directed primarily to the amplitude characteristics of basically impulsive signals. The most popular technique has been to use a piezoelectric ceramic disc encapsulated in an epoxy shoe. Each time an emission stress wave is received, a proportional electrical charge is produced on faces of the ceramic. Unfortunately, most elements exhibit strong mechanical resonances in the range from 100 kHz to 1 MHz and consequently the commonly observed electrical output is a ringing type response at one or more of these natural frequencies. This is satisfactory for event detection where frequency of occurence (and the location) of an event are of prime importance. The approach is also useful when an analysis of the emission energy per event is performed. On these grounds, acoustic emission analysis has been successfully employed for flaw location in pressure vessels and other structures, weld inspection, fatigue studies and fracture mechanics in metals and composite fibrous materials.

Deflagrating solid propellants produce much more of a uniform acoustic emission level with little pulsable behavior noted above. Consequently it is more useful to consider the emissions as realizations of a random process with energy distributed over a broad frequency band. The approach taken in the present study involved a combination of both spectral and temporal techniques best

suited to the continuous type acoustic emission signal observed during deflagration. The auto power spectrum provided the means to study the frequency distribution of power in the signal. This type of analysis was performed on digitized sample records of the recorded signal. In addition, an analog circuit was designed to provide a simultaneous rms acoustic emission signal (averaging time adjustable) whose spectral content and temporal behavior were analyzed.

Study of the ultrasonic emission spectrum must, at present, be general in nature for basically three reasons. First, the general meaning of the spectrum has yet to be formulated in any area of study. For solid propellants the inability to precisely define the propellant acoustical properties and its inhomogeneity greatly complicate data interpretation. Secondly, a suitable acoustic emission transducer with adequate bandwidth and relatively uniform response above 100 kHz is unavailable. Finally, frequency dependent attenuation of the waves caused by their dispersive propagation through the propellant and signal distortion produced by reflection at interface complicates data interpretation.

To account for the lack of flat transducer response on the spectral analysis, a transducer calibration spectrum was used to correct the measured spectra. At the outset, a calibration curve determined by the manufacturer using an impulsive acoustic emission technique was used for this purpose. This curve shows a smooth behavior from about 50 kHz to the 300 kHz limit of the tape recorder.

In order to provide finer spectrum detail, an alternate qualitative calibration technique was used (Bell, Craig, Strahle). Instead of measuring the transducer output for a known input stress wave (pressure), the electrical impedance of the transducer was measured over the frequency range of interest.

Because of the reversible nature of the piezoelectric effect, the transducer's driven electrical impedance will generally show a strong qualitative

similarity to the actual stress wave calibration. The electrical impedance was measured for the as-mounted configuration and quantitatively matched at the peak response (near 100 kHz) to the absolute calibration wave furnished. The most notable difference was the presence of several small (1-3 dB) peaks near 180 kHz and above 300 kHz. Rolloff at 100 kHz for the "impulse" calibration reflects the rolloff of the preamp used by the manufacturer in this test.

The temporal characteristics are also affected by the nonhomogeneities and geometric irregularities in the transmission media. As a result, the received signal may bear little resemblance to the pressure wave produced at the emission source. Three mechanisms can be immediately noted:

(a) material dispersion in the viscoelastic, heterogeneous propellant

(b) geometric dispersion for a stress wave propagating in a prismatic bar

(c) attenuation due to acoustic impedance mismatch at material interfaces in the transmission path.

The first two are difficult to define quantitatively; however, qualitatively, geometric dispersion is most pronounced at wavelengths about equal to the corss-section dimensions of the propagation medium. Since the estimated wavelengths in the propellant at from 100 kHz to 1 MHz are much less than the typical strand cross sections used in the experiments, geometric dispersion should be small, but dispersion due to propagation through the heterogeneous material containing AP particles comparable in size to emission wavelengths will be larger.

Attenuation due to acoustic impedance mismatch will occur at the propellant-holder, the holder-end-plate, and the endplate-transducer interfaces (Figure 1). To a first approximation the overall attenuation for complex waves may be represented as:

$$\text{Attenuation} = \frac{2}{1 + \frac{\rho_2 c_2}{\rho_1 c_1}}$$

where ρ = density, c = wavespeed, and propagation is from 1 to 2. For the present experimental configuration, the net attenuation is approximately 0.0026 so that less than 1% of the energy at the source will arrive at the transducer element.

The temporal characteristics of the acoustic emissions were studied by analysis of the rms signal recorded simultaneously. Three aspects of the signal behavior can be examined in this way:

(a) Signal power as a function of burn time. During the deflagration, the propellant strand effective length is decreasing continuously so that the acoustic emission path length is changing accordingly. Changes in the rms level with time can therefore be related to attenuation characteristics or to burn rate effects.

(b) Propellant imperfections. Abrupt changes or irregular behavior in the rms signal are indicative of amomalies in the deflagration process. In the simplest arrangement, this can be used to determine burn times.

(c) Spectral properties. When the rms averaging time is adjusted to a sufficiently short period (less than the period of the highest frequencies of interest), it is possible to computed an auto power sepctrum for the rms signal.

The first technique can be used to determine the attenuation characteristics, and then in reverse, to estimate the emission source power as a function of propellant formulation and test conditions. The second technique has been employed by several groups (4,5) to determine the quality of a burn. The spectral properties of the rms signal can be computed over the audible range of frequencies by adjusting the rms averaging time to on the order of 100 measurements. In this way, a comparison between the audible and acoustic emissions can be

made. For example, if the acoustic emissions are affected by microscopic level changes in the burn rate, it would be anticipated that under conditions of strong feedback (eg. in a driven impedance tube or a "T" burner) peaks would appear in the rms spectra at the driving frequencies. On the other hand, if the audible emissions are largely the result of gas phase effects occuring at relatively large distances from the propellant surface, there would be little correlation with the rms acoustic emission spectra.

In order to provide a firmer basis for the exploratory work, several mechanisms were considered as potential sources for the measured emissions. They can be broadly grouped as:

(a) solid phase effects such as dislocation kinetics or crystal fracture,

(b) gas phase phenomena such as ignition transients or combustion kinetics.

Since for these tests, energy has been analyzed over a 50 kHz to 300 kHz band, the sources can be further grouped according to characteristic frequencies. Solid phase effects are commonly observed as sources for acoustic emissions in materials tests, however, the characteristic times are in the sub-micro-second range so that the major energy release would occur well above the present band (and outside the range of all but the most exotic equipment). Furthermore, should this energy excite individual particles to vibrate, the characteristic frequencies (AP particles, for example) would again fall above 1MHz.

Chemical kinetics times, on the other hand, are typically on the order of 10 microseconds so that energy in the 50kHz to 1MHz range can be anticipated. Three potential mechanisms can be hypothesized:

(i) Laminar flame moving through a small volume of fuel immediately above an AP particle,

(ii) AP ignition transient as the gas above a particle igniter,

(iii) Explosive ignition of a fuel-oxidizer mixture near the surface.

While the characteristic times are all comparable, the resultant pressure disturbances can range from about 50 to 5000 microbar at the transducer for the first two cases, or in the third case to more than 1 bar.

These general observations have been systematically explored in the present study and the observations and conclusions are reported on in the following sections.

IV. Results and Discussion

Burn Rate

The physical properties of the propellants tested are presented in Table 1. These propellants are basically hydroxyl terminated polybutadine - ammonium perchlorate (AP) with and without aluminum (Al) and some additives. Parameter variations are systematically made in AP size, aluminum coating (AFCAM), catalyst and percentage of binder.

The burn rates for combustion in nitrogen and helium are shown in Table 2 at mean chamber pressures of from five to 30 Atm. For the MC propellant series a mass weighted average of the particle sizes was taken. Although no direct observation of the burn rate was possible, it was determined from the onset and termination of the ultrasonic signals. Assuming a power law dependence on binder ratio F, pressure, speed of sound in the tube, and AP diameter, the burn rate obtained by regression analysis using the data in Table 2 is

$$\dot{r} \sim F^{-.83} \bar{p}^{.5} c_t^{.15} D_{AP}^{-.26}$$

By analysis of the cross correlation coefficients, the burn rate is essentially independent of the tube speed of sound, as expected. To within the scatter in the experimental results, an AFCAM coating does not significantly affect the burn rate. Introduction of the catalysts increases the burn rate from 50 to 100 per cent.

From the regression analysis, the burn rate decreases with increasing binder ratio and AP size. Increasing the pressure increases the burn rate.

Experimental Results for Audible Emissions

The combustion noise efficiency and half power frequency for those propellants for which reliable emission data were obtained are presented in Table 2. Although considerable effort was made to ensure consistent sample preparation, large variations in the combustion noise efficiency are evident which makes data

interpretation qualitative at best. The efficiency is computed by integrating the audible spectrum over the frequency range from 40 to 1000 Hz. These parameters were also obtained from 40 to 10,000 Hz using the analysis given in Section III which accounts for the transverse modes existing in the tube above the cutoff frequency of 2000 Hz. For tests conducted in nitrogen the data indicate that most of the noise is produced at frequencies above this value as shown in Fig. 5. To isolate the tube effects from the propellant noise spectra, tests were conducted using helium rather than nitrogen as the wave propagation medium since the speed of sound is greater in helium by a factor of 2.88. Therefore, the cutoff frequency is increased from two to approximately six kiloHertz. From Fig. 5 the effect of helium is to shift the entire power curve to the right. This type of behavior would occur if (1) the noise from the propellant is dependent upon the tube speed of sound or (2) the propellant emits essentially white noise and the spectral features are entirely tube dependent. Regardless of the cause, the analysis in Section III can be used above the cutoff frequency to determine the deduced freefield spectra. However, above this frequency the data are considered qualitative since, in the theoretical analysis in Section III, the propellant combustion noise is assumed to arise from a point source at the center of the tube and at the position $x = 0$. In reality the combustion is distributed over a finite area, the sample length is finite and, because of localized combustion on the surface of the propellant sample, the source may not coincide exactly with the tube axis. Thus, tangential modes could be excited above the cutoff frequency, so the spectral details could be attributed to the cuton of tangential modes rather than deflagration behavior. Because of these uncertainties, the data is presented only over the range from 40 to 2000 Hertz and η and $\omega_{\frac{1}{2}}$ computed over the range from 40 to 1000 Hz.

The deduced free field spectra for the MC, NT, and T propellant series' are presented in Figs. 6, 7, and 8 respectively. Certain spectral features are common to each propellant. First there is an overall decrease in power level from 100 to approximately 1000 $\pm$ 200 Hz for the tests run in nitrogen. Upon reaching a minimum at 1000 Hz, the power level increases again from one to two kiloHertz. The cause of this behavior is not known and attempts to relate this phenomenon to the tube acoustics have been unsuccessful. Secondly, the tests performed in helium yield power levels approximately 10db lower than the nitrogen runs over the frequency range from 100 to 2000 Hz.

For the aluminized propellants, the effects of propellant properties and pressurization gas on the measured spectra are presented in Fig. 6. Comparison of the curves for MC-177 burned in air and nitrogen indicates a 10 to 15 db rise in sound power level for the run with air. The difference in the results appears to be caused by aluminum afterburning. The effect of an AFCAM coating can be observed from comparison of the spectra for MC-170 and 172. The propellant without AFCAM has a slightly higher noise output over the frequency range from 200 to 2000 Hz.

Also shown on Fig. 6 are the burn-through frequencies computed from $\nu = \dot{r}/D_{AP}$ using the MC-170 burn rate for various AP and Al particle sizes. Because of variations in granularity, it is seen that the spectrum is rather densely occupied by available frequencies. No apparent correlation of the observed spectra with these frequencies is evident - either from the figures or from the half-power frequencies presented in Table 2. None was really expected to be clear because of the roughness of the estimate of frequency, the usual spread of particle size about the stated value and the dense population of the spectrum with these particle frequencies. Also the frequencies for the 200 and 400 μ particle sizes are below the rolloff frequency of the transducer system. Moving from

MC-170 to MC-177, which increases the mean particle size and decreases the burn rate (see Tables 1 and 2), there is a general decrease in the spectral power level from 100 to 2000 Hz.

In contrast to the aluminized propellants, the spectra for the non-aluminized NT series propellants, shown in Fig. 7, indicates a general increase in noise with decreasing particle size over the 1000-2000 Hz range. Comparison of the curves show a general increase in the sound levels from 300 to 2000 Hz probably caused by the higher burn rate of NT-4. Below 300 Hz no general trend can be ascertained. From 40 to 1000 Hz $\omega_{\frac{1}{2}}$ increases noticeably with decreasing particle size for NT-2 and NT-3 in nitrogen. However, the shift in the half power frequency is not as large as expected.

For the T series non-aluminized propellants, no general trend can be determined concerning the variation in the spectra with particle size. The binder to oxidizer ratio does appear to have an influence. There is an increase in power level from the 273 to the 81 micron particle sizes, possibly due to the increase in burn rate. However, a decrease of five to 10db in power level occurs for the propellant with the 48 micron particle size which has the lowest burn rate because of its relatively high binder to oxidizer ratio.

Comparison of Theory and Experiment

Because of the lack of any marked change in the shape of the power spectra with propellant composition, a regression analysis was performed to determine the dependence of the combustion noise efficiency η and half-power frequency $\omega_{\frac{1}{2}}$ on (1) percentage of binder F, (2) chamber pressure, (3) tube speed of sound, (4) AP particle diameter, and (5) burn rate. Including the area of the propellant in this analysis shows that η and $\omega_{\frac{1}{2}}$ are independent of this parameter, which is consistent with previous results.[8] The results of the regression analysis are presented in Table 3 and the following empirical relations are obtained

from 0 to 1000 Hz.

$$\omega_{\frac{1}{2}} \sim F^{.38}\ \bar{P}^{.09}\ C^{-.49}\ D^{-.07}\ \dot{r}^{-.19}$$

$$\eta \sim F^{-.5}\ \bar{P}^{-1.9}\ C^{-1.4}\ D^{-.16}\ \dot{r}^{-1.5}$$

The correlation coefficients given in Table 3 are an indication of the interdependence of the dependent and independent variables. A coefficient which has a magnitude of unity indicates complete dependence, whereas a value of zero means no dependence whatsoever. For the half-power frequency, the only relatively strong correlation is with the speed of sound; and little correlation exists with the other variables. There is a strong correlation between η and $\bar{P}$, C, and r.

From the frequency spectra and the data of Table 3, the experimental frequency content shows the curious behavior that it is invariant with virtually any parameter. It was initially thought that the low frequency content (0-1000 Hz) would correlate with particle burnthrough times ($D/\dot{r}$), whereas the high frequency content would correlate with gas phase reaction times (τ_r). Clearly, however, the frequency content in both the high and low frequency regimes appears to be caused by the same mechanism. Allowing that another relevant time might be a molecular diffusion time ($\mu/\rho D^2 p = \tau_d$), it is tempting to attempt a correlation of the form

$$\omega_{\frac{1}{2}} = 1/(\tau_r^a\ \tau_b^b\ \tau_d^c)$$

with $a + b + c = 1$ to preserve dimensional homogeneity. The reaction time, if one assumes a global single-step equivalent reaction, would take the form

$$\tau_r = K\ F^m\ p^{1-n}$$

Here n is the effective overall order of the reaction and the F^m factor is empirical to take into account the fuel mass fraction effects and temperature

effects in the Arrhenius factor. It is expected that $m<0$, since the propellants are fuel rich and an increase in F would lower the temperature and increase the reaction time. Since $\tau_d \propto 1/pD^2$ and $\tau_b = D/\dot{r}$, comparison with the 0 - 10,000 Hz empirical law from Table 3,

$$\omega_{\frac{1}{2}} \propto F^{.1}\, p^{-.1}\, c^{.2}\, D^{o}\, \dot{r}^{.1},$$

yields

$$a = .85 \quad b = .1 \quad c = .05 \quad m = 1.0 \quad n = 0.8$$

with similar results for 0 - 1000 Hz. These numbers are plausible, and, if the approach is correct, the frequency is primarily dependent upon the gas phase reaction time.

The empirical dependence upon the tube speed of sound may also be explained through the gas phase reaction time. Since the speed of sound was varied by using He instead of N2 as the pressurization gas and He has a very low molecular weight, the diffusion of He into the reaction zone may have affected the reaction rates.

All attempts at explaining the behavior of η have failed. At this time, therefore, the physical cause for makeup of the source term D_ω is unknown. Using an approach similar to that of Ref. 2, the η law may be coarsely explained by reasoning with Eq. (9). However, the agreement between theory and experiment is not as good as desired and those results will not be presented here.

Ultrasonic

Ultrasonic acoustic emission data were obtained for all propellants in Table 1 and consist of (1) power spectra and (2) rms amplitude plots taken during the course of the burn. In an effort to determine a relation between the physical properties of the propellant and the spectral features, the effect of the following variables on the spectral data are investigated: (1) AP particle size,

(2) pressurization gas, (3) aluminum particles, (4) AFCAM coating, and (5) catalyst. In addition, the chamber pressure was varied from 20 to 50 Atm, and the corresponding spectra were studied to gain insight into the nature of the source characteristics. The details of the data reduction methods are given in Ref. 6.

While a satisfactory explanation for the emission power spectra has not been formulated in all cases, there are nonetheless certain features that are present in all spectra regardless of the propellant type. During the ignition and burnout transients, the emission level is abnormally high and the spectra considerably distorted. In between, the signal exhibits stationary properties and an ensemble averaged estimate of the power spectrum can be calculated. Figures 9 through 13 show power spectra computed this way using from 260 to 1000 averages each. Each spectrum is characterized by large power around 100 kHz with secondary peaks between 175 and 200 kHz. The secondary peak was also observed in an earlier study[4] at Princeton at pressures on order of magnitude higher than for the present work. In almost every test to date, a mild nonstationary character was observed in the spectrum with the noise power over the 200-300 kHz range smoothly increasing during the course of the burn as shown in Fig. 14. This behavior is most likely due to the dispersive attenuation of the stress waves as they pass through a decreasing length of propellant before arriving at the transducer.

In general agreement with the Princeton work, the ultrasonic emission power spectra when corrected for background noise and transducer response tend to exhibit no readily distinguishable features which could be used to recognize a particular propellant. A more detailed discussion for each property considered follows:

AP Particle Size. For the nonaluminized propellants AP particle size has little effect on either the overall sound power level or the location of the peaks in the spectrum as shown in Fig. 9. Based on these data no correlation appears to exist between the spectral peaks and the particle size. Since in the T series propellants the particle sizes and mixing were carefully controlled to ensure uniformity of size and distribution, the lack of any pronounced effect on the spectra cannot be attributed to nonuniformities in propellant preparation.

Effect of Pressurization Gas. The burning of MC-177 in air as opposed to nitrogen products a definite shift in both spectral peaks and peak power as shown in Fig. 10. In air there is a stronger high frequency content than in nitrogen. There is also a general smoothing of the spectra for air at the frequencies below 125 kHz. These effects are most probably caused by aluminum afterburning although correlation between the spectral peaks and the combustion process is presently not clear.

Aluminum Particle Addition. As shown in Fig. 9, AP particle size does not have a pronounced effect on the spectra of the acoustic emissions. However, the addition of aluminum does. Comparison of the spectra for aluminized (MC-177) and nonaluminized (NT-2) propellants in Fig. 11 indicate markedly different spectral features. The spectrum of the aluminumized propellant has a large noise content at the low frequency range below 125 kHz. Also, the peaks in the aluminized propellant spectrum are more distinct in the 125 to 225 kHz range. Above 225 kHz. however, relatively little difference is apparent in the two spectra. Whether the cause of the differences is the emission source itself or propagation of the ultrasonic waves through the aluminized nonaluminized propellant cannot be ascertained.

Effect of AFCAM Coating. As reported in Ref. 6 there was a general increase in overall sound power when the aluminum is coated with AFCAM for MC-177 and MC-178. This trend is not exhibited for MC-170 and MC-172 as shown in Fig. 12, although the spectral peaks are different.

Effect of a Catalyst. In Fig. 13 catalyzed MC-173 and MC-179 propellants are compared to an uncatalyzed MC-170. The most distinct effects of a catalyst are evident in the overall sound power level and relative noise content.

Variation of the Spectra during Deflagration

Typical variations in the spectra taken at different times during a burn are shown in Fig. 14 for MC-170. The two most noticeable differences with time are relatively high acoustic emission levels below 100 kHz during ignition and a relative increase in noise content at the higher frequencies with increasing time. This trend is shown quantitatively by the shift to higher values in half-power frequency as the burn progresses. General spectral features, however, remain essentially unchanged from 100 to 300 kHz. The broad peak about 125 kHz and the secondary peak between 175 and 200 kHz are evident throughout the burn.

Effect of Chamber Pressure on the Acoustic Emission Spectra

The effect of increasing the chamber pressure is to increase the overall sound power levels as shown in Fig. 15. However, no marked change in the spectral features is observed for either the aluminized or non-aluminized propellant.

Source Characteristics. Based on the earlier observations reported in Ref. 6, it was strongly suspected that the AP deflagration mechanism was primarily responsible for the observed emission spectra. The consideration summarized in Section III of this paper provide a crude theoretical basis for this hypothesis as well. The rms acoustic emission levels at the transducer consistently range between about 800 to 3500 μ Bar. These levels are somewhat above the range for

the laminar flame model but are generally consistent with the AP ignition transient model. The chemical kinetics times associated with both of these processes are on the order of 10^{-5} sec so that the accompanying unsteady pressures would be expected to show relatively larger spectral energy content near 100 kHz. Again, this is consistent with the earlier observations of a large peak in the emission power spectra around 100 kHz. Furthermore, since these characteristic times should be only weakly affected by pressure and unaffected by AP size, the principal alteration in the emission spectra should be a change in the relative height of the 100 kHz peak as AP sizes and burn rates are varied. In this case, the change in level is associated with the changing source areas.

Unfortunately, as shown in Fig. 9, there is no clear difference in the shape or level of the emission spectra as the AP size is varied from 50 μ to 200 μ (NT series) although the level of the spectra increases in the 100 - 300 kHz range for the T series as the particle size decreases. The spectra show some fine structure but are basically flat within the tolerance of the calibration curve used. On the other hand, as shown in Fig. 11, it is much more likely that the observed peak at 100 kHz can be attributed to the Al present in the more complex MC propellants. This possibility has not yet been fully explored in tests to date, although several comments might be made. From the levels involved, the signals would likely be produced before the Al agglomerates have left the burning surface (there is some indication, however, that the peak may be due to Al particle impact on the inner tube wall, although a neoprene rubber sheet is used to line the tube and minimize this effect.) Emissions from the solid phase Al due to dislocation activity or micro-fracture are well above the 100 kHz range. Propellants with a range of Al sizes and quantities will have to be tested in order to further clarify these observations. For example, insensitivity to Al size could indicate a

source mechanism associated with the agglomerate phase.

In addition to spectral analysis, the rms levels of the ultrasonic emissions have also been obtained. In Fig. 16, a comparison between the rms level of tests conducted with NT-2 is presented. During one of the tests the burn rate of the NT-2 was abnormally high. The corresponding ultrasonic emission levels are significantly higher and exhibit much greater variations with time than the propellant with the low burn rate. These data are in agreement with the observations reported in Ref. 5 in a similar study conducted at Princeton. The Princeton group found that, for propellants with abnormally large mean burn rate deviations, an increase in both the level and unsteadiness of the acoustic emissions was observed. They conclude that such information can be of use in diagnosing the quality of the burning and, thus, of the propellants.

To confirm these conclusions, the behavior of the rms levels was investigated in the present study. To systematically evaluate the use of the emission levels as a diagnostic aid, three tests were conducted with MC-177 with flaws intentionally added. The first consisted of a half-inch slit in the center of the propellant parallel to the centerline of a ¼" by ¼" strand. The next flaw consisted of a 1/16" - diameter hole drilled through the center of the strand perpendicular to the centerline. In the last test two such holes were drilled one inch apart. The results of these tests are presented in Fig. 17. In all three tests the presence of the flaws are characterized by an abrupt increase in the rms levels. The large amplitude at the initiation of the burns is attributed to the igniter paste and typically lasts for approximately one second. The large increase in amplitude at the termination of the burns is caused by the burning of the epoxy which holds the propellant strand to the mounting plate.

These anomalous fluctuations in the rms levels were also observed in the nonaluminized propellants as shown in Fig. 18 for T-81. Upon examination of

the propellant, spherical cavities caused by bubbles in the manufacture of the propellant were observed and are probably responsible for the sharp increase in rms level which occur at various times during the burn. It appears, then, that the ultrasonic rms emission can be used to reliably detect irregularties in the propellant.

As shown in Figs. 19 and 20 the rms levels strongly depend upon the chamber pressure over the range from 5 to 30 Atm and the particle size. The general increase in the rms acoustic emission levels with chamber pressure shown in Fig. 19 may be caused by the alteration of the combustion zone and/or the increasing burn rate. In Fig. 20 the rms levels are seen to be definitely dependent upon AP particle size and increase in magnitude with decreasing size. Although the burn rate decreases for the 48 micron particle size because of a large binder percentage (30% vs. 15% for T-273 and 16.9% for T-81), the acoustic emission level is the highest. Thus, in addition to the level being a function of burn rate, as reported in Ref. 5, it is also a strong function of AP particle size.

In the final study conducted under this contract, a coherence analysis was performed between the audible signal and the rms fluctuations of the acoustic emissions. The results are shown in Fig. 21 for MC-170. Two hundred samples were taken over the course of the burn and the spectral averages of the audible and ultrasonic signals are presented. Although the rms fluctuations are on the same time scale as the audible signal, the coherence between the two is statistically insignificant.

V. Conclusions

Audible Emissions

1. The source of the audible output in the range 0-1000 Hz is presently unknown. Theories are presented to explain the behavior of the frequency and noise emission levels. The frequency appears to be primarily dependent on the gas phase reaction time; however, all attempts to explain the behavior of the combustion noise efficiency have been somewhat unsuccessful.

2. The strength of the audible signal is insufficient to account for the roughness levels in the rocket motor chamber pressure observed in practice. Therefore, some other causes must be responsible.

3. The main frequency content of the audible output appears to be between 3-10 kHz in nitrogen, and the signal is not altered by the variables investigated in the lower frequency range. It is currently conjectured that gas phase kinetic phenomena are responsible, but the high frequency content does not appear useful for combustion diagnostics.

Ultrasonic Signal

1. The ultrasonic spectra in the range 50-300 kHz are insensitive to propellant variables and are relatively flat. Overall emission spectral features are not sufficiently distinct to identify either a propellant or its deflagration characteristics from its acoustic signature alone.

2. The rms ultrasonic emission signal is a useful indicator of propellant flaws, bad burns, and propellant burn times. It is also a function of chamber pressure and AP particle size. Increasing the pressure and decreasing the particle size increases the rms signal.

3. The rms signal fluctuates on the time scale of the audible signal but is found incoherent with the audible signal. While it is suspected that both signals are causally related through the burn rate, the complex propagation path of the ultrasonic signal probably destroys phase coherence.

While the general tone of the conclusions appears negative, it must be pointed out that spectral analysis of acoustic emission signals in many other fields has been notably unsuccessful. The work reported here has improved the measurement techniques over previous studies, primarily by simplifying the transmission path from propellant to transducer response. In the time domain, the rms emission levels can be used to accurately measure burn times and to detect irregularities in the delfagration. It now appears that features in the rms signal may prove of more value as a diagnostic tool.

VI. Nomenclature

c	speed of sound
D	source function defined by Eq. (9)
d_p	width of propellant sample
d_R	length of gas phase reaction and mixing zone
G	one sided spectral density
k	wavenumber
ℓ	tube length
ℓ_p	mean particle size
M	Mach number
$\dot{m}$	total mass flow rate
m	mass flow rate/unit area
p	pressure
r	radial coordinate
$\dot{r}$	burn rate
S	tube area
S_p	propellant area
S_{cor}	area of correlated elements on the propellant surface
u	axial velocity
$\underrightarrow{v}$	vector velocity
x	axial distance
β	dimensionless specific acoustic admittance
γ	ratio of specific heats
δ	source function, $\int_{S_p} D \, dS$

η	acoustic efficiency
θ	angular coordinate
$\varkappa$	eigenvalue
λ	wavelength
ν	frequency
ρ	density
σ	entropy fluctuation
Ψ	eigenfunction
ω	angular frequency
$\nabla_{r,\theta}$	"del" operator in r and θ directions
$< >$	time mean operation

Superscripts

$'$	perturbation quantity
$-$	mean quantity

Subscripts

a	acoustic or dilatational part
mn	mn^{th} mode
p	pertaining to pressure or propellant gases
v	vortical or rotational part
δ	pertaining to δ
ω	Fourier transform

VII. References

1. Strahle, W. C., "Some Results in Combustion Generated Noise," Journal of Sound and Vibration, 23, 113-125, 1972.

2. Strahle, W. C. and Shivashankara, B. N., "A Rational Correlation of Combustion Noise Results from Open Turbulent Premixed Flames," Fifteenth Symposium (International) on Combustion, The Combustion Institute, Pittsburgh, 1974, pp. 1379-1385.

3. Strahle, W. C., and Shivashankara, B. N., "Combustion Generated Noise in Gas Turbine Combustors," Journal of Engineering for Power, Vol. 98, No. 2, April 1976, pp. 242-246.

4. Saber, A. J., Johnston, M. D., Caveny, L. H., Summerfield, M., and Koury, J., "Acoustic Emissions from Burning Solid Propellant Strands," 11th JANNAF Combustion Meeting, CPIA Publication No. 261, December 1974, pp. 409-428.

5. Caveny, L. H., Saber, A. J., and Summerfield, M., "Propellant Combustion and Burning Rate Uniformity Identified by Ultrasonic Acoustic Emissions," J. Spacecraft and Rockets, Vol. 14, No. 7, July 1977, pp. 434-437.

6. Craig, J. I., Strahle, W. C., and Palfrey, J., "Audible and Ultrasonic Acoustic Emissions from Composite Solid Propellants," AFOSR-75-2805, July 1975.

7. Morse, P. M. and Ingard, K. U., Theoretical Acoustics, Mc-Graw Hill, New York, 1964, Chapter 9.

8. Bell, W. A., Craig, J. I., and Strahle, W. C., "Study of Unsteady Combustion of Heterogeneous Solid Propellants by Analysis of Acoustic Emissions," AIAA Paper No. 77-15, Presented at the 15th Aerospace Sciences Meeting, Los Angeles, CA, January 1977.

9. Acoustic Emission, American Society of Testing and Materials, Special Technical Publication, STP-505, Phila., 1972.

10. Dunegan, H. L., and Harris, D. O., "Acoustic Emission Technique," Experimental Techniques in Fracture Mechanics, ed. A. S. Kobayashi, SESA Monograph No. 1, Iowa State Univ. Press, p. 38, 1973.

VIII. Tables

Table 1. Physical Properties of the Propellants Tested

Specimen	R-45M	AP Size	AP %	Al	Dioetyl dipate	Indopol	IPDI	Catalysts
MC-170	9.31%	200 μ 14 μ 6 μ	26.8 20.4 20.8	20% 5 μ		2%	0.69%	
MC-172	9.31%	200 μ 14 μ 6 μ	26.8 20.4 20.8	20% 5 μ AFCAM		2%	0.69%	
MC-173	9.31%	200 μ 14 μ 6 μ	26.8 20.4 20.8	20% 5 μ	2%		0.69%	Fe_2O_3 2%
MC-179	9.31%	200 μ 14 μ 6 μ	26.8 20.4 20.8	20% 5 μ	2%		0.69%	Copper fluoride 2%
MC-174	10.24%	6 μ 0.5 μ	26 40	20% 5 μ		3%	0.76%	
MC-175	10.24%	6 μ 0.5 μ	26 40	20% 5 μ AFCAM		3%	0.76%	
MC-177	9.31%	400 μ 200 μ 50 μ	44 18 6	20% 5 μ		2%	0.69%	
MC-178	9.31%	400 μ 200 μ 50 μ	44 18 6	20% 5 μ AFCAM		2%	0.69%	

Table 1. Physical Properties of the Propellants Tested (Cont'd)

Specimen	R-45M	AP		Al
		Size	%	
NT-2	20%	200 μ	80	0%
NT-3	20%	90 μ	80	0%
NT-4	20%	50 μ	80	0%
T-273	15%	273 μ	85	0%
T-81	16.9%	81 μ	83.1	0%
T-48	30%	48 μ	70	0%

Table 2. Burn Rates, Combustion Efficiency, and Half-Power Frequency for the Propellants Tested over the Range of Frequencies from 40 to 1000 Hertz.

MC SERIES

Specimen	Percentage of Binder	Chamber Pressure (ATM)	Tube Speed of Sound (Relative)	AP Diameter (Microns)	Burn Rate (in/sec)	Half-Power Frequency (Hertz)	$P/(\dot{m} r^2)$ (Dimensionless)
MC-170	12	20	1	83	.432	237	.241
MC-170	12	20	1	83	.360	153	.947
MC-172	12	20	1	83	.416	223	.174
MC-172	12	20	1	83	.424	236	.0067
MC-173	12	20	1	83	.620	211	.0746
MC-173	12	20	1	83	.768	218	.308
MC-174	14	20	1	2.4	.936	400	.0111
MC-174	14	20	1	2.4	.597	222	.105
MC-175	14	20	1	2.4	.752	310	.121
MC-175	14	20	1	2.4	.920	214	.0591
MC-177	12	20	1	316	.176	211	.383
MC-177	12	15	1	316	.178	220	.270
MC-177	12	5	1	316	.123	164	9.75
MC-177	12	10	1	316	.153	359	1.28
MC-177	12	20	1	316	.212	293	.0987
MC-177	12	25	1	316	.217	211	.0839
MC-177	12	30	1	316	.241	183	.0622
MC-178	12	20	1	316	.237	322	.206
MC-179	12	20	1	83	1.37	-	-
MC-179	12	20	1	83	.677	361	.273

Table 2. Burn Rates, Combustion Efficiency, and Half-Power Frequency for the Propellants Tested over the Range of Frequencies from 40 to 1000 Hertz.

NT SERIES

Specimen	Percentage of Binder	Chamber Pressure (ATM)	Tube Speed of Sound (Relative)	AP Diameter (Microns)	Burn Rate (in/sec)	Half-Power Frequency (Hertz)	$P/(\dot{m} r^2)$ (Dimensionless)
NT-2	20	20	1	200	.200	217	.481
NT-2	20	20	1	200	.221	222	.081
NT-2	20	20	2.88	200	.223	151	.0552
NT-2	20	5	1	200	.0974	282	5.18
NT-2	20	10	1	200	.140	405	1.05
NT-2	20	15	1	200	.171	321	.274
NT-2	20	20	1	200	.202	264	.150
NT-2	20	25	1	200	.217	265	.0899
NT-2	20	30	1	200	.258	176	.0435
NT-2	20	20	1	200	.222	296	.223
NT-3	20	20	1	90	.358	326	.0181
NT-3	20	20	2.88	90	.297	129	.0325
NT-3	20	20	2.88	90	.310	101	.0127
NT-3	20	20	1	90	.290	364	.0800
NT-4	20	20	2.88	50	.331	335	.0233
NT-4	20	20	2.88	50	.331	224	.0249
NT-4	20	20	2.88	50	.358	84	.0255
NT-4	20	15	2.88	50	.308	54	.0560
NT-4	20	30	2.88	50	.441	147	.00598
NT-4	20	23	2.88	50	.378	282	.0209

Table 2. Burn Rates, Combustion Efficiency, and Half-Power Frequency for the Propellants Tested over the Range of Frequencies from 40 to 1000 Hertz.

T SERIES

Specimen	Percentage of Binder	Chamber Pressure (ATM)	Tube Speed of Sound (Relative)	AP Diameter (Microns)	Burn Rate (in/sec)	Half-Power Frequency (Hertz)	$P/(\dot{m} r^2)$ (Dimensionless)
T-81	16.9	15	1	81	.298	312	.369
T-81	16.9	10	1	81	.244	439	1.05
T-81	16.9	30	1	81	.476	307	.0558
T-81	16.9	20	1	81	.357	308	.674
T-81	16.9	5	1	81	.162	249	5.52
T-81	16.9	25	1	81	.408	312	.102
T-81	16.9	20	1	81	.394	347	.296
T-273	15	20	1	273	.325	200	.0775
T-48	30	20	1	48	.148	435	.435
T-48	30	20	1	48	.150	395	.451
T-48	30	20	1	48	.152	405	.329
T-273	15	20	1	273	.267	283	.139
T-48	30	20	2.88	48	.158	498	.0683
T-273	15	20	2.88	273	.294	421	.0736

Table 3. Results of the Regression Analysis Using the Data from Table 2.

Variable	Definition
x_1	Percentage of binder
x_2	Chamber pressure
x_3	Chamber sound speed
x_4	AP particle diameter
x_5	Burn rate
x_6	Dependent variable - $\omega_{\frac{1}{2}}$ or η

$$\omega_{\frac{1}{2}},\ \eta \sim (x_1)^a\ (x_2)^b\ (x_3)^c\ (x_4)^d\ (x_5)^e$$

Cross Correlation Coefficient	Frequency Range			
	0-1000 Hz		0-10 kHz	
	$\omega_{\frac{1}{2}}$	η	$\omega_{\frac{1}{2}}$	η
R_{16}	.154	-.097	.340	.082
R_{26}	-.054	-.742	.198	-.622
R_{36}	-.409	-.510	.855	-.643
R_{46}	-.050	.288	-.047	.431
R_{56}	-.148	-.600	.123	-.717
a	.38	-.50	.14	2.9
b	.09	-1.9	-.06	-2.8
c	-.49	-1.4	.24	-4.1
d	-.07	.16	.04	.38
e	-.19	-1.5	.13	-1.6

IX. Figures

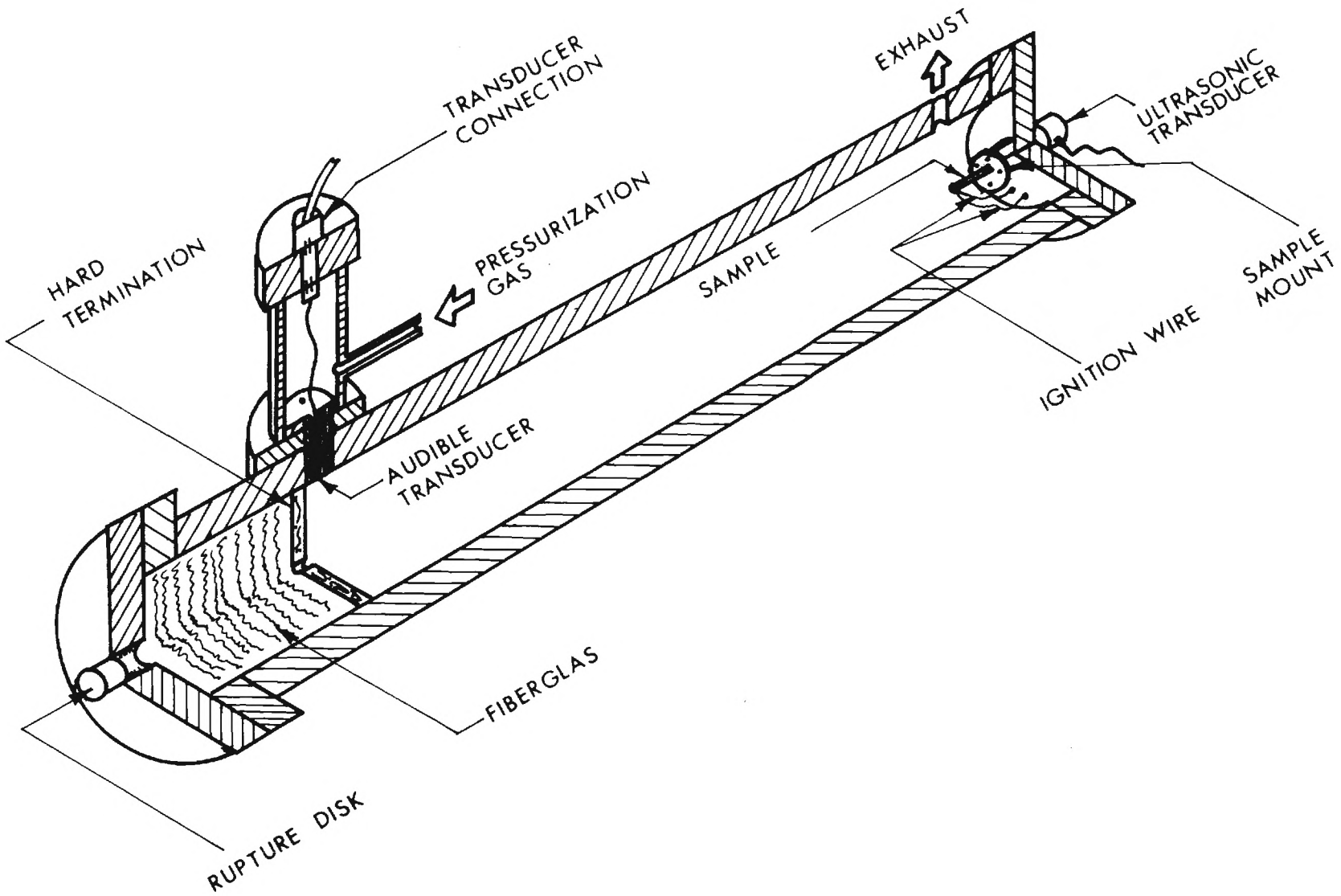

FIGURE 1. SCHEMATIC OF DEFLAGRATION TUBE.

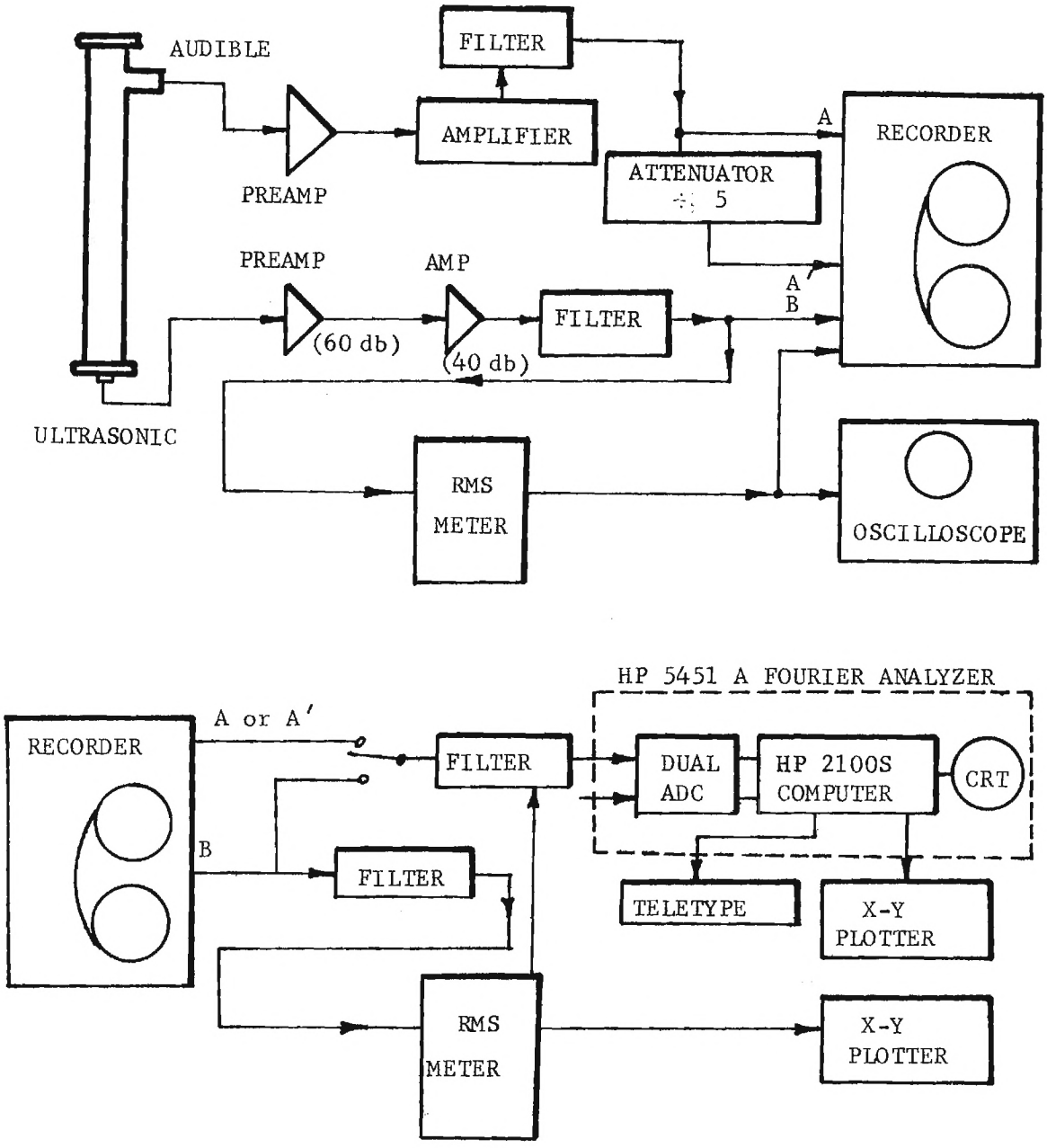

FIGURE 2. DATA ACQUISITION AND ANALYSIS SCHEMATIC

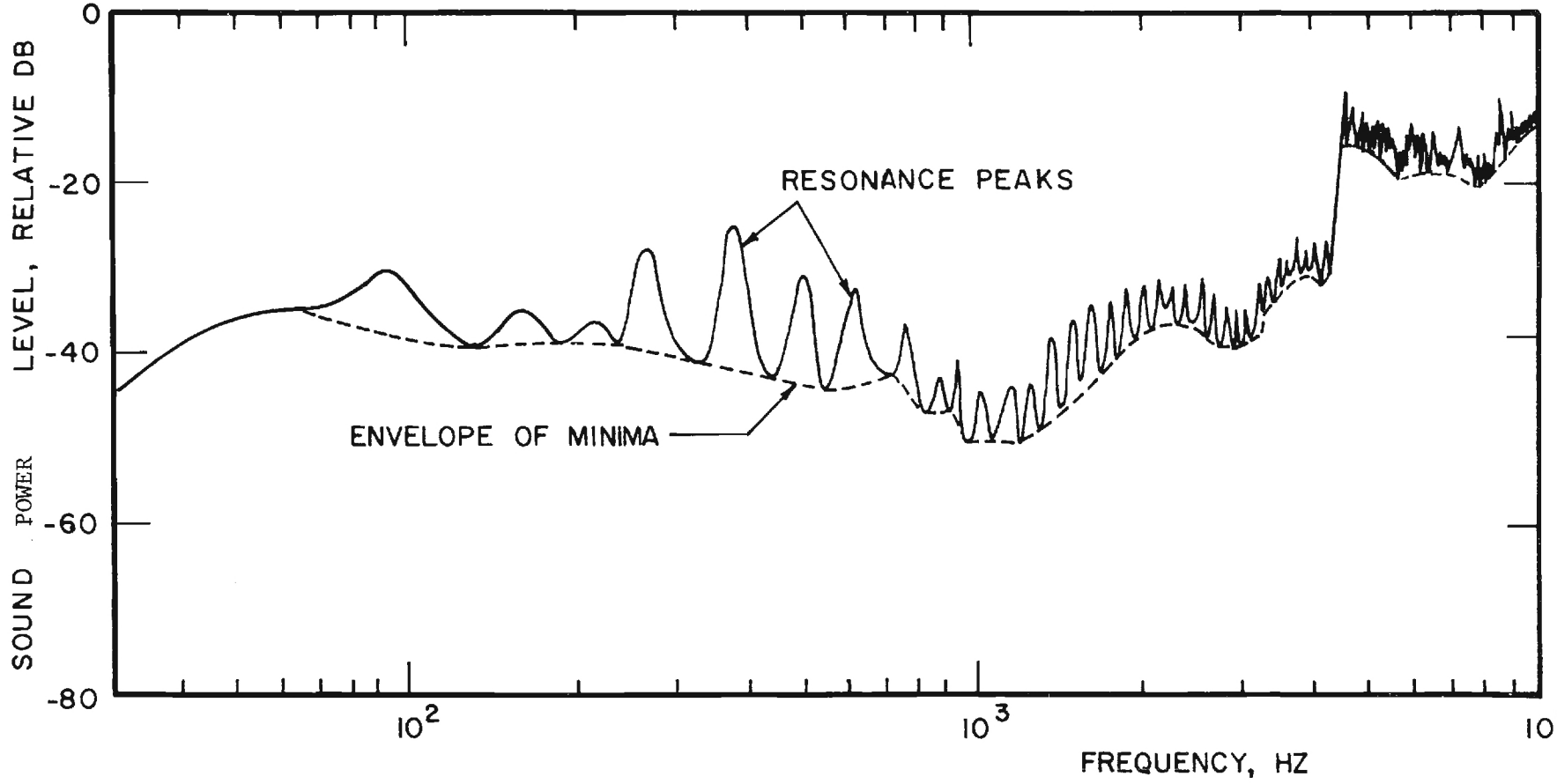

FIGURE 3. RAW SPECTRUM FOR NT-2 BURNING IN NITROGEN AT 300 PSIA.

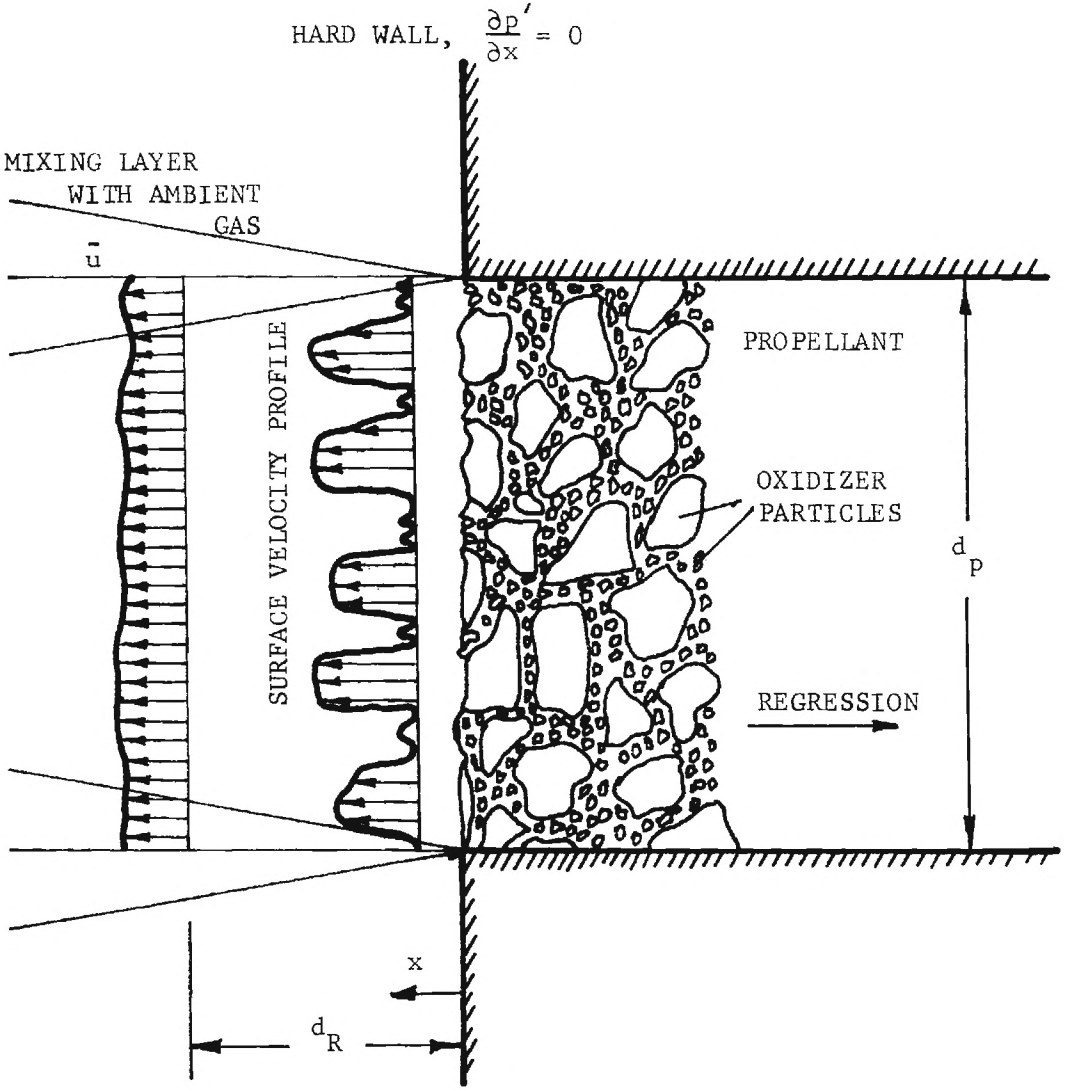

FIGURE 4. DIAGRAM OF THE COMBUSTION REACTION ZONE

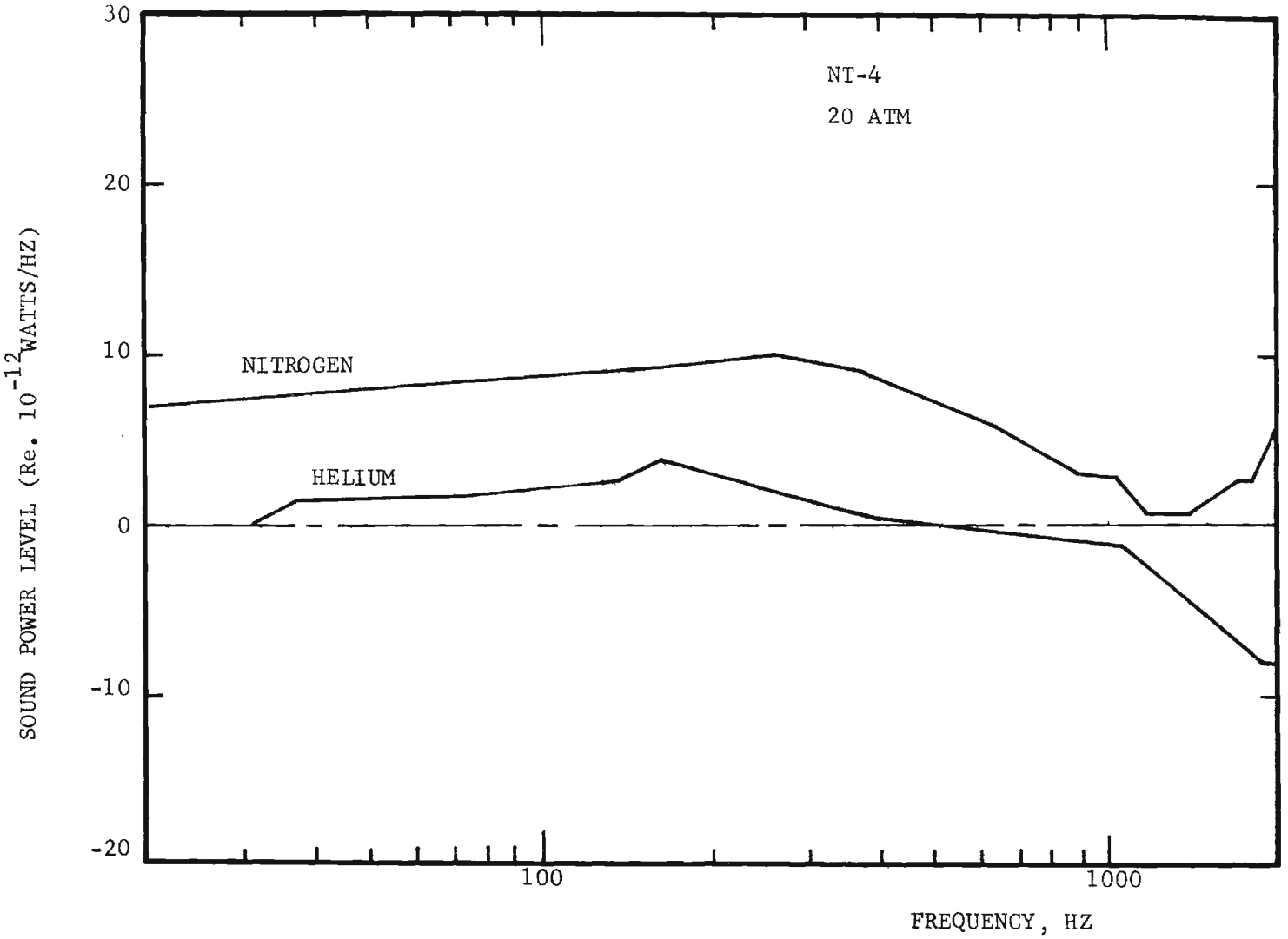

FIGURE 5. EFFECT OF CHAMBER GAS ON DEDUCED FREE FIELD POWER SPECTRUM

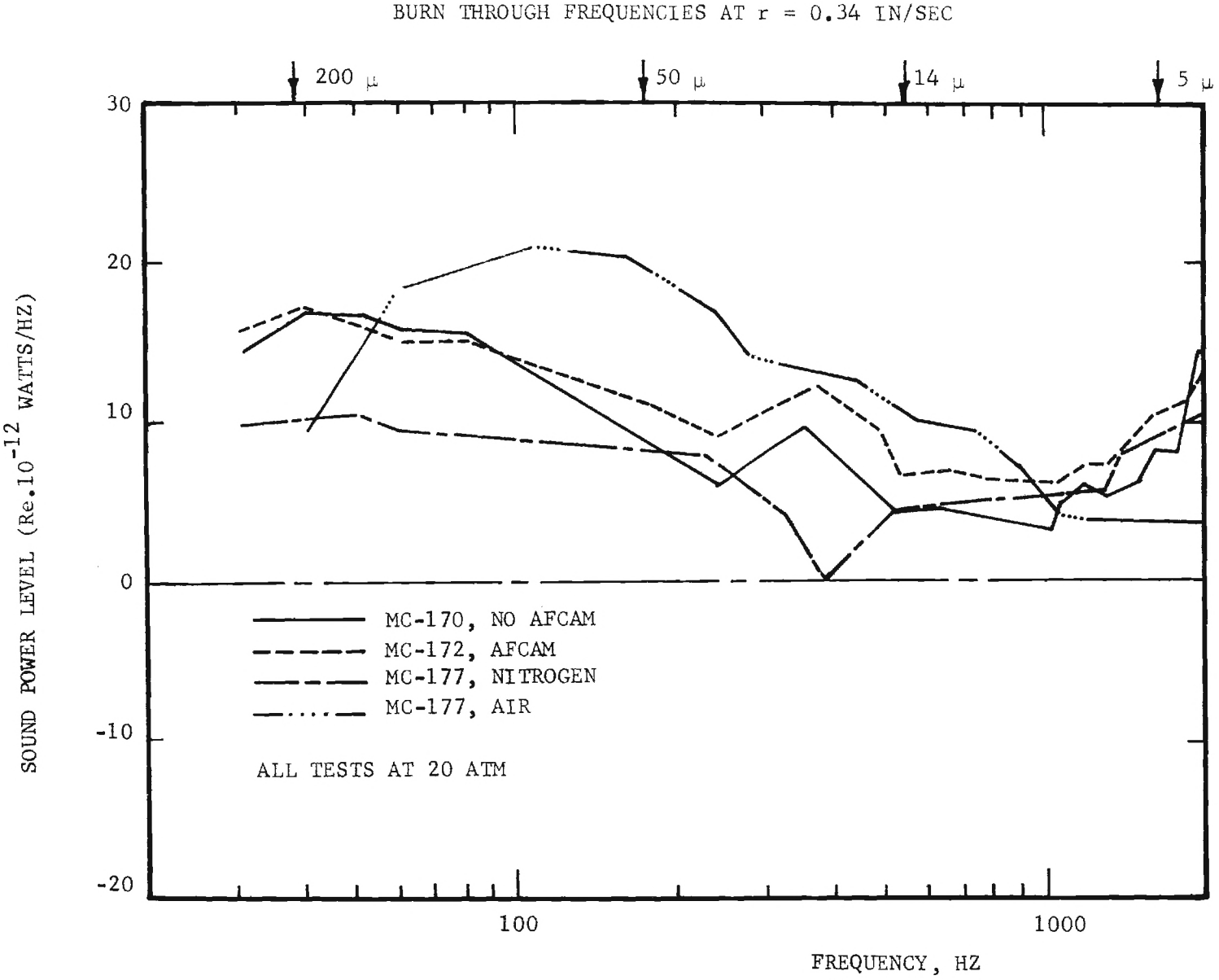

FIGURE 6. EFFECTS OF AP PARTICLE SIZE, AFCAM TREATMENT, AND CHAMBER GAS ON DEDUCED FREE FIELD SPECTRA.

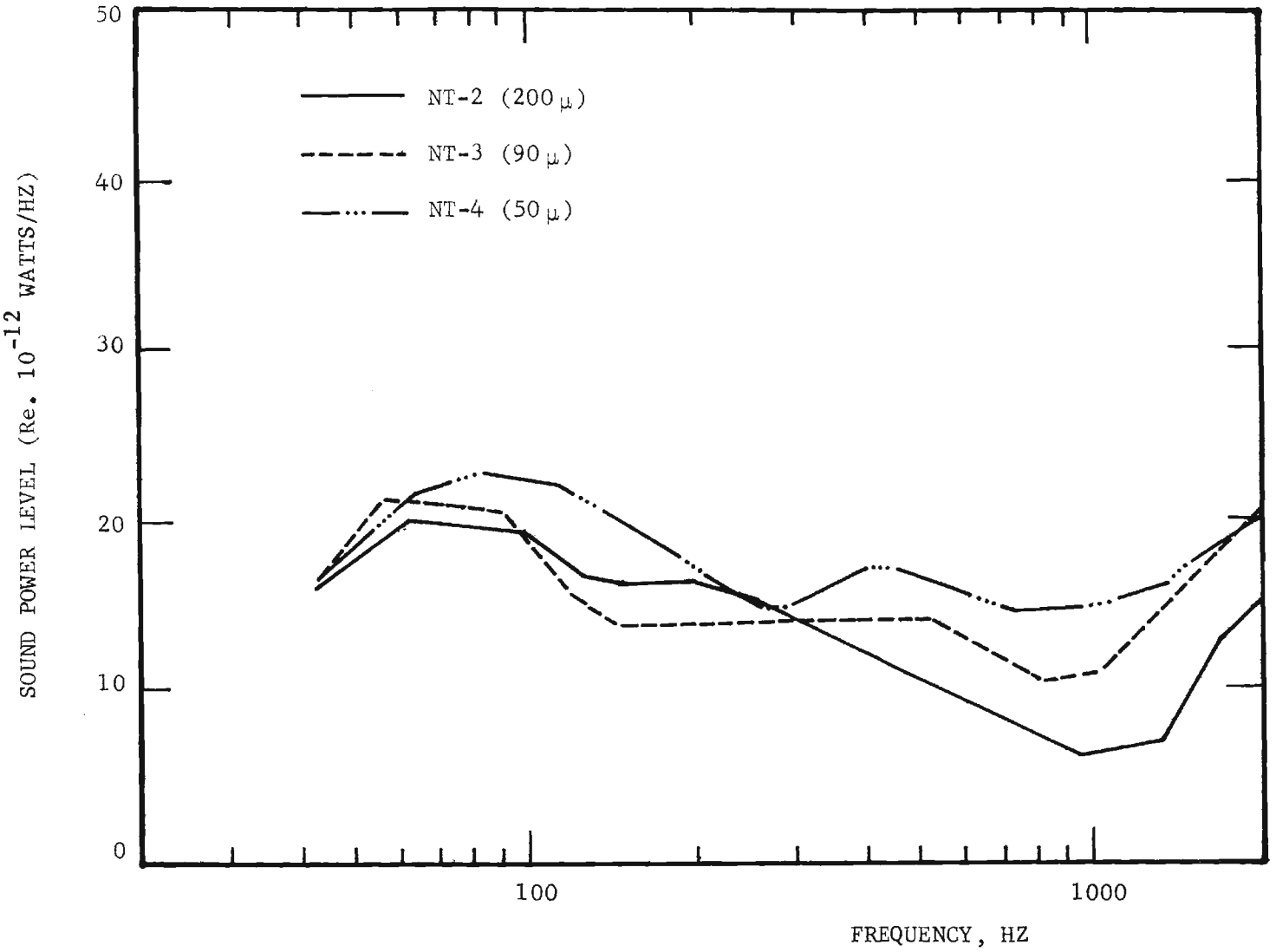

FIGURE 7. COMPARISON OF DEDUCED FREE FIELD SPECTRA FOR NONALUMINIZED PROPELLANTS BURNED AT 300 PSIA IN NITROGEN

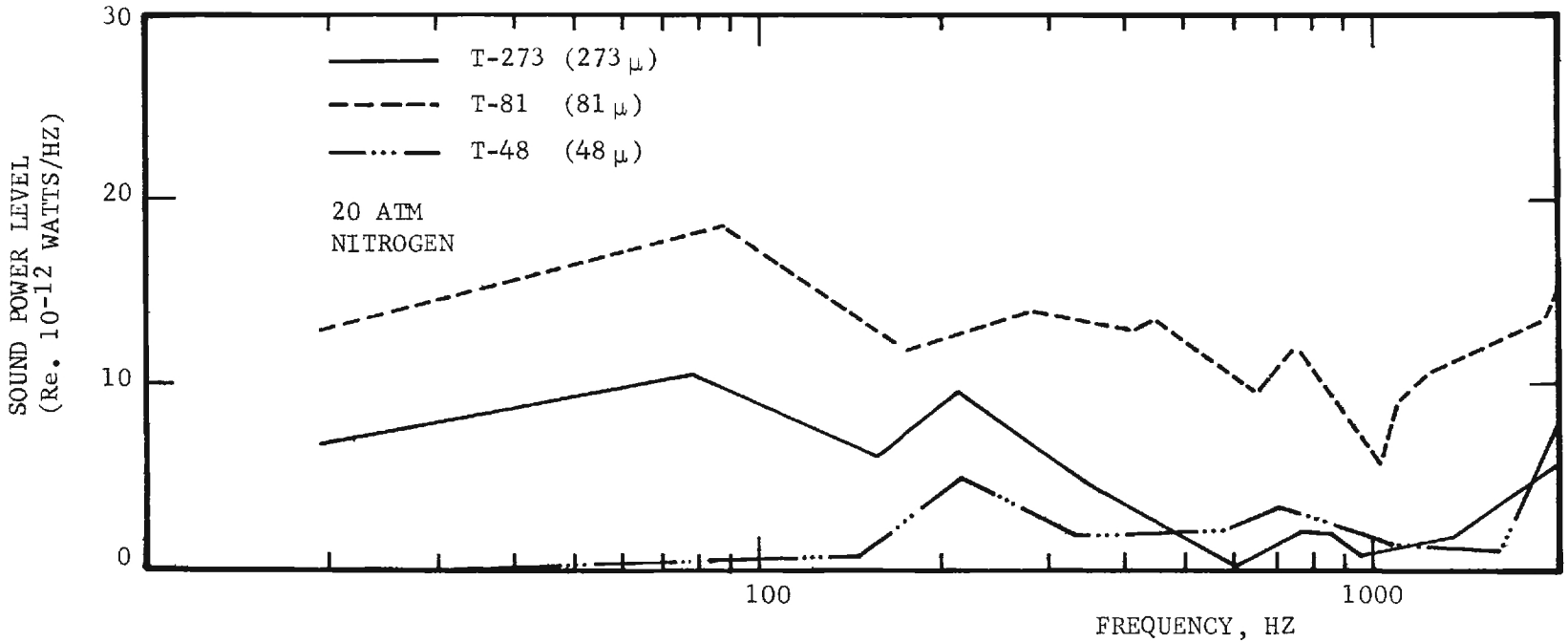

FIGURE 8. EFFECT OF PARTICLE SIZE ON DEDUCED FREE FIELD SPECTRA FOR NONALUMINIZED PROPELLANTS, T-SERIES

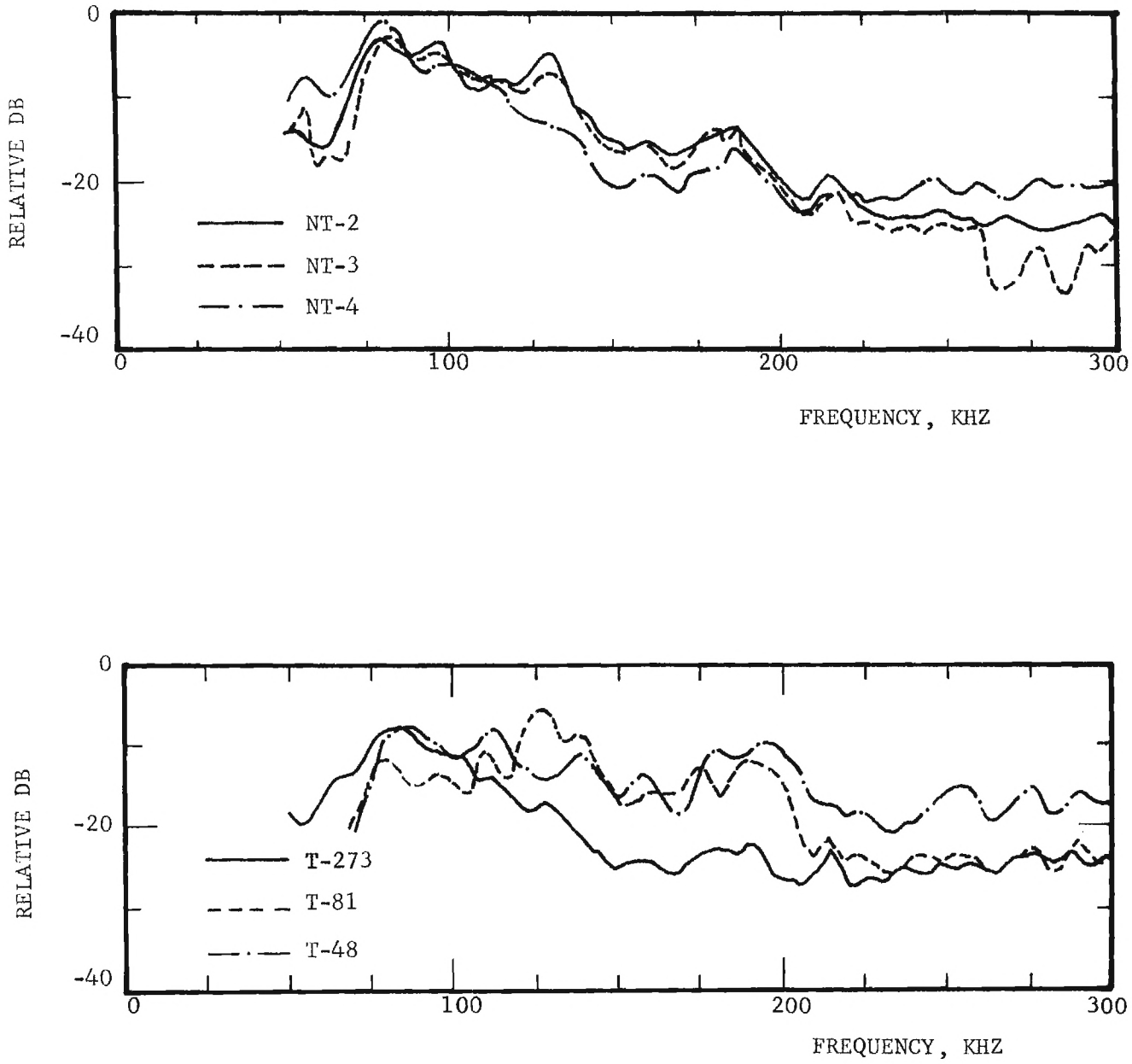

FIGURE 9. EFFECT OF AP PARTICLE SIZE ON THE ACOUSTIC EMISSION SPECTRA FOR THE NONALUMINIZED PROPELLANTS BURNED IN NITROGEN AT 300 PSIA.

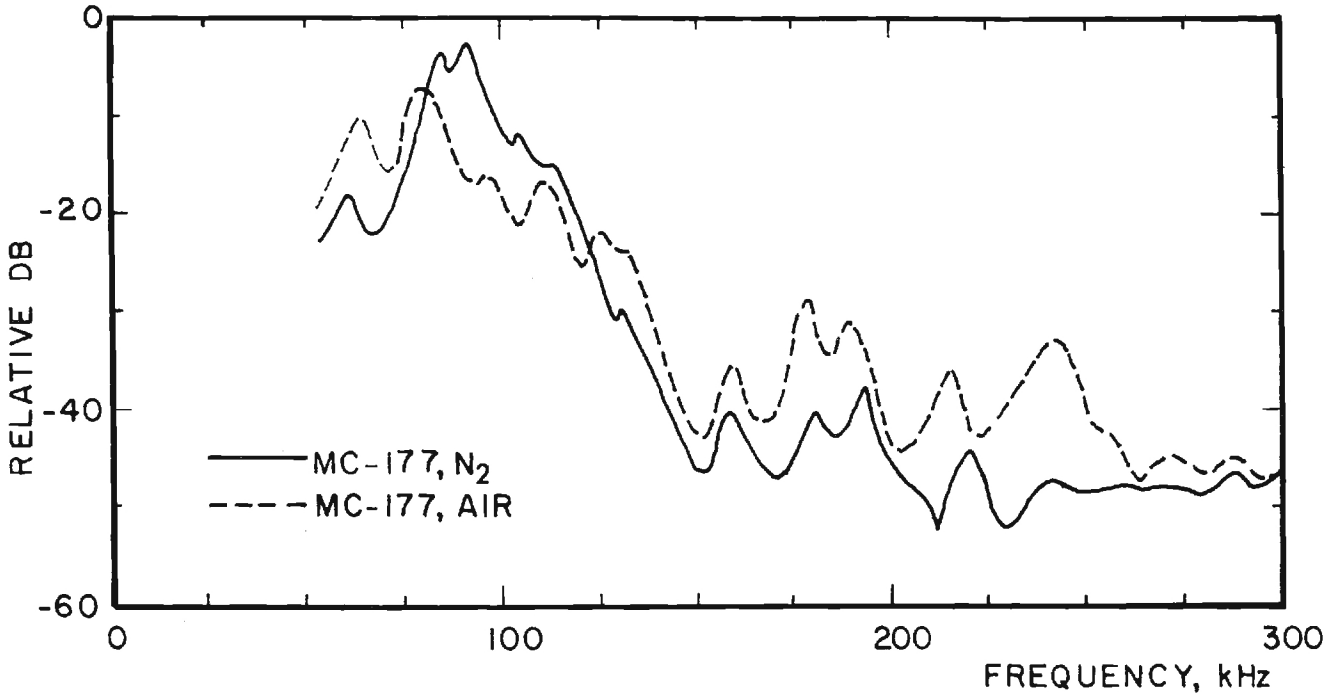

FIGURE 10. EFFECT OF PRESSURIZATION GAS ON THE ULTRASONIC SPECTRA OF MC-177 AT 300 PSIA

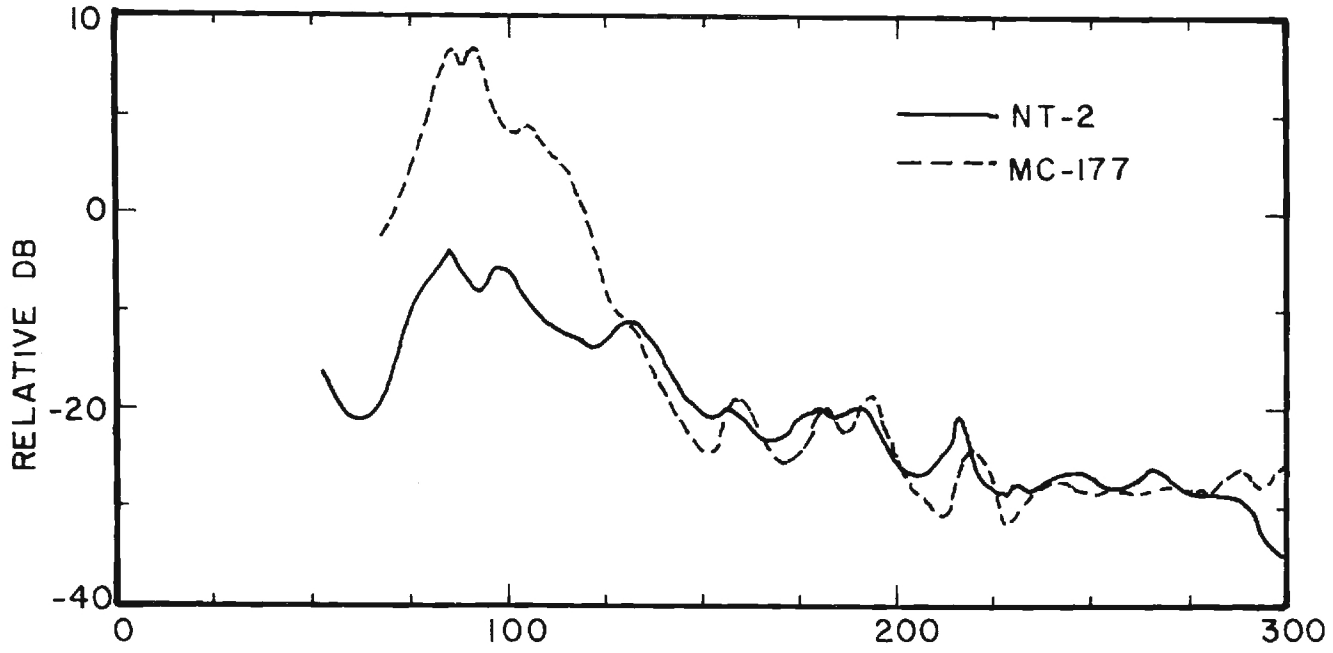

FIGURE 11. EFFECT OF ALUMINUM ADDITION ON THE ULTRASONIC SPECTRA AT 300 PSIA BURNED IN NITROGEN.

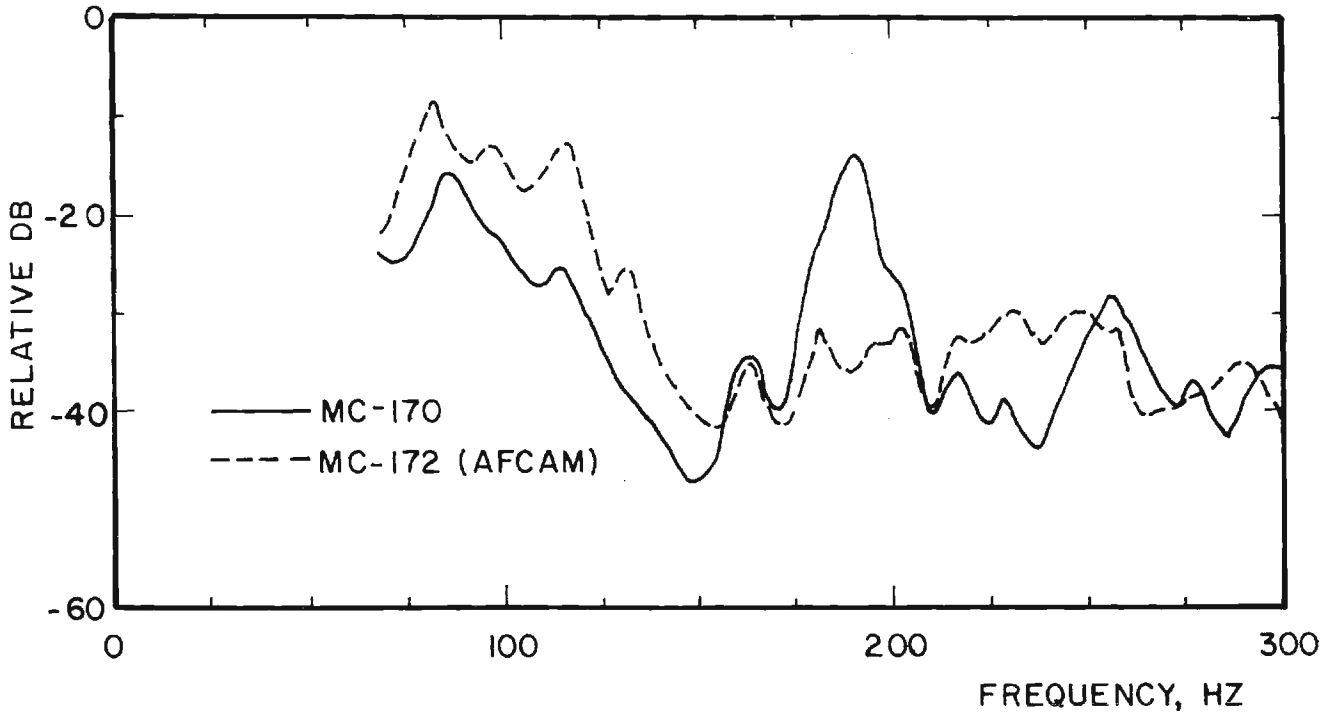

FIGURE 12. EFFECT OF AFCAM COATING OF THE ALUMINUM PARTICLES AT 300 PSIA IN NITROGEN.

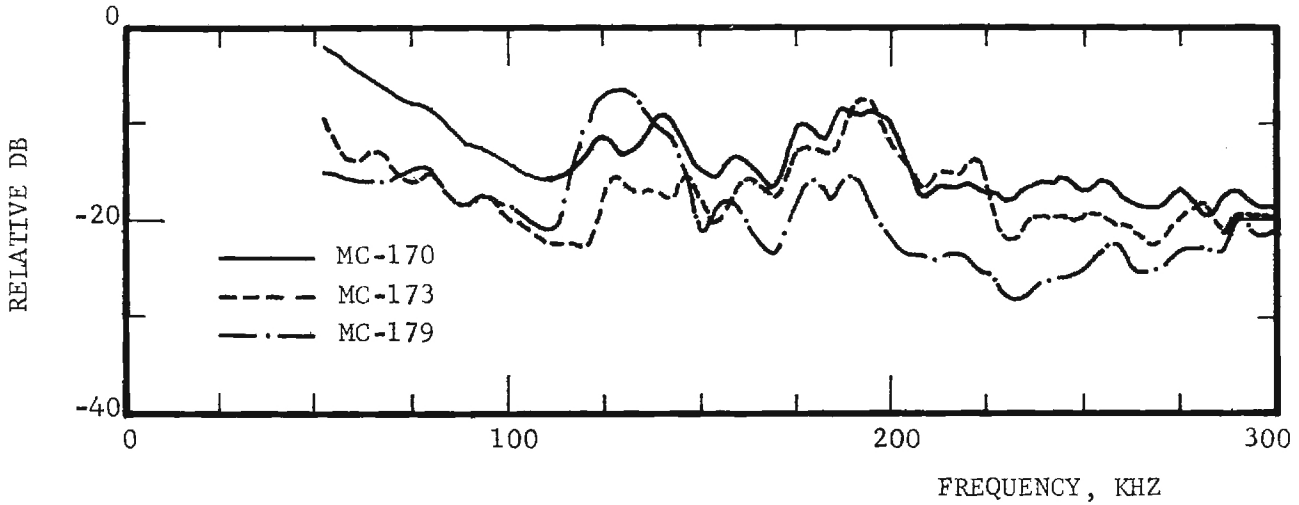

FIGURE 13. EFFECT OF CATALYSTS ON THE SOUND POWER SPECTRA FOR THE ACOUSTIC EMISSIONS.

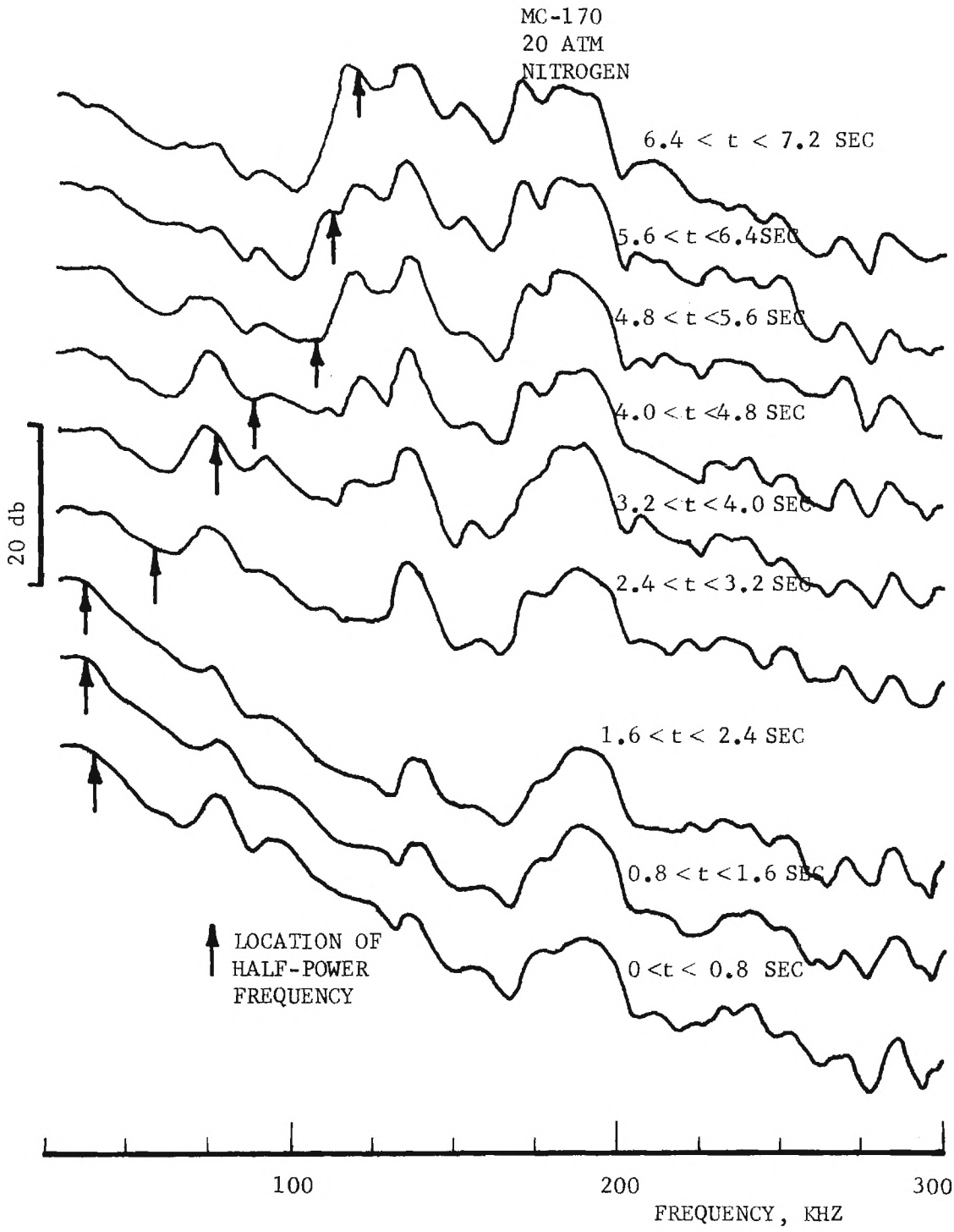

FIGURE 14. NONSTATIONARITY OF THE ACOUSTIC EMISSIONS DURING DEFLAGRATION AS TIME INCREASES.

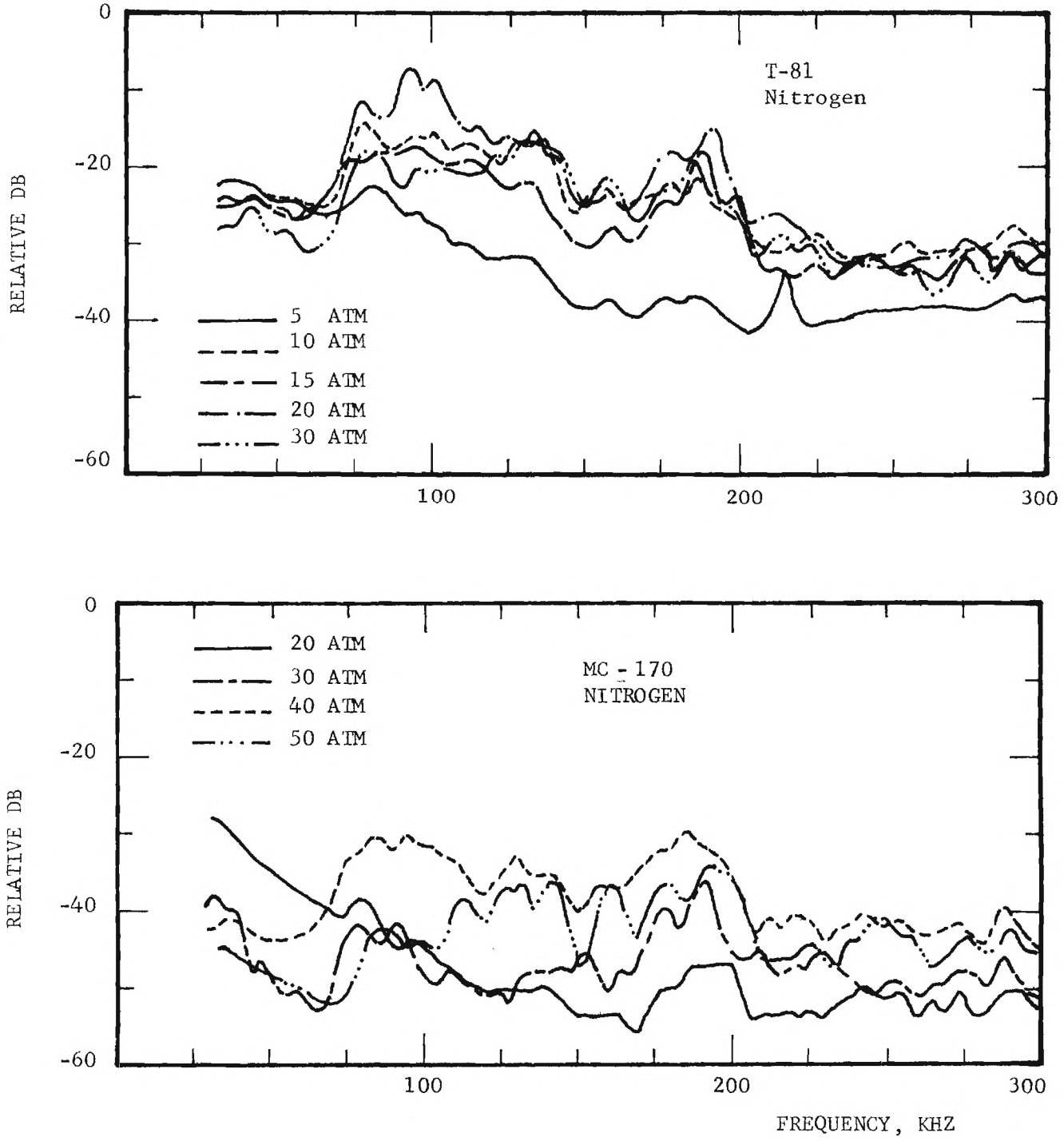

FIGURE 15. EFFECT OF CHAMBER PRESSURE ON THE ACOUSTIC EMISSION SOUND POWER SPECTRA FOR NONALUMINIZED AND ALUMINIZED PROPELLANTS.

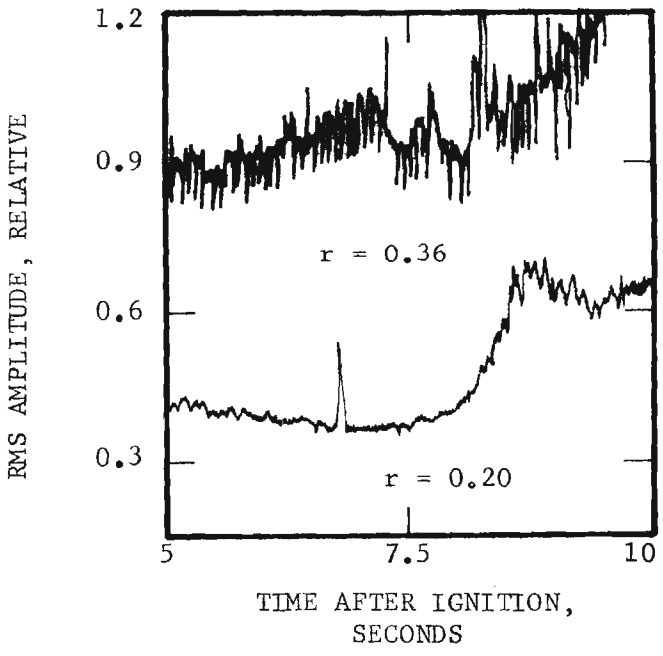

FIGURE 16. INCREASE IN ACOUSTIC EMISSIONS WHICH ACCOMPANIES AN ABNORMALLY HIGH BURN RATE FOR NT-2 at 20ATM IN NITROGEN.

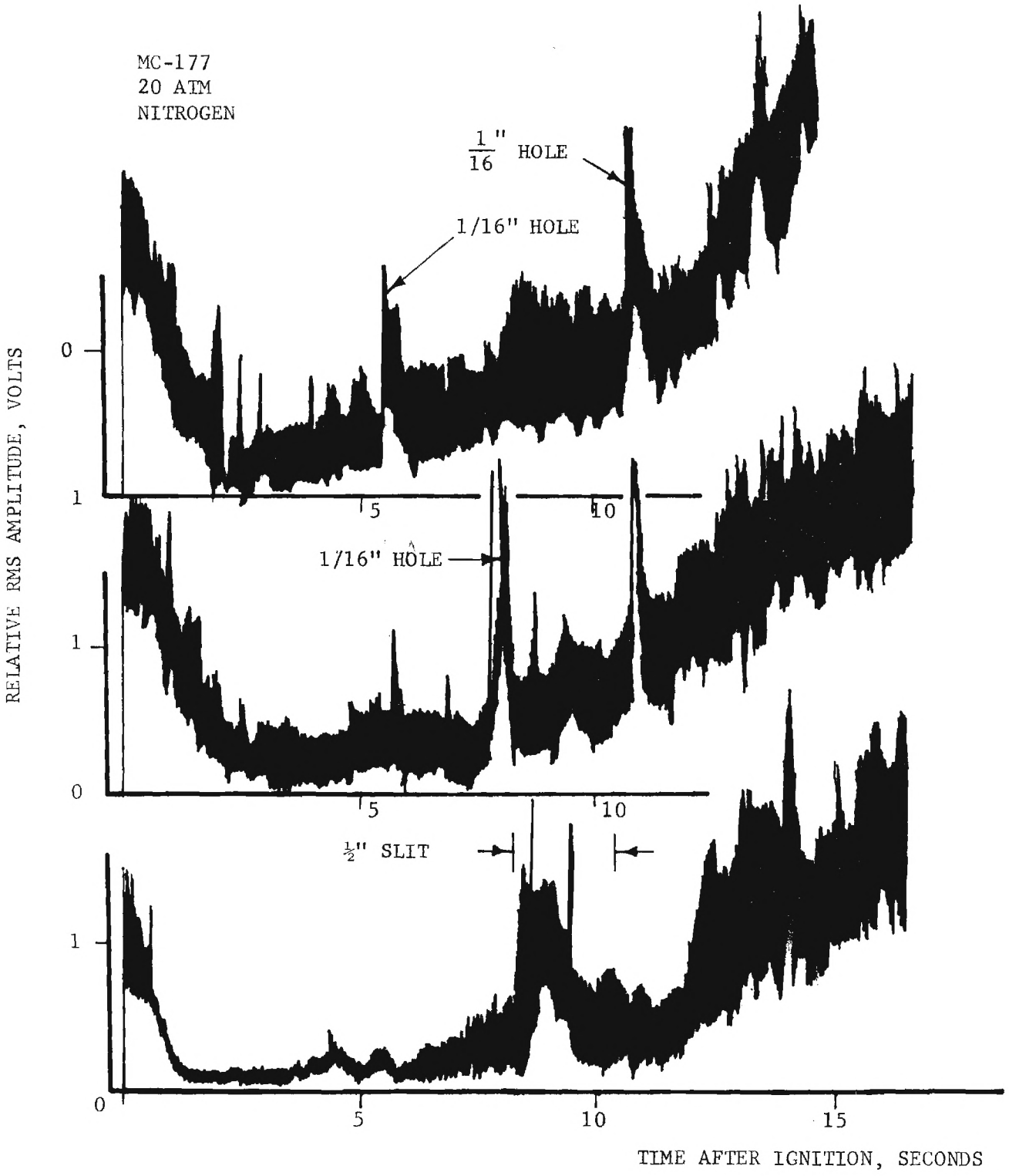

FIGURE 17. EFFECT OF IMPERFECTIONS SYSTEMATICALLY INTRODUCED IN THE PROPELLANT SAMPLE ON THE RMS LEVELS OF THE ACOUSTIC EMISSIONS.

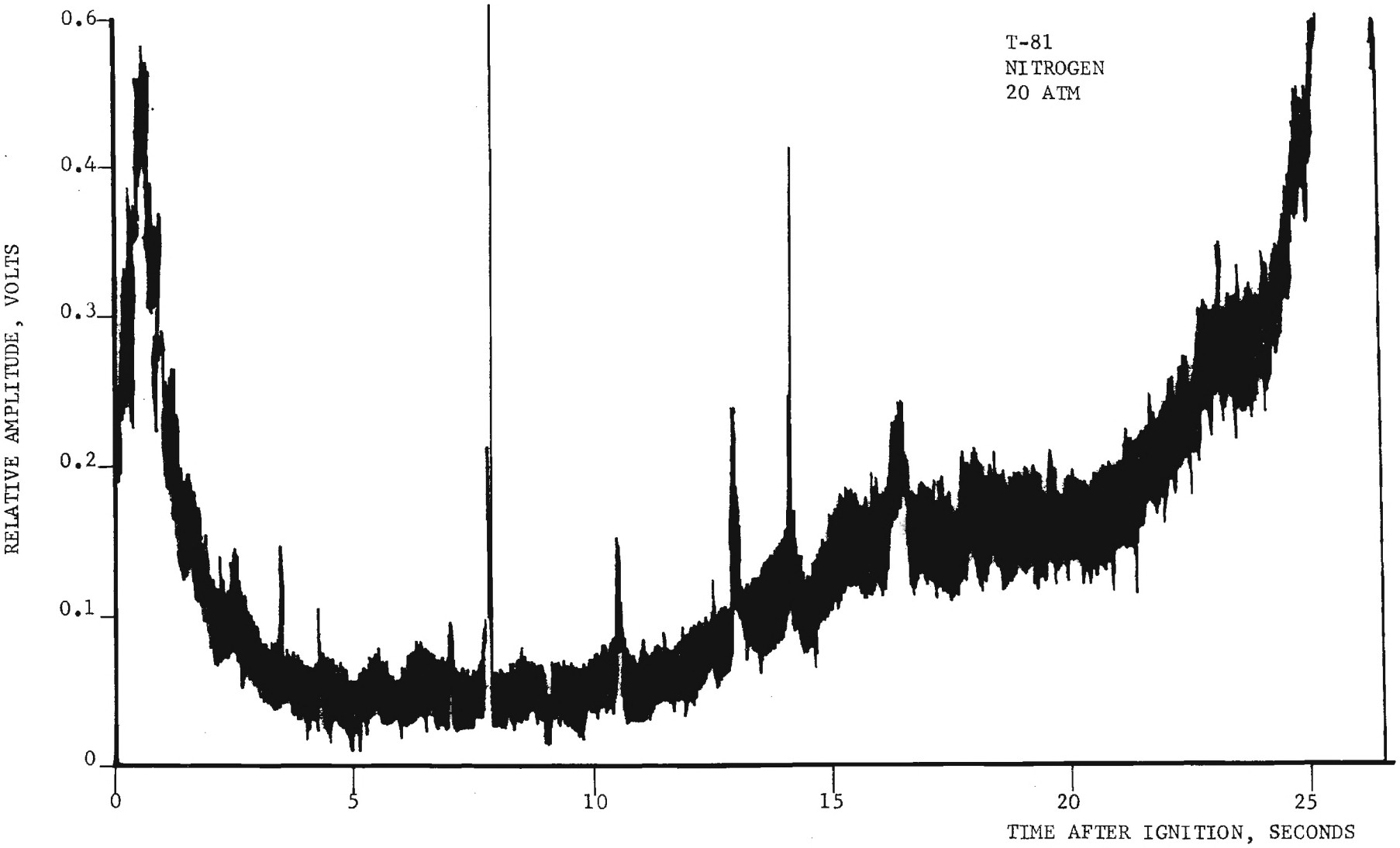

FIGURE 18. ANOMALOUS BEHAVIOR OF THE RMS ACOUSTIC EMISSION LEVELS. THE "SPIKES" ARE PROBABLY CAUSED BY BUBBLES IN THE PROPELLANT INTRODUCED DURING PREPARATION.

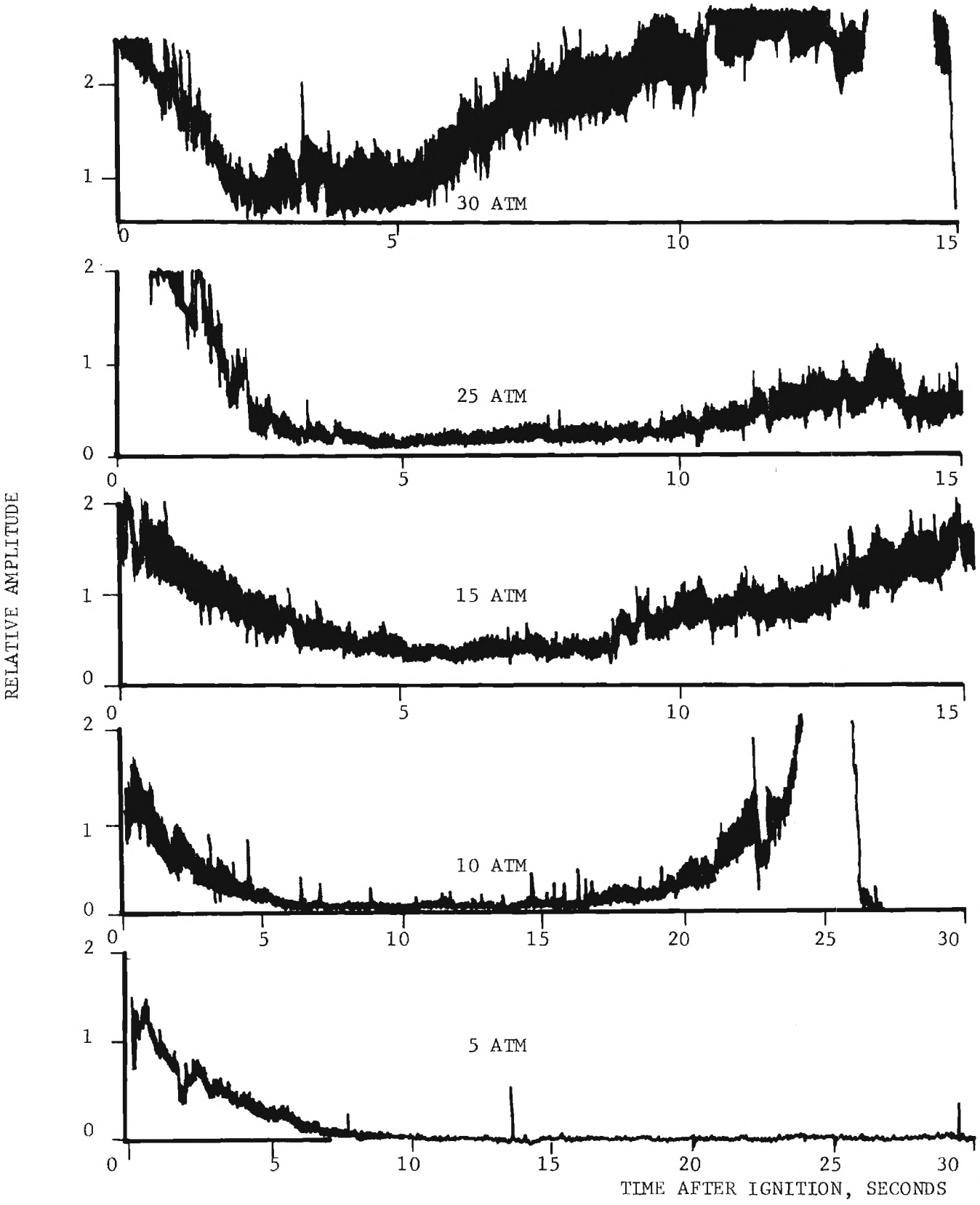

FIGURE 19. EFFECT OF CHAMBER PRESSURE ON THE RMS ACOUSTIC EMISSION LEVELS FOR NT-2 IN NITROGEN.

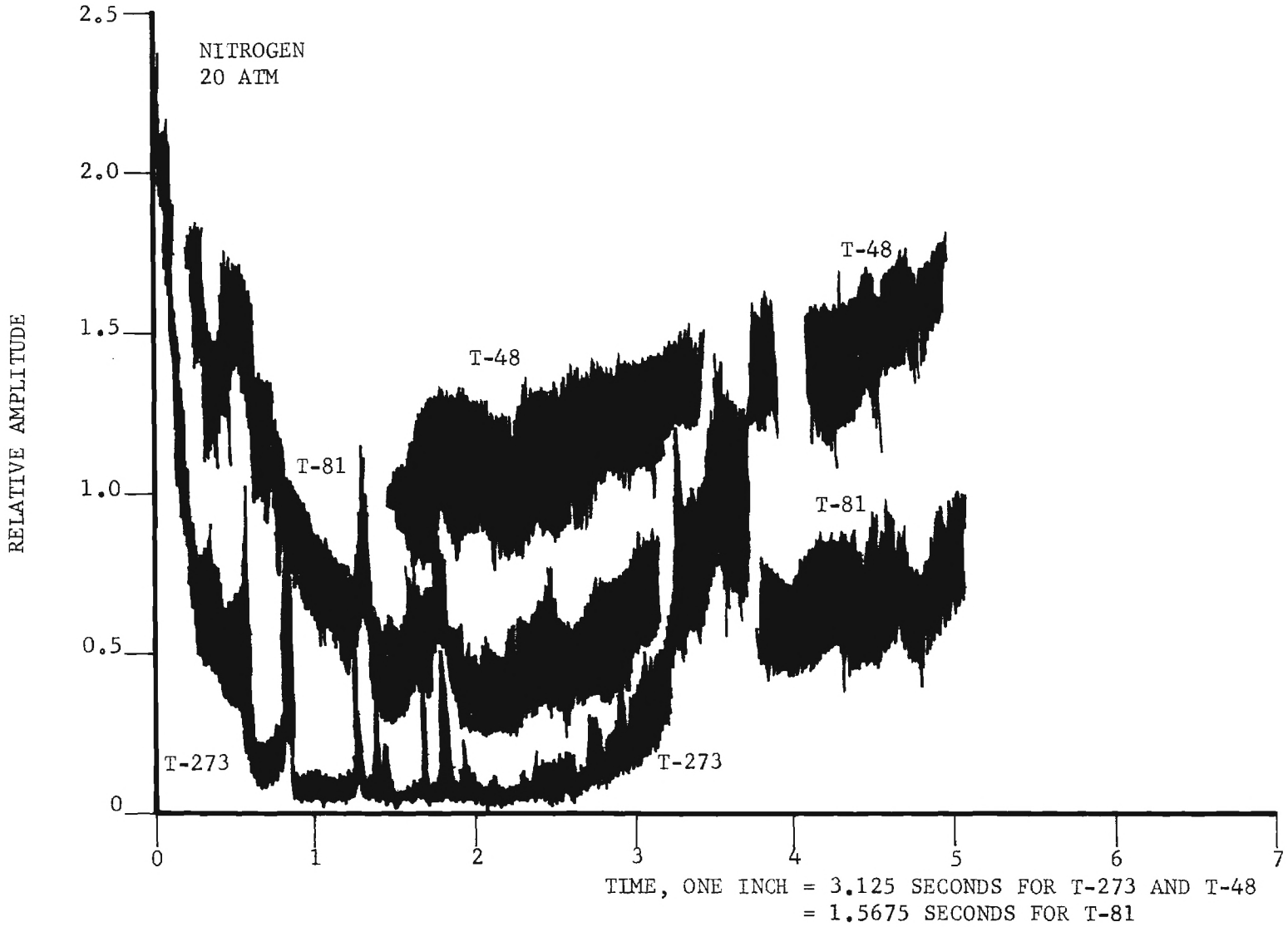

FIGURE 20. EFFECT OF PARTICLE SIZE ON THE RMS ACOUSTIC EMISSION LEVELS FOR A NON-ALUMINIZED SERIES OF PROPELLANTS.

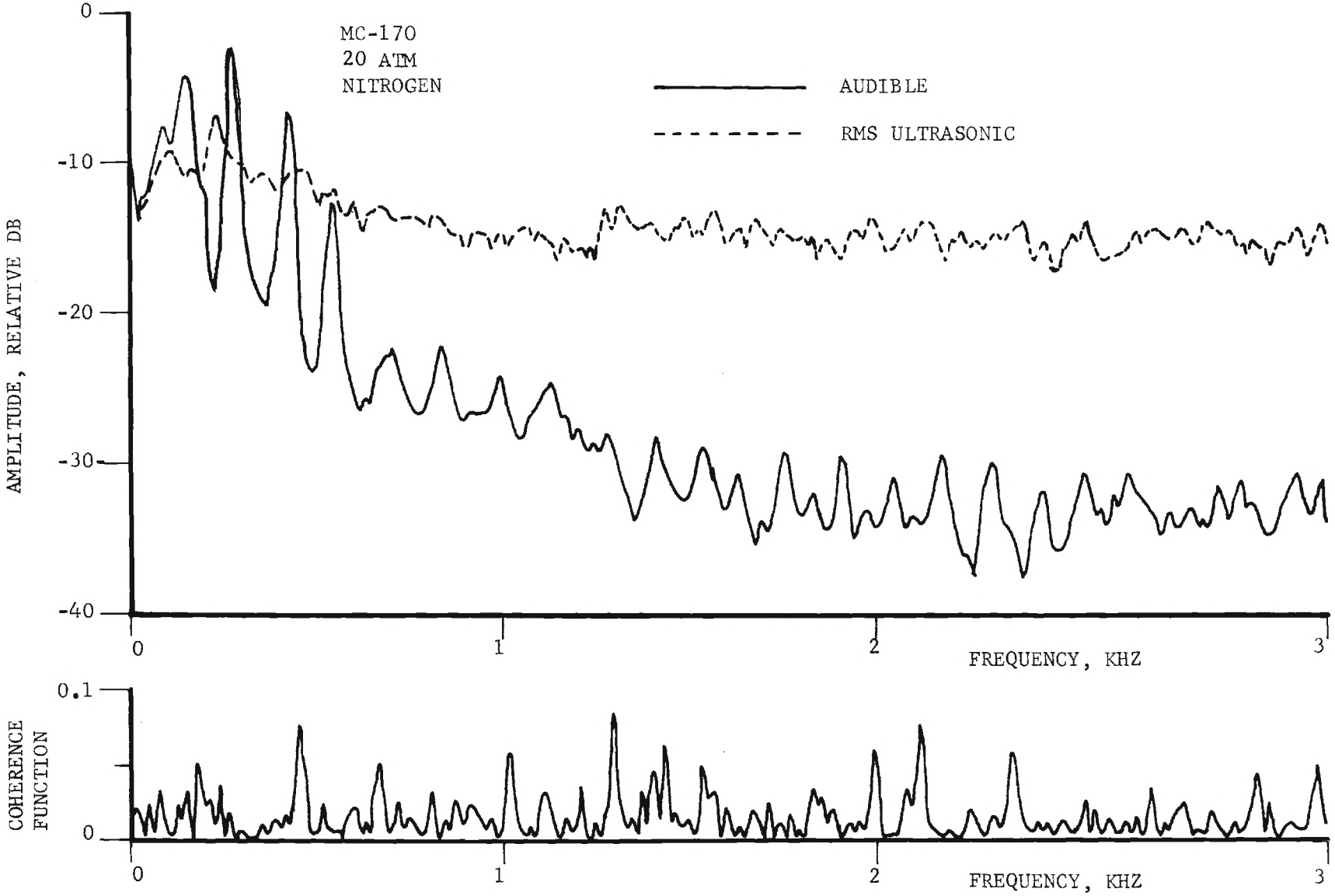

FIGURE 21. CORRELATION OF THE RMS ACOUSTIC EMISSION SIGNAL WITH THE AUDIBLE SIGNAL FOR AN ALUMINIZED PROPELLANT.